PB87-227658

Mesoscale Acid Deposition Model: Preliminary Applications and a Guide for User Interface

Iowa Univ., Iowa City

Prepared for

Environmental Protection Agency, Research Triangle Park, NC

Aug 87

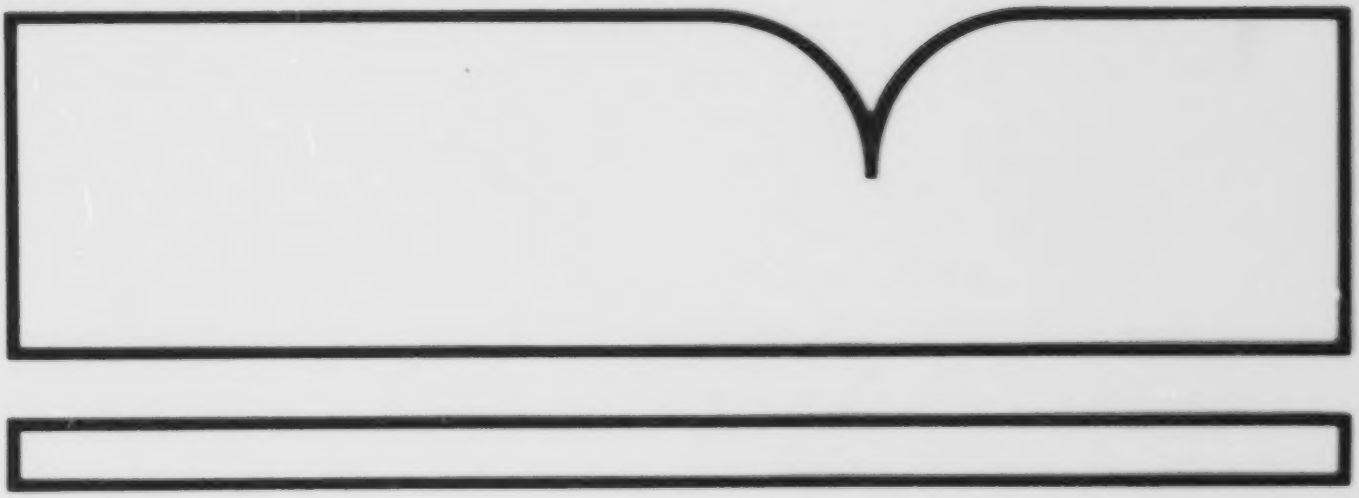

U.S. Department of Commerce
National Technical Information Service
NTIS

PB87-227658

EPA/600/3-87/027
August 1987

A MESOSCALE ACID DEPOSITION MODEL

Preliminary Applications and a Guide for User Interface

by

Gregory R. Carmichael
Department of Chemical & Materials Engineering
University of Iowa
Iowa City, IA 52242

and

Leonard K. Peters
Department of Chemical Engineering
University of Kentucky
Lexington, KY 40506

DW80931289

Project Officer

Francis S. Binkowski
Meteorology and Assessment Division
Atmospheric Sciences Research Laboratory
Research Triangle Park, NC 27711

ATMOSPHERIC SCIENCES RESEARCH LABORATORY
OFFICE OF RESEARCH AND DEVELOPMENT
U.S. ENVIRONMENTAL PROTECTION AGENCY
RESEARCH TRIANGLE PARK, NC 27711

REPRODUCED BY
U.S. DEPARTMENT OF COMMERCE
NATIONAL TECHNICAL
INFORMATION SERVICE
SPRINGFIELD, VA. 22161

TECHNICAL REPORT DATA
(Please read Instructions on the reverse before completing)

1. REPORT NO.	2.	3. RECIPIENT'S ACCESSION NO.
EPA/600/3-87/027		PB87 227658/AS

4. TITLE AND SUBTITLE	5. REPORT DATE
A MESOSCALE ACID DEPOSITION MODEL Preliminary Applications and a Guide for User Interface	August 1987 6. PERFORMING ORGANIZATION CODE

7. AUTHOR(S)	8. PERFORMING ORGANIZATION REPORT NO.
Gregory R. Carmichael and Leonard K. Peters	

9. PERFORMING ORGANIZATION NAME AND ADDRESS	10. PROGRAM ELEMENT NO.
University of Iowa, Iowa City, IA 52242 University of Kentucky, Lexington, KY 40506	N104/C/05/05-5062 (FY-87) 11. CONTRACT/GRANT NO.
	DW 80931289

12. SPONSORING AGENCY NAME AND ADDRESS	13. TYPE OF REPORT AND PERIOD COVERED
Atmospheric Sciences Research Laboratory--RTP, NC Office of Research and Development Environmental Protection Agency Research Triangle Park, NC 27711	Interim 5/85-4/87 14. SPONSORING AGENCY CODE EPA/600/09

15. SUPPLEMENTARY NOTES

16. ABSTRACT

In 1984 the U.S. EPA initiated a Mesoscale Acid Deposition Study. This study was organized to assess and understand the interactions and importance of local emissions in mesoscale precipitation scavenging. One important component of the project is the simulation of the field events using a detailed meteorological and chemical modeling framework (called MesoSTEM). A dynamical meteorological model, Mesoscale Atmospheric Simulation System (MASS) is used to predict the meteorological fields, including precipitation rates. These fields are used as inputs to a comprehensive chemical model Sulfur Transport Eulerian Model (STEM-II). The three-dimensional models are used to quantify the relationships between emissions, chemical production, and wet deposition on the mesoscale. The linkage of the models, and the application of MesoSTEM to the May 2nd and 3rd, 1985 Philadelphia Mesoscale Field Study data set is the subject of this progress report.

17. KEY WORDS AND DOCUMENT ANALYSIS

a. DESCRIPTORS	b. IDENTIFIERS/OPEN ENDED TERMS	c. COSATI Field Group

18. DISTRIBUTION STATEMENT	19. SECURITY CLASS (This Report)	21. NO. OF PAGES
RELEASE TO PUBLIC	UNCLASSIFIED	125
	20. SECURITY CLASS (This page)	22. PRICE
	UNCLASSIFIED	PC A18.95

EPA Form 2220-1 (Rev. 4-77) PREVIOUS EDITION IS OBSOLETE

NOTICE

The information in this document has been funded by the United States Environmental Protection Agency under an interagency agreement (DW80931289) to National Aeronautics and Space Administration.

It has been subjected to the Agency's peer and administrative review, and it has been approved for publication as an EPA document. Mention of trade names or commercial products does not constitute endorsement or recommendation for use.

ABSTRACT

In 1984 the U.S. EPA initiated a Mesoscale Acid Deposition Study. This study was organized to assess and understand the interactions and importance of local emissions in mesoscale precipitation scavenging. One important component of the project is the simulation of the field events using a detailed meteorological and chemical modeling framework (called MesoSTEM). A dynamical meteorological model, Mesoscale Atmospheric Simulation System (MASS) is used to predict the meteorological fields, including precipitation rates. These fields are used as inputs to a comprehensive chemical model Sulfur Transport Eulerian Model (STEM-II). The three-dimensional models are used to quantify the relationships between em ssions, chemical production, and wet deposition on the mesoscale. The linkage of the models, and the application of MesoSTEM to the May 2nd and 3rd, 1985 Philadelphia Mesoscale Field Study data set is the subject of this progress report.

CONTENTS

Abstract.....iii

Figures.....vi

Tables.....viii

Acknowledgement.....ix

1. Introduction.....1-1

2. Overview of MesoSTEM Model Equations.....2-1
   Model Equations.....2-1
   QA/QC of Numerical Advection Algorithm.....2-6

3. MesoSTEM Computer Code.....3-1

4. Application of MesoSTEM to May 2nd & 3rd Field Data.....4-1
   Coarse Grid Simulation.....4-9
   Fine Grid Simulations.....4-13
   Nested Grid Capabilities.....4-29
   Simulation Execution Time.....4-31

5. Related Activities.....5-1
   Influence of Transition Metal Ions on Sulfate Formation.....5-1
   Cumulus Cloud Scavenging Studies.....5-2
   Acidification of Non-Precipitating Cumulus Clouds.....5-3
   Improved Numerical Schemes.....5-5
   Evaluation of Source Receptor Relations in the MesoSTEM Model.....5-8
   Investigation of Gas Phase Acid Formation using Sensitivity Analysis.....5-9

6. Summary.....6-1

7. References.....7-1

8. Appendix A.....8-1

FIGURES

Number

1 Interaction diagram of chemical/physical processes treated in STEM+ASM.....2-3

2 One-dimensional pure convection test of the Crank-Nicolson Galerkin finite element method with piecewise linear basis functions.....2-8

3 Flow diagrams for STEM-II model.....3-2

4 Philadelphia mesoscale acid deposition study domain.....4-2

5 Model region for MesoSTEM application.....4-3

6 Elevated point sources and area emissions for NO.....4-4

7 Elevated point sources and area emissions for SO_2.....4-5

8 Elevated point sources and area emissions for ammonia.....4-6

9 Elevated point sources and area emissions for $SO_4^=$.....4-7

10 Elevated point sources and area emissions for toluene.....4-8

11 Level one wind fields generated by MASS.....4-10

12 3 hour precipitation predicted by MASS.....4-11

13 Measured total deposition of (a) H^+, (b) HNO_3, and (c) $SO_4^=$.....4-12

14 Initial conditions for NO and SO_2.....4-14

15 Initial conditions for HNO_3 and ammonia.....4-15

16 Initial conditions for $SO_4^=$ and NO_2.....4-16

17 Initial conditions for O_3 and H_2O_2.....4-17

18 Ground-level aerosol $SO_4^=$ concentration.....4-18

19 Ground-level gas phase H_2O_2 concentration.....4-20

20 Total 18 hour wet deposition amounts of nitrate (top) and sulfate (bottom).....4-23

FIGURES (CONTINUED)

21 Total 18 hour wet deposition amounts of H_2O_2(top) and H^+ (bottom).....4-24

22 (a) Precipitation field at grid (8,2), (b) precipitation field at grid (4,8), (c) rain water concentration at grid (8,2), (d) rain water concentration at grid (4,8), (e) cumulative deposition at grid (8,2), and (f) cumulative deposition at grid (4,8).....4-25

23 Budget calculations for (a) HNO_3, (b) sulfate, and (c) SO_2.....4-27

24 Grid system for the regional scale simulation.....4-30

25 Variation of relative error 5-7

26 The response of sulfate at the receptors with respect to a positive perturbation of SO_2 sources in the vicinity of Gary, Cincinnati, and Pittsburgh.....5-10

TABLES

Number		Page
1	Numerical Analogs of Domain Moment Integrals	2-9
2	Subroutine List	3-8
3	Chemistry Subroutine List	3-10
4	Variable List	3-12
5	Chemical Species List	3-15
6	Budget Calculations of Selected Species for the 18 Hour Simulation for the Coarse and Fine Grid Domains	4-28

ACKNOWLEDGMENTS

Special thanks to Dr. Ari Patrinos of Brookhaven National Laboratory for supplying the deposition data, to Dr. Mike Kaplan and Glen Coats for preparation of the meteorological fields, to Dr. J. M. Hales of Pacific Northwest Laboratories for supplying the Advanced Scavenging Model, Dr. David Powell of Pacific Northwest Laboratories for providing the gridded precipitation data for the regional scale work, Prasad Kasibhatla at the University of Kentucky for preparing the emission fields, and Shang-gyoo Shim at the University of Iowa for carrying out the STEM model simulations.

1. INTRODUCTION

The STEM (Sulfur Transport Eulerian Model) models were developed to provide a theoretical basis to investigate the relationships between the emissions, the atmospheric transport, chemistry and removal processes, and the resultant distribution of air pollutants and depositions. The development of an Eulerian model, the STEM-I model, to describe the transport/transformation and removal of SO_2 and sulfate began in 1975. This STEM-I model simulates the transport and chemical processes of SO_2 and sulfate in three-dimensions and makes use of a set of 27 reactions to describe SO_2 gas phase photo-oxidation. This model is described in detail in Carmichael and Peters (1984a and 1984b) and subsequently has undergone extensive comparison with the July 1974 and 1978 SURE data bases (cf, Dronamraju et al., (1987a & b)).

Work began in 1980, with NASA funding, to extend the STEM model to include a more detailed treatment of N_xO_y, hydrocarbon, and H_xO_y species and wet removal processes. This activity, and subsequent work with Pacific Northwest Laboratories related to wet removal, led to the development of the STEM-II model, which currently treats some 60 chemical species. The important atmospheric processes are incorporated into the model using chemical, dynamical and thermodynamical parameterizations having sufficient detail to accommodate boundary layer-free troposphere exchange in cloudy and cloud-free environments, and in-cloud and below-cloud wet removal and chemical processes. The STEM-II model (Carmichael, et al., 1986) is described in detail later in this report. The STEM-II model and its components have already been used for a variety of applications. Some of these are: a) transport of SO_2/NO_x/hydrocarbon urban plumes to the background troposphere (Balko and Peters, 1983); b) sulfate and nitrate formation in the presence of land/sea breeze (Kitada, et al., 1984); c) effects of in-cloud and below-cloud scavenging on homogeneous gas-phase chemistry (Carmichael et al., 1983); d) detailed analysis of mixing-limited chemical reaction of NO emissions (Karamchandani and Peters, 1986); and e) the investigation of sulfate production in orographic storms (Hong and Carmichael, 1986). Many other applications are currently ongoing and some will be discussed later in this report. Also, the STEM-II model has been applied to problems on various

spatial scales utilizing horizontal grid sizes from 80 km down to 5 km (cf, Kitada, et al., 1986).

In 1984 the U.S. EPA initiated a Mesoscale Acid Deposition Study. This study, involving scientists from EPA, Brookhaven National Laboratory, NASA, Meso, Inc. and the Universities of Iowa and Kentucky, was organized to assess and understand the interactions and importance of local emissions in mesoscale precipitation scavenging. The study consists of a field component, diagnostic calculations, and the application of a combined mesoscale meteorological and chemical modeling framework (called MesoSTEM). The STEM-II model is being used in this project. This report summarizes our activities during the two year period May, 1985 - May, 1987. These activities have focused on the linkage of the dynamic mesoscale meteorological model (i.e., the MASS (Mesoscale Atmospheric Simulation System) model (cf, Kaplan et al., 1982) and the STEM-II model, the testing of the MesoSTEM model, and the diagnostic analysis of field data collected on May 2nd and 3rd, 1985 around Philadelphia, PA.

2. OVERVIEW OF STEM-II MODEL

The diagnostic analysis in this project is being carried out by use of the STEM-II model (Carmichael, et al., 1986). The STEM-II model is an Eulerian combined transport/chemistry/removal model which treats chemical species in the gas, cloud, rain and snow phases. Thirty-nine species are advected, while twenty-one species are short-lived and are modeled using pseudo-steady state methods.

MODEL EQUATIONS

The advected species satisfy the following equations

Gas Phase:

$$\frac{\partial C_i}{\partial t} + \frac{\partial (U_j C_i)}{\partial x_j} = \frac{\partial}{\partial x_j}\left[K_{jj} \frac{\partial C_i}{\partial x_j}\right] + R_i + E_i + G_i \qquad i=1,\cdots,39 \qquad (1)$$

Cloud, Rain, and Snow Phases:

$$\frac{\partial (S_m C_{im})}{\partial t} + \frac{\partial}{\partial x_j}(U_j - V_{sm}) S_m C_{im} = \frac{\partial}{\partial x_j}\left(K_{jjm} C_{im} \frac{\partial S_m}{\partial x_j}\right) + R_{im} + G_{im} \qquad (2)$$

$i=1,\cdots,39$; m = 1 for cloud ($V_{sm} = 0$)
= 2 for rain
= 3 for snow

where C_i's denote the gas phase concentrations in molecules/cm^3

C_{im}'s denote the liquid phase concentrations in moles/liter

U_j's are velocity components in m/s

S_m's are the condensed water contents in m^3water/m^3air

E_i's are the elevated emissions in molecules/cm^3/s

V_{sm}'s are the settling velocities of the hydrometeors in m/s

K_{jj}'s are the eddy diffusivities in m^2/s and

K_{jjm}'s are the eddy diffusivities of the condensed water phases in m^2/s

R_i gas phase chemical reaction rate for species i, molecules/cm^3/s

R_{im} condensed water phase chemical reaction rates for species i, moles/liters/s

G_i gas phase mass transfer rates, molecules/cm^3/s

G_{im} condensed water phase mass transfer rates, molecules/cm^3/s

The STEM-II model is structured to treat wet removal processes in detail. A schematic of the processes that are included in the model analysis is presented in Figure 1. In this model, the in-cloud scavenging of sulfate aerosol is presumed to occur totally by nucleation. Both cloud and aerosol size distributions are assumed to be monodispersed. Once the cloud forms, the number of sulfate aerosols activated and dissolved to form aqueous sulfate is assumed to be the same as the number concentration of cloud droplets. Rain drops are also assumed to be monodispersed. Secondary sulfate is treated in the same way as primary sulfate and is allowed to be reinjected into the aerosol phase as hydrometeors evaporate.

In this project the cloud parameters are calculated by the ASM (Advanced Scavenging Module) cloud scavenging model (Easter and Hales, 1984). The ASM model treats the cloud microphysics, and calculates the cloud and precipitation distributions, and interconversion rates. ASM calculates a self consistent and realistic meteorological data set of the simulated storm. The precipitation formation processes are treated in a parameterized fashion. The parameterizations of rain formation are adapted from Berry and Reinhardt (1974), Scott (1982), Kessler (1969), and Lin et al., (1983). The snow formation is parameterized based on schemes similar to that developed by Lin et al. and Scott. The scheme lumps water into four categories: water vapor, cloud water, rain and snow. The cloud related parameters calculated in ASM are transferred to the STEM-II model where the transport/chemistry/removal of pollutants is calculated.

For the gas phase, the reaction mechanism of Atkinson et al., (1982), which includes 85 reactions and 60 chemical species, is used. Of these species, 39 long-lived species are advected while the remaining 21 short-lived species such as free radicals are modeled using the Pseudo-Steady State Approximation.

For the liquid phase, 17 equilibrium dissociation reactions, 3 chemical kinetic expressions, and 22 ionic species based on the work of Chameides (1984) are included in the STEM-II code. Detailed solution equilibria and chemical kinetics are solved using a modified semi-implicit method while

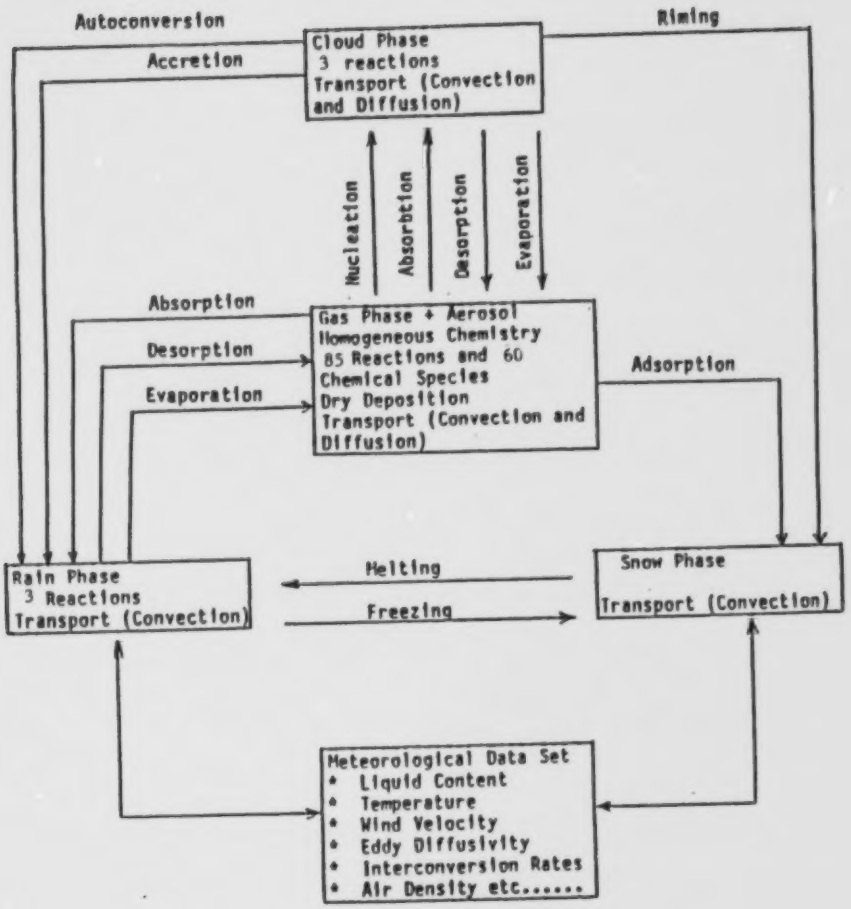

Figure 1. Interaction diagram of chemical/physical processes treated in the STEM+ASM model.

satisfying the electrical-neutrality constraint. Also, the mass transfer associated with absorption into and desorption from droplets is included.

The effect of clouds on the solar flux values is also included in this analysis. The following empirical correlation relating photon flux to cloud cover (Kaiser and Hill (1976)) is employed,

$$F = F_c\left(1 - AC^{1.75}\right) \tag{3}$$

where F_c is the photon flux for clear sky, C is the cloud cover fraction, and A is a constant dependent on cloud type. The effect of multiple layers of clouds is not explicitly treated in this analysis.

The simulation of transport/chemistry described by Equations (1) and (2) requires numerical integration. The method presently used is a combination of the concept of fractional time steps and the one-dimensional finite element method. This is referred to as the Locally One-Dimensional, Finite-Element Method (LOD-FEM). The LOD procedures (Mitchell, 1969) split the multi-dimensional partial differential equation into time dependent, one-dimensional problems which are solved sequentially. The time-split equations are of the form

$$\frac{\partial C_\ell}{\partial t} + L_x C_\ell = 0 \tag{4a}$$

$$\frac{\partial C_\ell}{\partial t} + L_y C_\ell = 0 \tag{4b}$$

$$\frac{\partial C_\ell}{\partial t} + L_z C_\ell = S_\ell \tag{4c}$$

and

$$\frac{\partial C_\ell}{\partial t} = R_\ell + G_\ell \tag{4d}$$

where the L's represent the one-dimensional transport operators

(e.g., $L_x C_\ell = \frac{\partial (U\ C_\ell)}{\partial x} - \frac{\partial}{\partial x}\left(K_{xx} \frac{\partial C_\ell}{\partial x}\right)$). The liquid phase equations have the same form. The chemical reaction and mass transfer terms are treated separately because many of the reactions have time scales much smaller than that for the transport. Splitting out these terms allows different time steps for the transport and the chemistry/removal processes.

The transport equations are solved using a Petrov-Crank-Nicolson-Galerkin (Heinrich et al., 1977) finite element technique. An important feature of this numerical procedure is that the computer code is structured to allow application to one, two and three dimensional time-dependent analysis.

The technique used to integrate the chemistry and mass transfer terms is an adaptation of the semi-implicit Euler method proposed by Preussner and Brand (1981). The method consists of writing Equation (4d) in the form

$$\frac{dC_i}{dt} = G_i \qquad (5)$$

$$\frac{dC_i}{dt} = G_{im} \qquad (6)$$

$$\frac{dC_i}{dt} = P_i - D_i\ C_i \qquad (7)$$

$$\frac{dC_{im}}{dt} = P_{im} - D_{im}\ C_{im} \qquad (8)$$

m = 1 for cloud
m = 2 for rain
m = 3 for snow

when P and D represent the chemical production and destruction terms. Over time step Δt, Equations (5) to (8) are solved analytically assuming all other concentrations are constant during the time period. These procedures have the important properties that C_I can never become negative provided that the reaction rates are positive and the initial values are non-negative, and that

in the limit as $t \to \infty$ the proper steady state concentrations are obtained; i.e.,

$$C_i^{ss} = \frac{P_i}{D_i} \quad (9)$$

Equation (7) is used in the model in the calculation of the advected species only. However, the terms P_i and D_i also contain the concentrations of the short-lived gas phase species (e.g., OH, HO_2, etc.), which are calculated using the pseudo-steady state approximations. The use of this approximation results in a set of algebraic equations that depends on the concentrations of the advected species. The calculation procedure to advance from t to $t + \Delta t$ uses $C_{i|t}$ to calculate the short lived species concentrations and then uses these concentrations to advance to $C_{i|t} + \Delta t$ using Equation (7) as a one-step predictor.

The accuracy of this technique is dependent on the species of interest and Δt_i For long lived species (e.g., SO_2, CO, and alkanes), relatively large Δt can be used, but for relatively reactive species much smaller time steps are required. Test calculations using the kinetic mechanism indicate that over a fifteen minute simulation (5 - 15 minutes are typical step sizes used for solution of the transport equations), the results obtained by this method and those obtained by the Gear method differ by less than 1%. This pseudo-analytic technique can execute ten times as fast as the Gear method for this chemical scheme. The chemistry time step used in this study is 5 sec.

QA/QC OF NUMERICAL ADVECTION ALGORITHM

The equations governing the transport and chemistry of trace species must be solved numerically for most realistic cases. The procedure used in STEM-II is a combination of the concept of fractional time steps and one-dimensional finite elements, referred to as the Locally One-Dimensional, Finite-Element Method (LOD-FEM). The multi-dimensional partial differential equations are split into three time dependent, one-dimensional problems which are solved sequentially.

The transport equations are solved using a Petrov-Galerkin finite element technique (Heinrich, et al., 1977) and spatial filtering (Forester, 1977; McRae, et al., 1982). This LOD-FEM procedure has been evaluated by others; for example, Kasibhatla (1984) has evaluated the advection algorithm used in STEM-II by investigating the accuracy of the one-dimensional advection equation. His tests were based on advection of triangle, sine and square wave distributions of moderately narrow width. In addition to visual observations of the advected waveforms, the first and second moments of the distributions, M_1 and M_2, were evaluated. Obviously, M_1 represents the mass conservation condition, while M_2 will be preserved only if there are no diffusive effects. Both M_1 and M_2 of the advected waveforms are exactly conserved, and the efficiency of any numerical method can be studied by evaluating these moments at various times.

Selected results from Kasibhatla's study are shown in Figure 2 and Table 1 for the three waveforms. These results demonstrate that the Crank-Nicolson Galerkin method, when applied to an advection-dominated problem, gives rise to numerical oscillations, primarily in the wake of the advected waveform. However, the upwinding scheme substantially minimizes this problem. From Table 1, it can be seen that mass is essentially conserved and wave shapes can be substantially retained. Part of the diffusion that occurs results from filtering of the data. The reduction in peak value of the concentration depends on the shape of the waveform. These results also clearly show the advantages of using the upwinding scheme and filtering routine. Greater stability of the numerical solution is obtained, and the method is readily applied to high Peclet number ($u\Delta x/K$) situations provided the Courant number ($u\Delta t/\Delta x$) is less than 1, where u is the wind velocity, Δx is the x-direction grid spacing, Δt is the time step, and K is the eddy diffusivity. For the MesoSTEM simulations filtering was not used. Sweeping in the LOD equations is done in the sequence x-direction, y-direction and z-direction.

A complete description of the STEM-II model is presented in Appendix I and the computer code is described in Section 3.

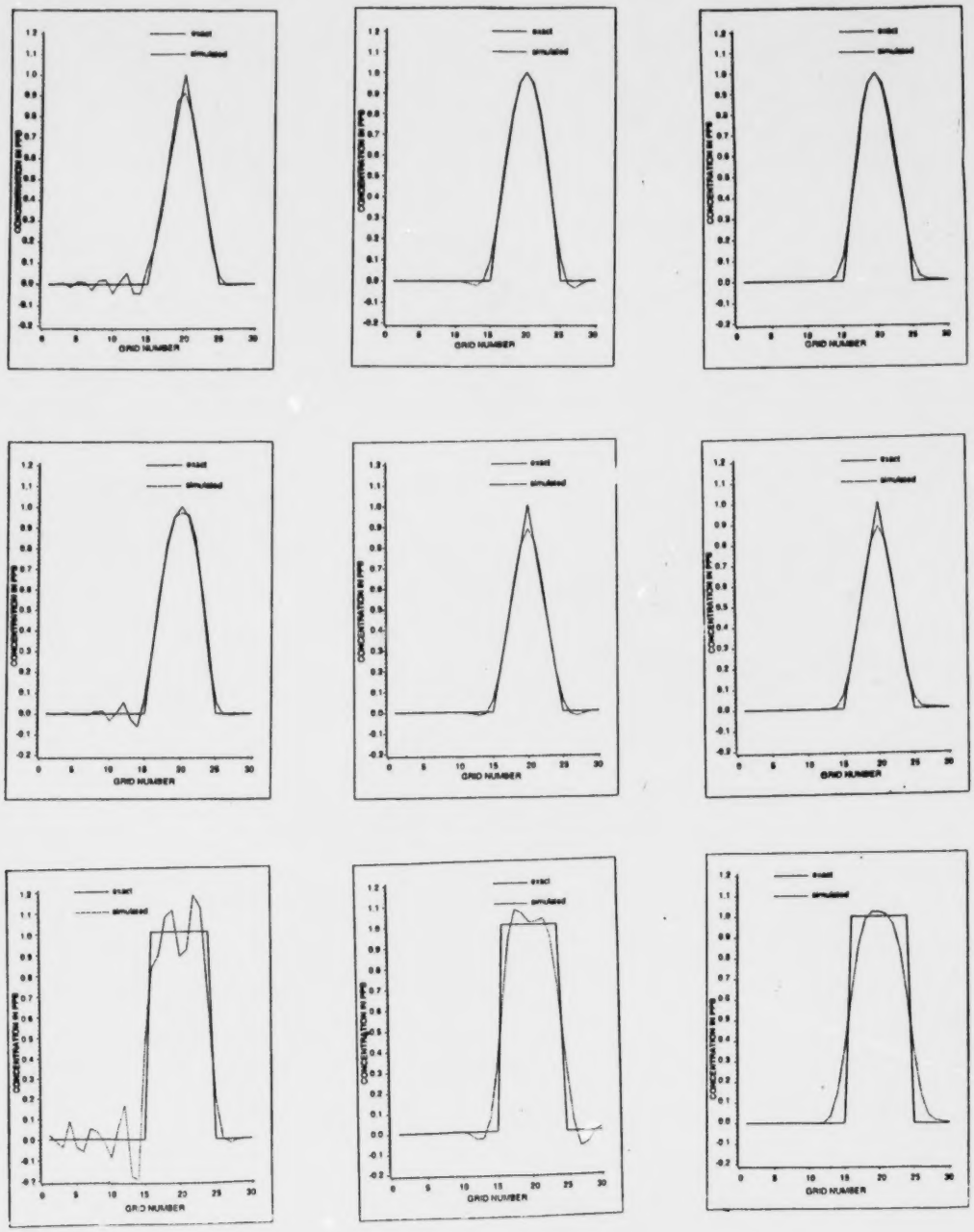

Figure 2. One-dimensional pure advection test of the Crank-Nicolson-Galerkin finite element method with piecewise linear base functions. Initial sine wave, triangle wave, and square wave forms are shown. The results are shown after 24 hours of transport (96 time steps) for cases without upwinding and filter (left), with upwinding and without filter (middle), and with upwinding and filter (right). Reprinted with permission of Atmospheric Environment.

TABLE 1

NUMERICAL ANALOGS OF DOMAIN MOMENT INTEGRALS

	Triangle Wave Test		Sine Wave Test		Square Wave Test	
	$\overline{M}_1$	$\overline{M}_2$	$\overline{M}_1$	$\overline{M}_2$	$\overline{M}_1$	$\overline{M}_2$
Initial Values	5.00	3.40	6.31	5.00	9.00	9.00
Values 24 hours from start						
1) Without upwinding and without filter	5.00	3.40	6.32	5.00	9.01	8.84
2) Without upwinding and with filter	5.00	3.22	6.32	4.70	9.00	6.94
3) With upwinding and without filter	5.00	3.29	6.32	4.88	9.01	8.28
4) With upwinding and with filter	5.05	3.24	6.39	4.77	9.06	7.53

3. STEM-II COMPUTER CODE

The STEM-II computer model is written in Fortran 77 and is structured so that it can easily be run in one, two or three dimensional modes. The domain and grid spacings can be readily changed; physical, chemical and mathematical components can be readily replaced, swapped, upgraded, etc.; and input variables can come from either objective analysis of observed fields or from external model predictions. A flow chart for the model is shown in Figure 3. As shown, the model consists basically of input procedures, transport integrators, chemical integrators, mass balance and deposition flux calculation procedures, and output writers. A listing of the subroutine function is presented in Table 2.

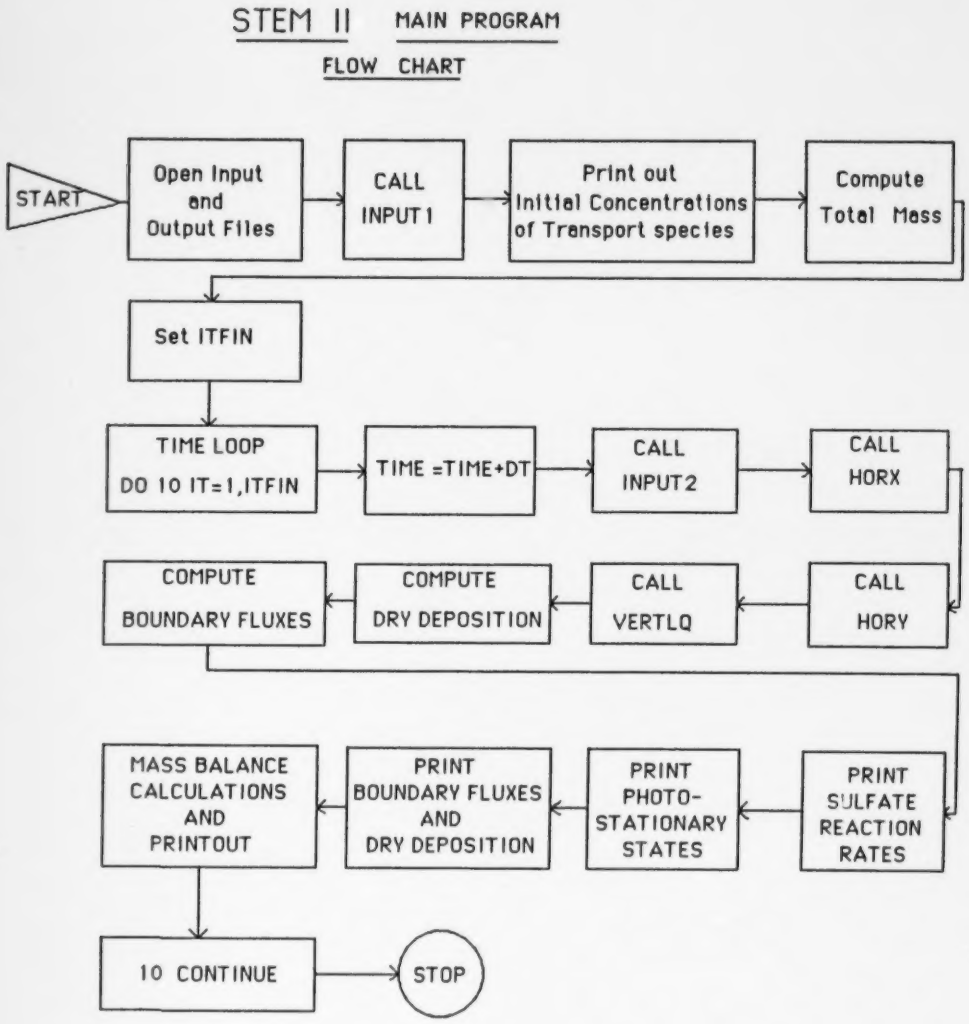

Figure 3. Flow Diagrams for STEM-II Model (Continued)

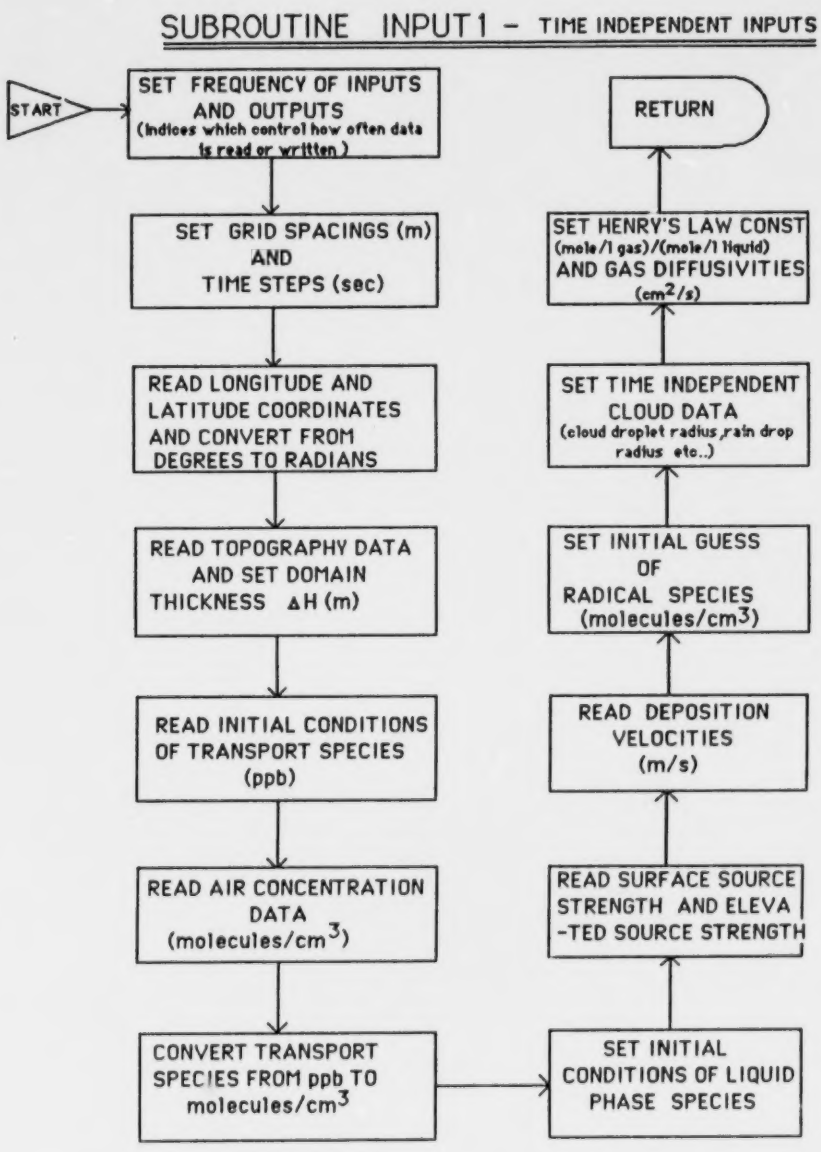
SUBROUTINE INPUT1 - TIME INDEPENDENT INPUTS
START
SET FREQUENCY OF INPUTS AND OUTPUTS
(indices which control how often data is read or written)
SET GRID SPACINGS (m) AND TIME STEPS (sec)
READ LONGITUDE AND LATITUDE COORDINATES AND CONVERT FROM DEGREES TO RADIANS
READ TOPOGRAPHY DATA AND SET DOMAIN THICKNESS ΔH (m)
READ INITIAL CONDITIONS OF TRANSPORT SPECIES (ppb)
READ AIR CONCENTRATION DATA (molecules/cm3)
CONVERT TRANSPORT SPECIES FROM ppb TO molecules/cm3
SET INITIAL CONDITIONS OF LIQUID PHASE SPECIES
READ SURFACE SOURCE STRENGTH AND ELEVA -TED SOURCE STRENGTH
READ DEPOSITION VELOCITIES (m/s)
SET INITIAL GUESS OF RADICAL SPECIES (molecules/cm3)
SET TIME INDEPENDENT CLOUD DATA
(cloud droplet radius, rain drop radius etc..)
SET HENRY'S LAW CONST (mole/l gas)/(mole/l liquid) AND GAS DIFFUSIVITIES (cm2/s)
RETURN

Figure 3. Flow Diagrams for STEM-II Model
(Continued)

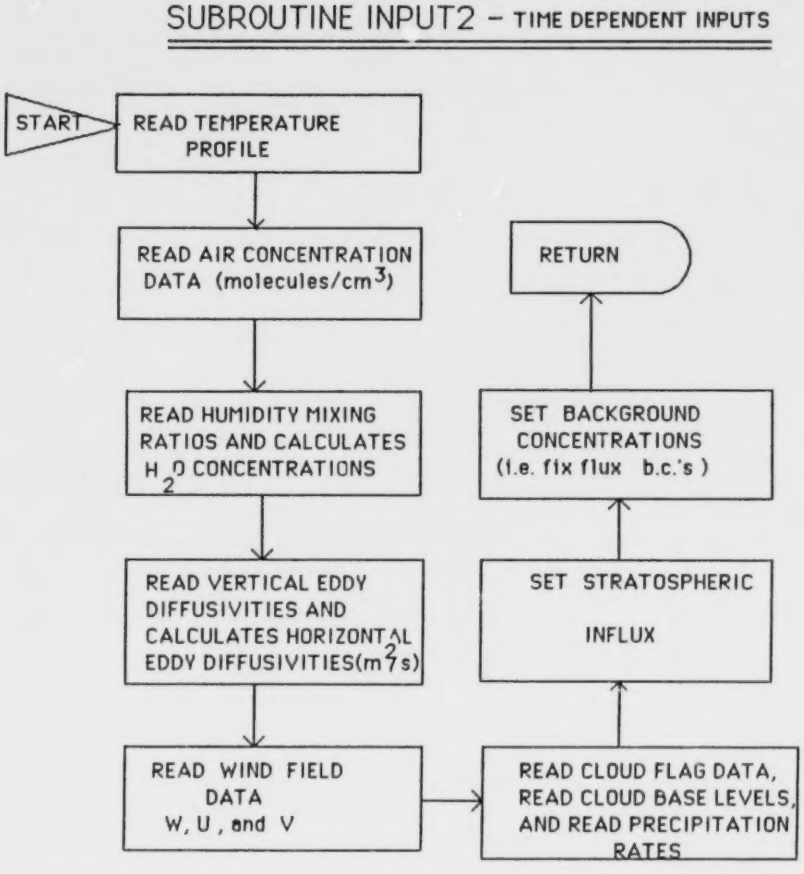
SUBROUTINE INPUT2 – TIME DEPENDENT INPUTS
START
READ TEMPERATURE PROFILE
READ AIR CONCENTRATION DATA (molecules/cm3)
READ HUMIDITY MIXING RATIOS AND CALCULATES H2O CONCENTRATIONS
READ VERTICAL EDDY DIFFUSIVITIES AND CALCULATES HORIZONTAL EDDY DIFFUSIVITIES(m2/s)
READ WIND FIELD DATA W, U, and V
READ CLOUD FLAG DATA, READ CLOUD BASE LEVELS, AND READ PRECIPITATION RATES
SET STRATOSPHERIC INFLUX
SET BACKGROUND CONCENTRATIONS (i.e. fix flux b.c.'s)
RETURN

Figure 3. Flow Diagrams for STEM-II Model
(Continued)

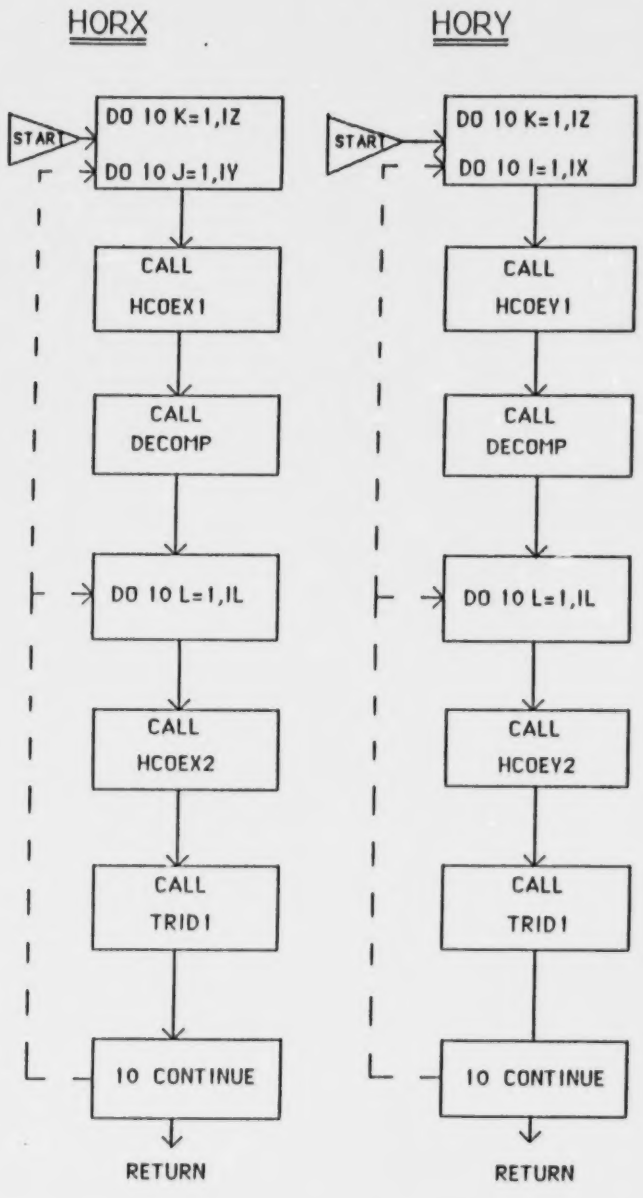

Figure 3. Flow Diagrams for STEM-II Model
(Continued)

SUBROUTINE VERTLQ

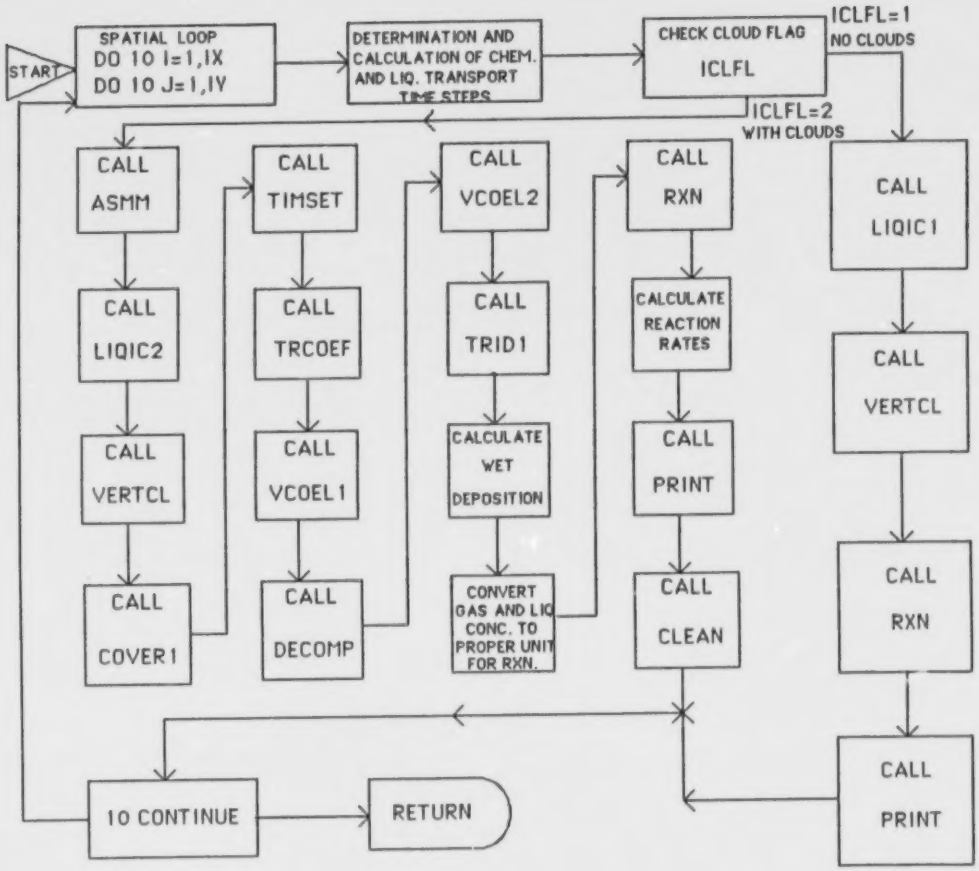

Figure 3. Flow Diagrams for STEM-II Model
(Continued)

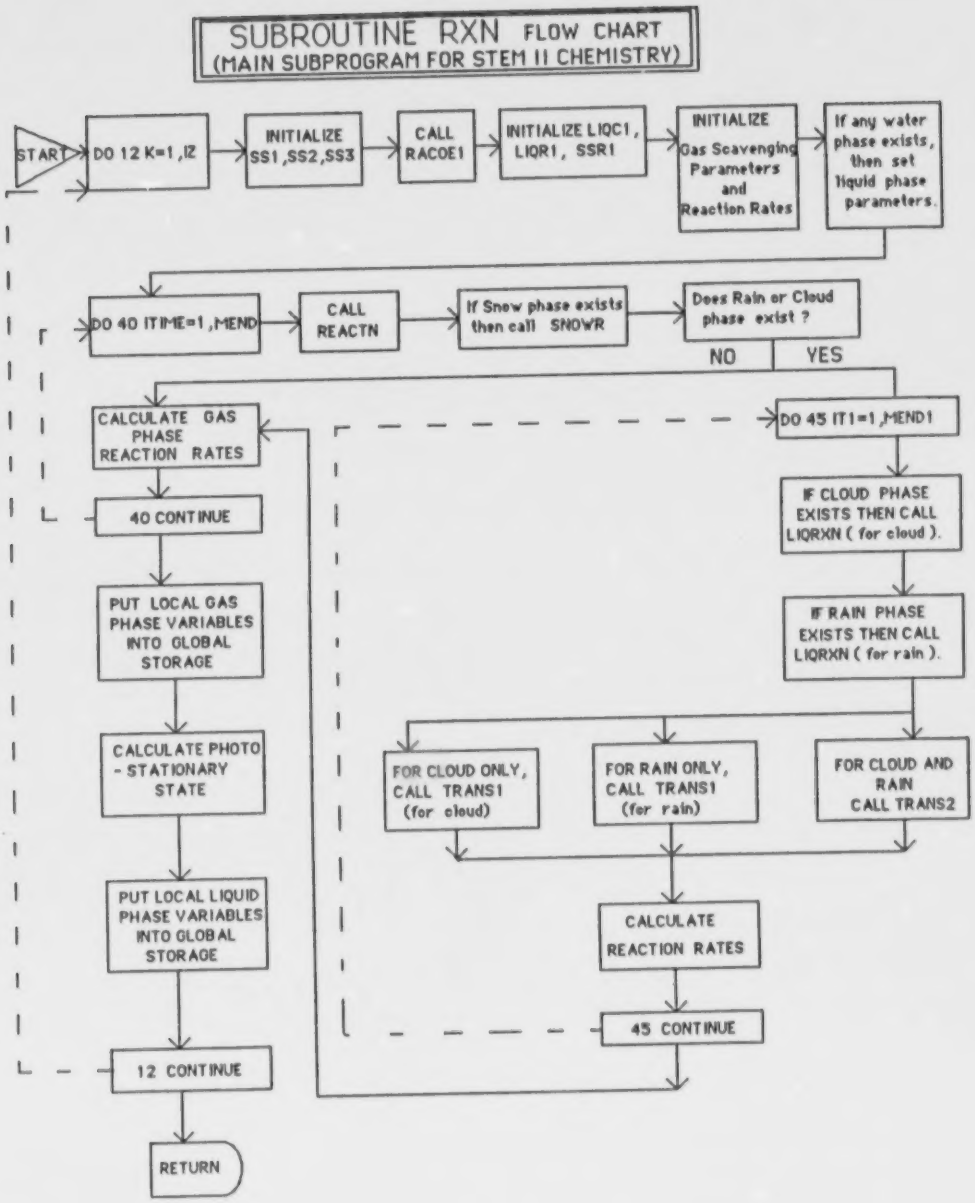
SUBROUTINE RXN FLOW CHART
(MAIN SUBPROGRAM FOR STEM II CHEMISTRY)
START
DO 12 K=1,IZ
INITIALIZE SS1,SS2,SS3
CALL RACOE1
INITIALIZE LIQC1, LIQR1, SSR1
INITIALIZE Gas Scavenging Parameters and Reaction Rates
If any water phase exists, then set liquid phase parameters.
DO 40 ITIME=1,MEND
CALL REACTN
If Snow phase exists then call SNOWR
Does Rain or Cloud phase exist ?
NO
YES
CALCULATE GAS PHASE REACTION RATES
40 CONTINUE
PUT LOCAL GAS PHASE VARIABLES INTO GLOBAL STORAGE
CALCULATE PHOTO - STATIONARY STATE
PUT LOCAL LIQUID PHASE VARIABLES INTO GLOBAL STORAGE
12 CONTINUE
RETURN
DO 45 IT1=1,MEND1
IF CLOUD PHASE EXISTS THEN CALL LIQRXN (for cloud).
IF RAIN PHASE EXISTS THEN CALL LIQRXN (for rain).
FOR CLOUD ONLY, CALL TRANS1 (for cloud)
FOR RAIN ONLY, CALL TRANS1 (for rain)
FOR CLOUD AND RAIN CALL TRANS2
CALCULATE REACTION RATES
45 CONTINUE

Figure 3. Flow Diagrams for STEM-II Model
(Continued)

Table 2. Subroutine List

INPUT1	- sets and reads input which is independent of time.
INPUT2	- sets and reads time dependent input.
HORX	- calculates horizontal transport in the X-direction.
HORY	- calculates horizontal transport in the Y-direction.
VERTLQ	- calculates gas or gas and liquid vertical transport and gas or gas and liquid chemical reactions.
VCOEF1	- calculates coefficient matrix for gaseous vertical transport.
VCOEF2	- calculates right-hand side vector for gaseous vertical transport.
HCOEX1	- calculates coefficient matrix for transport in the X-direction.
HCOEX2	- calculates right-hand side vector for transport in the X-direction
HCOEY1	- calculates coefficient matrix for transport in the Y-direction.
HCOEY2	- calculates right-hand side vector for transport in the Y-direction.
TRID	- computes solution of tri-diagonal matrix.
ASMM	- interfaces STEM II with ADVANCED SCAVENGING MODULE.
LIQIC1	- initializes cloud droplets columnwise and also initializes cloud radiation factor.

Table 2 (continued)

LIQIC2	- initializes liquid concentration at each time step.
VERTCL	- main subroutine for vertical transport calculation (only does transport calculations).
RXN	- main subroutine for complete chemistry.
COVER1	- calculates cloud effect of sunlight.
TIMSET	- determines time stepof transport calculation of liquid phase such that COURANT NUMBER ≤0.9 to 1.0
TRCOEF	- computes Eddy diffusivity and updraft of liquid phase(depending upon phase identity-computes Kv and precipitation velocity).
VCOEL1	- computes coefficient matrix for vertical calculation of liquid phase.
VCOEL2	- computes right-hand side vector for vertical calculation of liquid phase.
DECOMP	- performs LU decomposition of tridiagonal matrix.
TRID1	- solves for LU decomposed tridiagonal matrix.
PRINT	- prints radicals and liquid phase related values.
CLEAN	- adds gaseous and liquid species contents in preparation for new transport calculations.

Table 3. Chemistry Subroutine List

CHEMISTRY SUBROUTINES

AQUPHA	- determines mass transfer coefficient.
COVER1	- calculates cloud cover effect of sunlight.
EQUIFN	- calculates parameters which connect gas and liquid phases.
INTCON	- calculates interactions among cloud, rain, and snow.
INTSOL	- gives solution for intermediate life species.
LIQRXN	- calculates liquid reactions.
MATSOL	- calculates the inverse of a 2x2 matrix.
PRINT	- print radicals and liquid phase related values.
RACOEF	- sets some G-3 species and rate coefficients.
RACOE1	- gives rate constants independent of time within Dt min.
RADATN	- calculates modifications of rate coefficients by cloud effects
RADSOL	- iteration solver for radicals, $NO_x \geq 2 \times 10^{-4}$ ppm
RAD1,RAD2	- iteration solvers for radicals, $NO_x < 2 \times 10^{-4}$ ppm
REACTN	- calculates results of chemistry for one time step

Table 3. (continued)

RXN	- main subroutine for STEM II chemistry.
SION	- ion iteration solver.
SNOWR	- solves differential equation for concentration of snow phase
TRANS1	- solves two-phase mass transfer into droplets (rain only or cloud only)
TRANS2	- solves three-phase mass transfer into droplets(rain and cloud)
TYR	- employs Taylor series to eliminate numerical errors of exponential function

Table 4. Variable List

LIST OF VARIABLES FOR STEM II

CF	coefficient KF in filter equation=0.2
CL1	coefficients derived from Galerkin formulation
CL2	"
CL3	"
CL4	"
CLOUDB	cloud base height (meters)
CO	cell Courant number
COMAX	maximum cell Courant number
CONCZ	amount advected at top of the boundary in gas phase for SO2,sulfate and HNO3 (molec)
CONCZL	amount of wet deposited at surface for SO2, sulfate and HNO3(molec.)
DH(I,J)	height of upper boundary from ground level (m)
DT	time step for transport equations (sec)
DTC	time step for chemical processes in gas phase (sec)
DTC1	time step for chemical processes in liquid phase (sec)
DVG	summation of amount deposited for SO2, sulfate and HNO3 (molec.)
DZ(K)	dimensionless distance between grid levels k and k+1 (m)
ELON	longitude at east end of calculation region (radians)
EM	elevated emission strength (molec/cu. cm/sec)
EM1	summation of elevated emission with time for SO2, sulfate and HNO3 (molec)
FZ	0.01 times flux at upper boundary (molec/sq. cm/s)
H(I,J)	topography relative to sea level (m)
HDZ(K)	dimensionless height of grid point
HENRY	Henry's Law Constant (mole/l-gas/mole/l-liq)
HH(I,J)	height of upper boundary relative to sea level (m)
ICLFL(I,J)	cloud or rain flag ICLFL(I,J)=1 no liquid phase ICLFL(I,j)=0 liquid phase
IHOUR	local time (hours)
IMIN	local time (minutes)
IDEP	frequency of input of dry deposition velocity

Table 4 (continued)

IEM	frequency of input of elevated emission
IL	number of advected species
IPRNT	frequency of printing
IT	calculation time step (sec)
ITER	number of applications of filter (usually=2)
ITSTAT	TSTAT/(3600*24) = number of days from start of simulation (cf. TSTAT)
IXT,IX	number of grid points in x-direction
IYT,IY	number of grid points in y-direction
IZT,IZ	number of grid points in z-direction
KH	horizontal eddy diffusivity (sq.m/sec)
KR	gas phase reaction rate constants(molec/cu.cm/sec)
KV	vertical eddy diffusivity (sq.m/s)
LIQC	water content of cloud (g/cu.m)
LIQR	water content of rain (g/cu.m)
LIQS	water content of snow (g/cu.m)
LIQC1	liquid concentration of species in cloud phase (mol/(liter ofcloud phase volume))
LIQR1	liquid concentration of species in rain phase (mol/(liter of rain phase volume))
NOLAT	latitude at north end of calculation region (radians)
Q	surface emission rate. Read in molec/sq.cm and converted to molec/(sq.cm*100)
Q1	accumulated surface emissions (molec)
RSO4(I,J,K,1)	amount of sulfate produced in gas phase in one transport time step (molec)
RSO4(I,J,K,2)	amount of nitric acid produced in gas phase in one transport time step (molec)
RSO4T(I,J,K,L)	summation of RSO4 with time (molec)
RSO4L(I,J,K,1)	amount of sulfate produce in liquid phase in one trasport time step (molec)
RSO4L(I,J,K,2)	amount of nitric acid produced in liquid phase in one transport time step (molec)
RSO4TL(I,J,K,L)	summation of RSO4L with time (molec)
S1(I,J,K,L)	concentrations of transport species (molec/cu.cm)
S4(I,J,K,1)	concentration of air (molec/cu.cm)
S4(I,J,K,2)	concentration of water (molec/cu.cm)
S4(I,J,K,3)	concentration of carbon monoxide (molec/cu.cm)
SI(30)	array of input data for filter subroutine

Table 4. (continued)

SL1(I,J,K,L,IPH)	concentration of liquid phase L=35; CL2 L=36; OH L=37; HO2 IPH=1; cloud phase mole/(liter of cloud phase volume) IPH=2; rain phase mole/(literof rain phase volume) IPH=3; snow phase mole/(liter of total space volume)
SO(30)	array for output from filter subroutine
SOLAT	latitude at south end of calculation region (radians)
SPRC(I,J)	surface precipitation (g-mol/sq.m-s)
SS1,SS2	temporary storage for concentrations of advected species (molec/cu.cm)
SS3(L)	temporary storage for concentrations of free radicals and other short lived species (molec/cu.cm)
SSL1(L)	temporary storage for concentration of liquid phase
STEMPO(30)	array of temporary storage of concentrations
TIME	Greenwich mean time
TIMELO	local time measured from midnight of the day simulation starts and calculated at the longitude corresponding to the west boundary of the region
TSTAT	constant to be specified, indicating time (in sec) of the start of the simulation measured from noon of the vernal equinox at Greenwich, UK: e.g. TSTAT=0 indicates that the simulation starts from the Greenwich noon of March 21
U	horizontal wind speed in x-direction (m/s)
V	horizontal wind speed in y-direction (m/s)
VG	deposition velocity (m/s)
W	vertical wind speed in z-direction (m/s)
WLON	longitude at west end of calculation region (radians)
WI	local Peclet number

Table 5. Chemical Species List

VARIABLE NAMES OF ALL CHEMICAL SPECIES

LONG LIVED SPECIES (ppm)

SS1(1) NO	SS1(9) Alkane	SS1(16) Xylene
SS1(2) NO2	SS1(10) Propene	SS1(17) MEK
SS1(3) HNO3	SS1(11) Butene	SS1(18) CH3COCH3
SS1(4) NH3	SS1(12) Ethene	SS1(19) PAN
SS1(5) SO2	SS1(13) Benzene	SS1(20) PPN
SS1(6) Sulfate	SS1(14) Cresol	SS1(21) EL-NO2
SS1(7) O3	SS1(15) Toluene	SS1(22) PBZN
SS1(8) Propane		

INTERMEDIATE SPECIES

SS2(1) H2O2	SS2(5) RCHO	SS2(8) DIAL
SS2(2) HONO	SS2(6) ARCHO	SS2(9) CHOCHO
SS2(3) HCHO	SS2(7) CH3COCHO	SS2(10) HCl

RADICAL SPECIES

SS3(1) N2O5	SS3(8) CH2O2	SS3(15) CH3CO3
SS3(2) HO2NO2	SS3(9) PO2	SS3(16) RCO3
SS3(3) NO3	SS3(10) AO2	SS3(17) ARCO3
SS3(4) OH	SS3(11) ARO2	SS3(18) EL
SS3(5) HO2	SS3(12) XO2	SS3(19) CH3CHOO
SS3(6) CH3O2	SS3(13) PhO2	SS3(20) ADD
SS3(7) C2H5O2	SS3(14) Phenoxy	SS3(21) ADD2

4. APPLICATION OF STEM-II TO MAY 2ND AND 3RD FIELD DATA

The STEM-II model described in Sections 2 and 3 is being used to analyze field data collected in the U.S. EPA Mesoscale Acid Deposition Study. The model was implemented on the VPS 32 machine at the NASA Langley Research Center. The current application work is focusing on the May 2nd and 3, 1985 study conducted in the Philadelphia area.

The modeling domain used for this analysis is shown in Figure 4. Two different grid systems are being used: a coarse grid with horizontal grid spacings of ~ 56 km; and a fine grid with horizontal spacings of 20 km (see Figure 5). The vertical domain is the same in each system with 14 vertical grids non-uniformly spaced between the surface and a height of 6 km. The 14 vertical grid points are located at 0, 0.2, 0.4, 0.8, 1.2, 1.6, 2.0, 2.4, 2.8, 3.2, 3.6, 4.0, 5.0, and 6.0 km. The wind, temperature, and surface precipitation fields predicted by the dynamic meteorological model MASS (Mesoscale Atmospheric Simulation System) (cf, Kaplan et al., 1982) were used as inputs to the STEM-II model. MASS has been evaluated independently by Koch (1985) and Koch et al. (1985). The predicted precipitation fields were used as inputs to the ASM cloud model to generate the microphysical parameters for the wet removal calculations.

The emission fields for the simulations were based on Version 5.2 of the U.S. EPA NAPAP (National Acid Precipitation Assessment Program) which includes SO_x, NO_x and speciated hydrocarbons. The point and area sources gridded to 20 km are shown in Figures 6 - 10. Elevated point sources were assigned to vertical grids by distributing the point emissions in molecules/s over the control volume centered around the grid point. For example, level 2 point emissions are given by dividing the point emissions by a control volume of ($2 \times 10^4 * 2 \times 10^4 * 200$) m^3. Presented are point source and area emissions for NO, SO_2, NH_3, sulfate and toulene. The spatial distributions of the NO, SO_2, sulfate and toulene emissions are similar with the major point sources in the northeast section (around New York) of the model domain and around Philadelphia. The area sources show a similar pattern but with appreciable values at each grid point. The NO area emissions are very large exceeding 1.1

Figure 4. Philadelphia mesoscale acid deposition study domain. The shaded regions denote the areas where the monitoring stations were deployed. The large slanted square represents the modeling region.

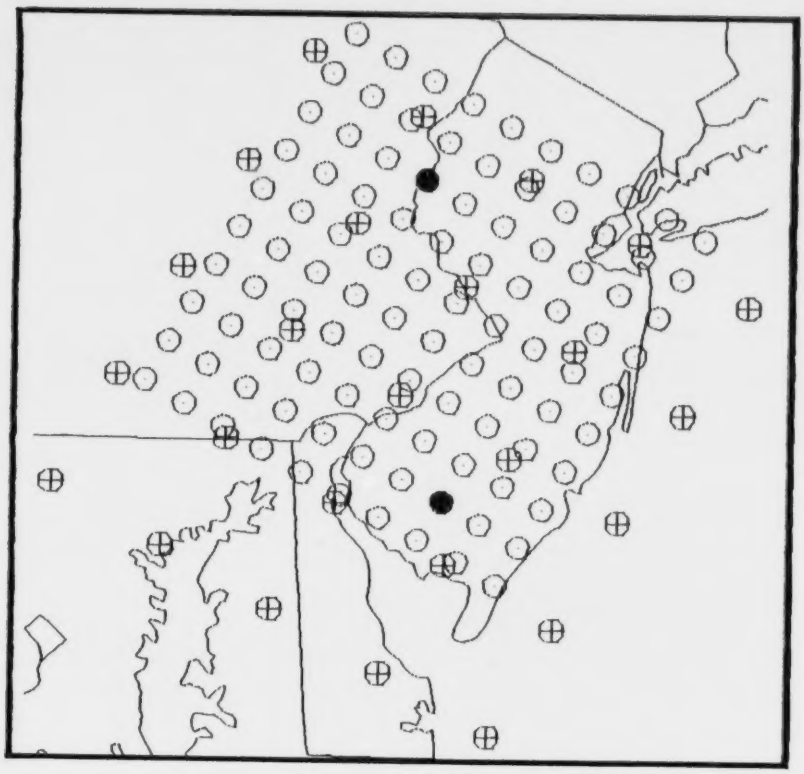

Figure 5 Model region for MesoSTEM application. Course grid and fine mesh grid systems are shown. Solid dots show grid points (8,2) and (4,8) in the New Jersey and Pennsylvania regions, respectively.

NO EMISSIONS

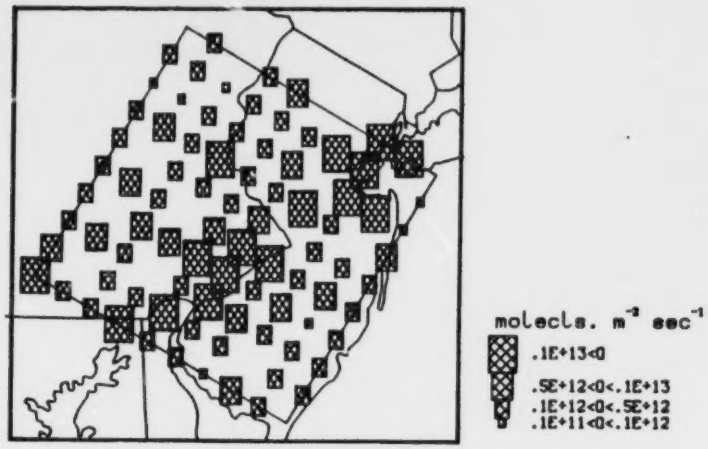

NO EMISSIONS(P)

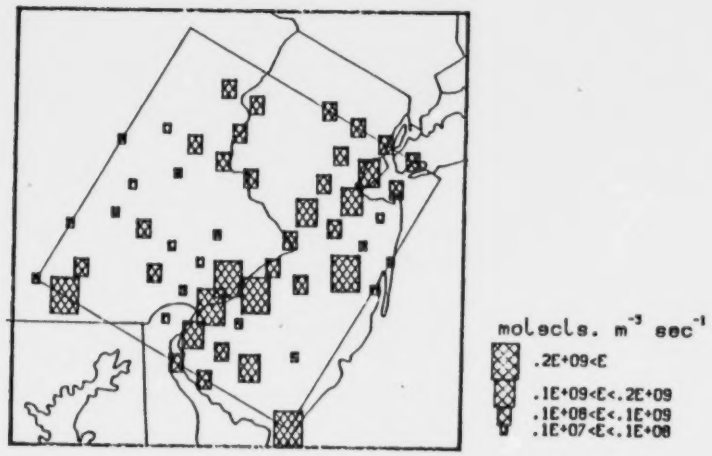

Figure 6. Elevated point sources (at level 2 corresponding to a height 200 m) and area emissions for NO

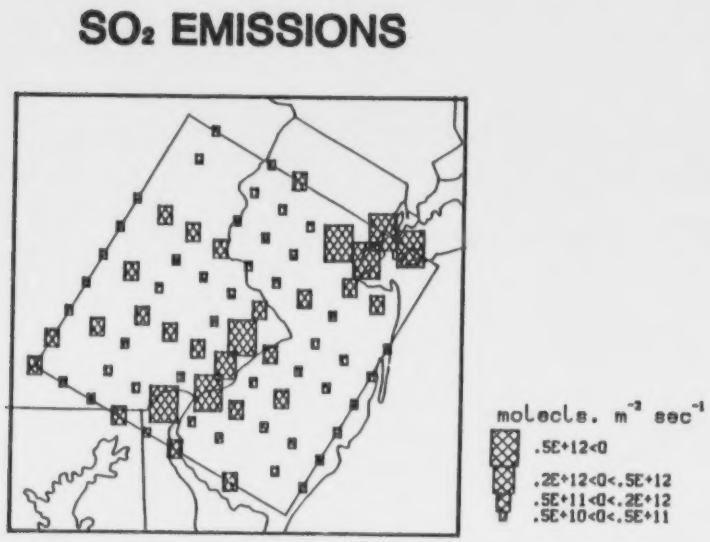

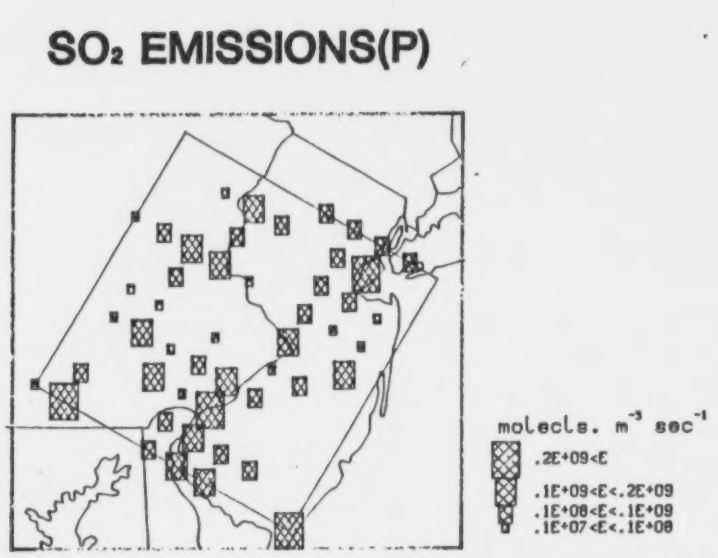

Figure 7. Elevated point sources (at level 2 corresponding to a height 200 m) and area emissions for SO_2

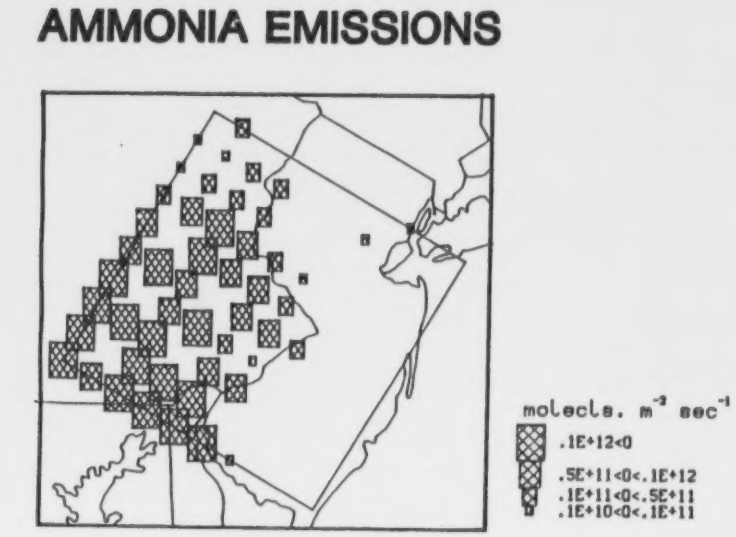

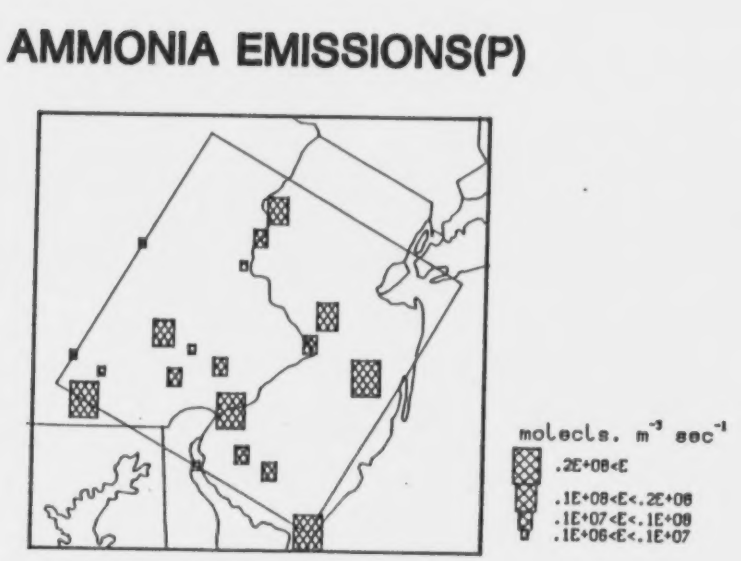

Figure 8. Elevated Point sources (at level 2 corresponding to a height 200 m) and area emissions for ammonia

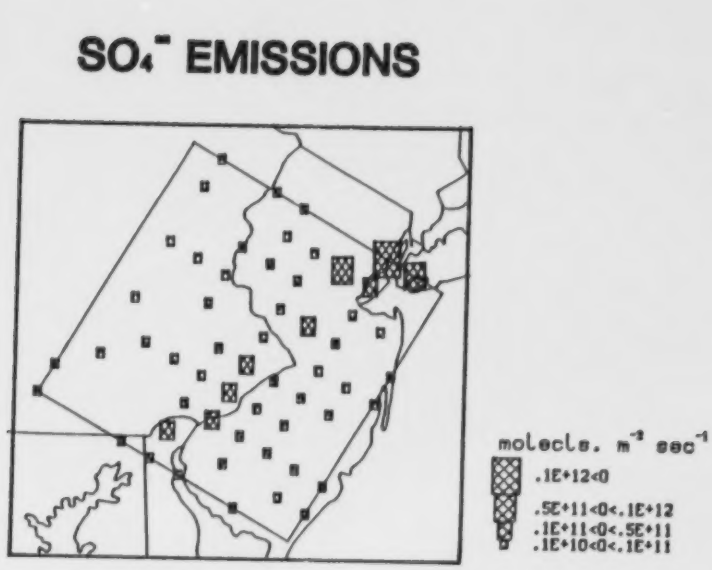

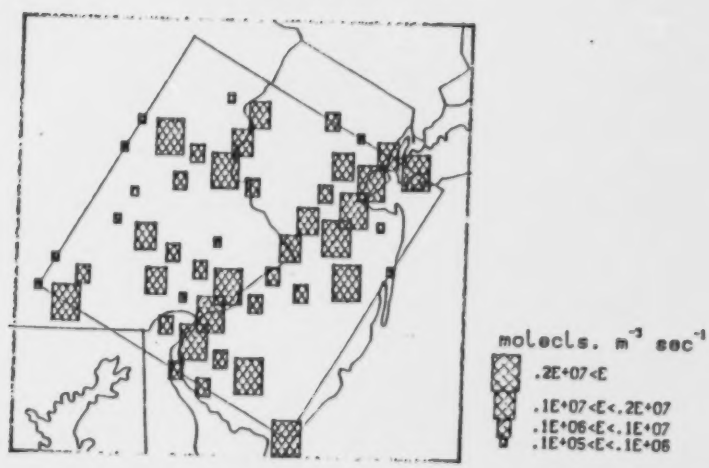

Figure 9. Elevated point sources (at level 2 corresponding to a height 200 m) and area emissions for $SO_4^=$

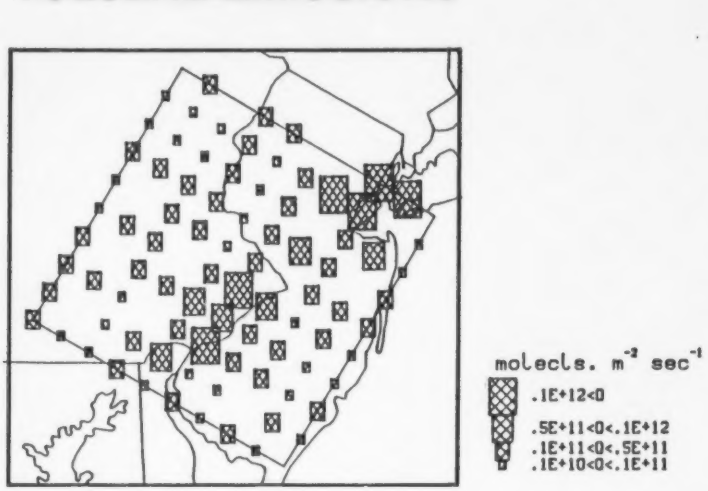

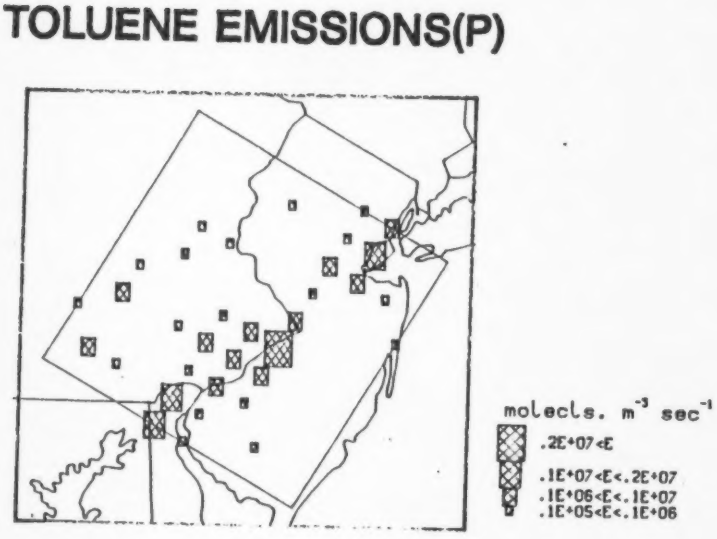

Figure 10. Elevated point sources (at level 2 corresponding to a height 200 m) and area emissions for toluene

x 10^{13} molecules/m^2-s at several locations. The area emissions of ammonia are quite different from the other species. As shown, there are very low ammonia emission in New Jersey and relatively large emissions on the Pennsylvania side of the model region.

The May 2nd event was an example of a slow moving frontal system which produced very heavy precipitation in the study area. The flow field in the modeling region at 14:00 LT (local time) was generally from the east and gradually shifted to the northeast after 22:00 LT. The level one wind speeds were high throughout the period with horizontal winds of 15 m/s. The precipitation came from the south and reached Philadelphia at 15:50 LT. Predicted flow and precipitation fields using the MASS model are shown in Figures 11 and 12. Output from the MASS model was used to provide the meteorological inputs for the STEM-II model.

The measured wet deposition loadings of nitrate and sulfate are shown in Figure 13. The general features show that for both species the loadings were higher on the Pennsylvania side. Furthermore, the nitrate loadings were slightly higher than those for sulfate on the New Jersey side.

COARSE GRID SIMULATIONS

Coarse grid model predictions have been obtained for an 18 hr period corresponding to 14:00 May 2nd to 8:00 May 3rd, 1985. The model was initialized by starting with rural conditions and then seasoning under no-flow conditions with real emissions for a period of 2-3 days. Initialization of the model is difficult because of the small domain size and large horizontal velocities. The model was initialized under no flow conditions so that the initial conditions would reflect the source characteristics of the model domain. Since no measurements were available to set the inflow boundary conditions, the chemical composition of the air masses transported into the model region (through the eastern and northern boundaries) was estimated by performing 1-dimensional model calculations reflecting the air mass histories. For example, the air entering through the eastern boundary has relatively low concentrations reflecting that it originated from the south and traveled along a wet trajectory, whereas the air mass entering the northern

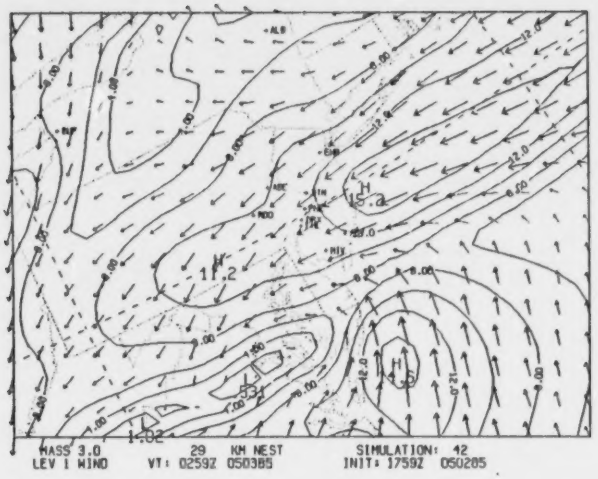

a)

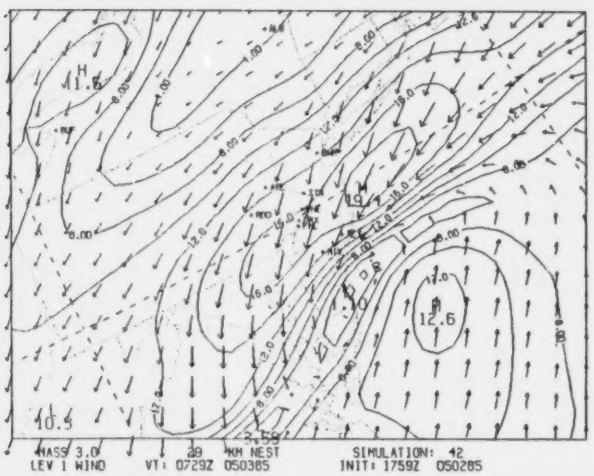

b)

Figure 11. Level one wind fields generated by MASS at a) 11 p.m. and b) 3:30 a.m. (m/s)

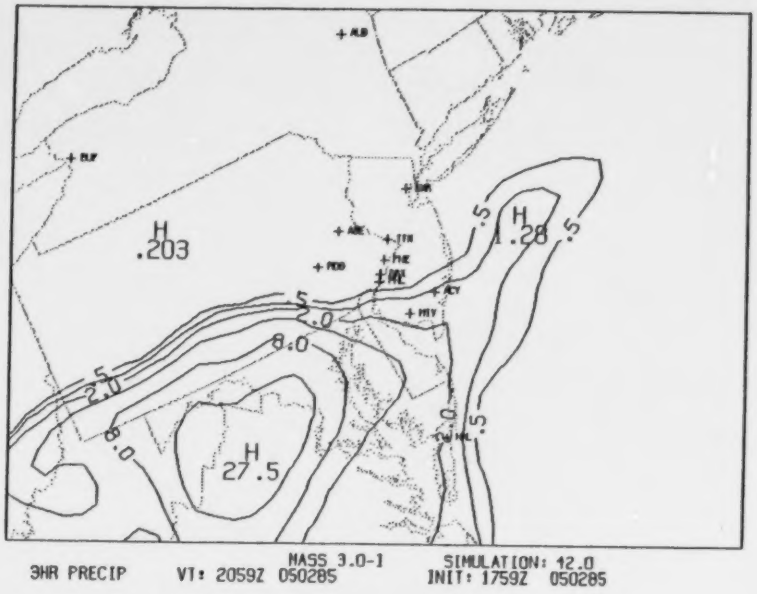

a)

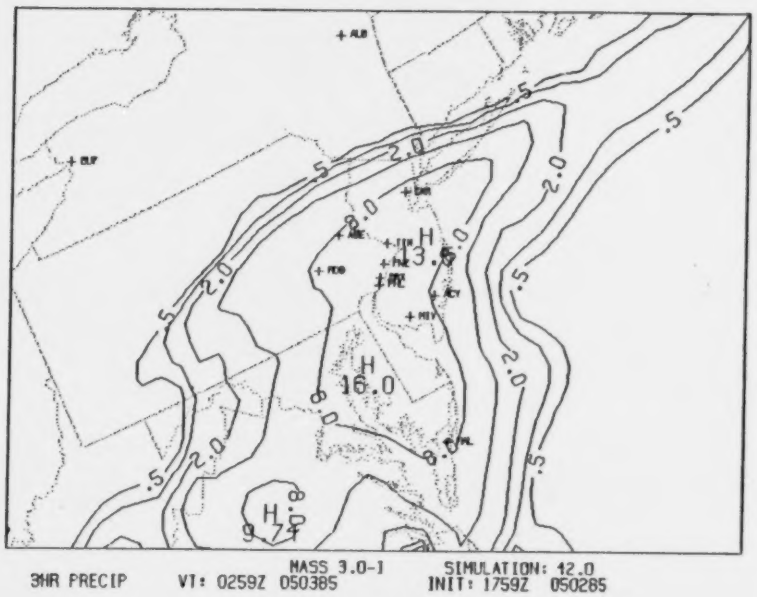

b)

Figure 12. 3 hour precipitation predicted by MASS at (a) 5 p.m. and (b) 11 p.m. (mm)

Figure 13. Measured total deposition of (a) H^+, (b) HNO_3, and (c) $SO_4^=$. The underlined values are for manually deployed bottle-funnel collectors and the others are for automatic wetfall collectors.

boundary has high concentrations of pollutants reflecting the high source regions upwind in New York. The results of the coarse grid simulation are discussed in a paper presented at the 16th International Technical Meeting on Air Pollution Modeling and Its Applications. A copy of the paper is included in Appendix A.

FINE GRID SIMULATION

Results using a fine grid of 20 km horizontal mesh spacing for the May 2nd and 3rd, 1985 case have also been obtained. The fine grid domain is shown in Figure 5 and covers a region 180 km x 180 km x 6 km with 1400 grid points (i.e., 10x10x14). The emissions inventory was discussed earlier and plotted for selected species in Figures 6 to 10. The initial conditions of selected species (corresponding to 2 p.m. local time) for the fine grid simulation are shown in Figures 14 to 17. The initial conditions of the primary pollutants (e.g., NO, NO_2, and SO_2) show large concentrations around New York City and Philadelphia areas. The initial conditions of ammonia reflect the large area sources on the Pennsylvania side of the model domain. Ground level NH_3 concentrations exceed 5 ppb in much of this region. The initial concentrations of the secondary pollutants (e.g., HNO_3, H_2O_2, O_3, and sulfate) show quite different behavior than the primary species. For example, the H_2O_2 surface concentrations are rather uniform from 3 - 6 ppb. The spatial distribution of the nitrate and sulfate initial conditions reflect the structure in the emissions of NO_x and SO_2, respectively. The surface O_3 initial concentrations are low reflecting the high NO_x emissions over the entire modeling region. The boundary conditions for the fine grid domain were derived from the predictions of the coarse grid simulations.

The surface concentrations of sulfate and H_2O_2 at various times are shown in Figures 18 and 19. The rain enters the domain around 14:00 on May 2nd and is completed by 6:00 on May 3rd. The sulfate and H_2O_2 surface concentrations reflect the rain patterns, with low values during the rain and the build up of concentration after the rain ends.

Results for the total wet deposition of selected species are presented in

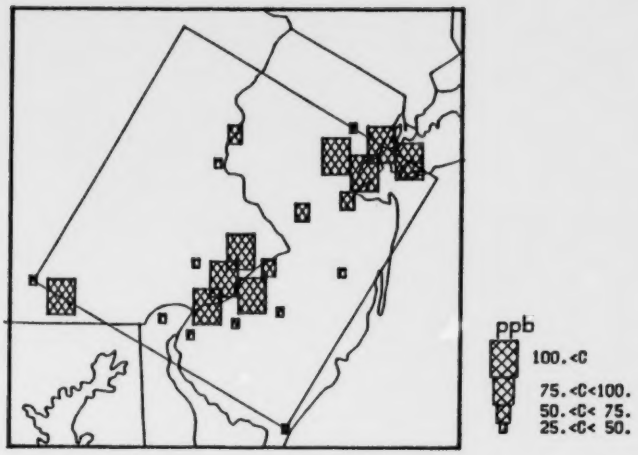

a)

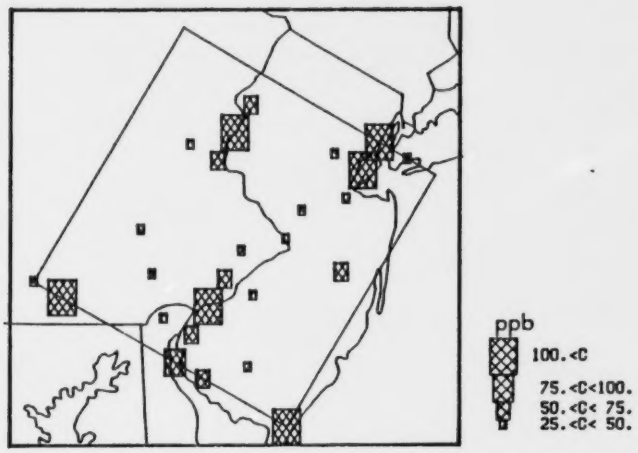

b)

Figure 14. Initial conditions for a) NO and b) SO_2

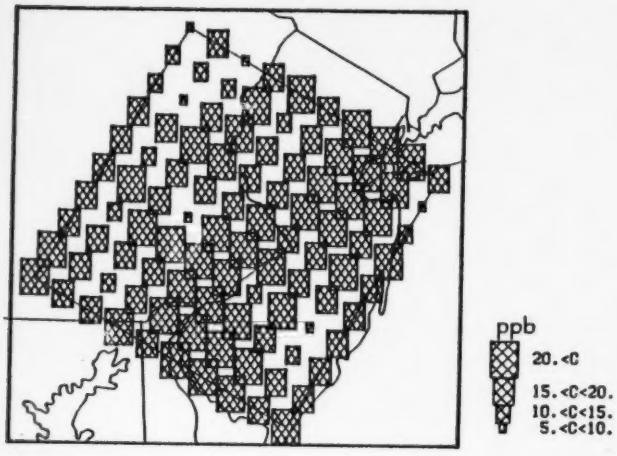

a)

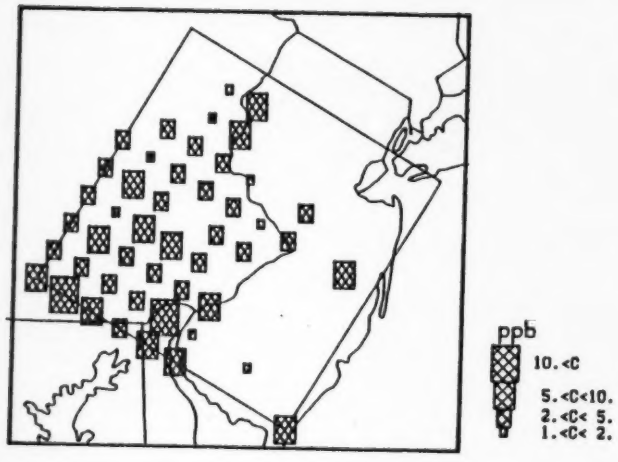

b)

Figure 15. Initial conditions for a) HNO_3 and b) ammonia

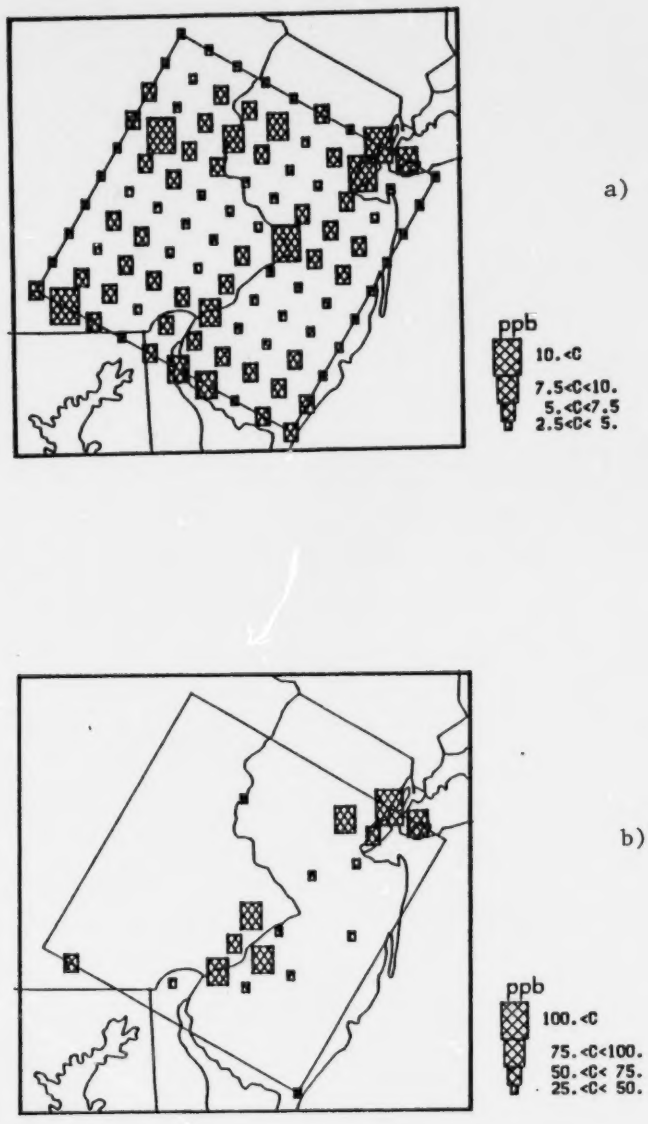

Figure 16. Initial conditions for a) $SO_4^=$ and b) NO_2

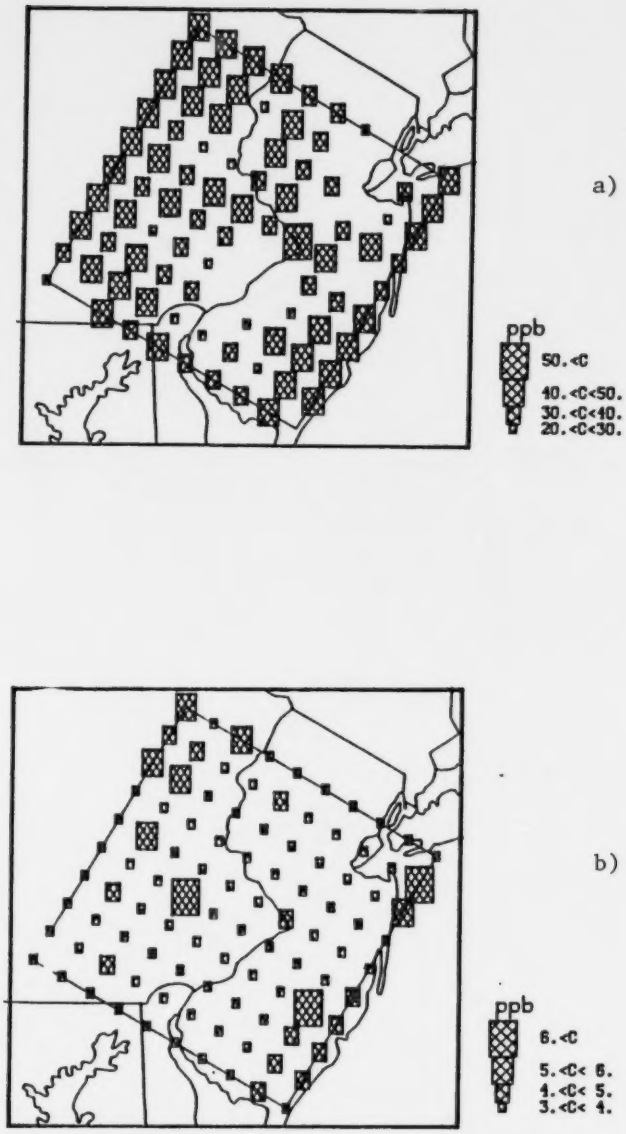

Figure 17. Initial conditions for a) O_3 and b) H_2O_2

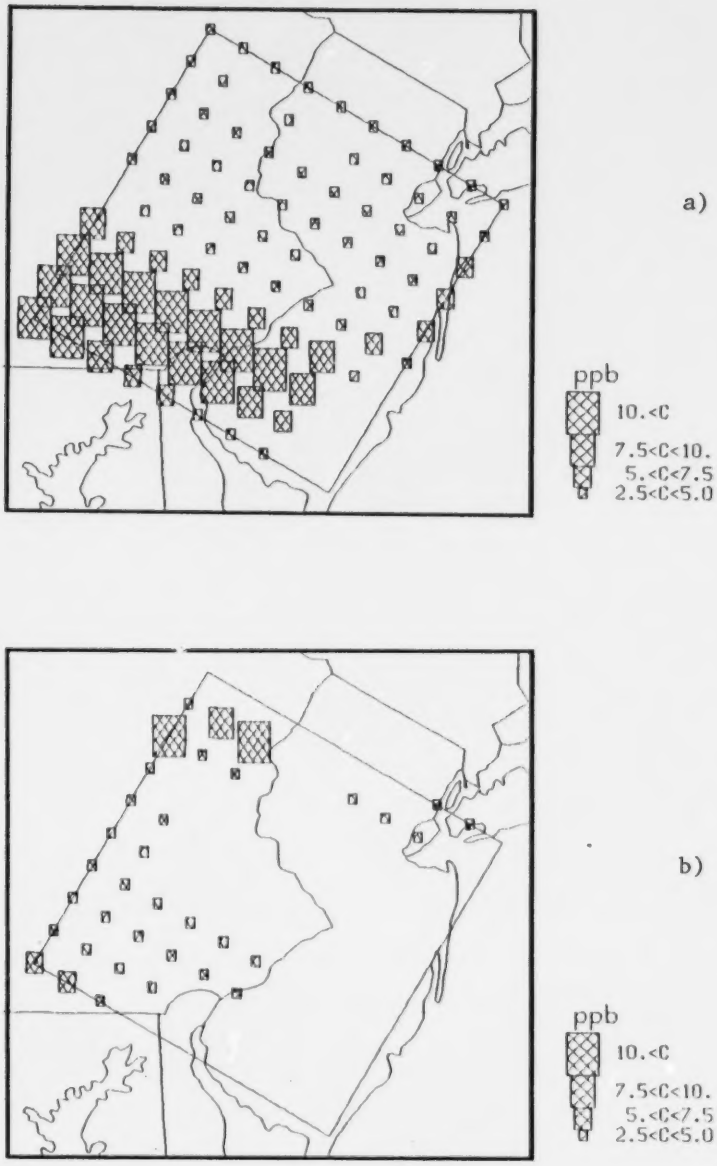

Figure 18. Ground-level aerosol $SO_4^=$ concentration at a) 2 p.m., b) 4 p.m., c) 2 a.m., and d) 8 a.m.

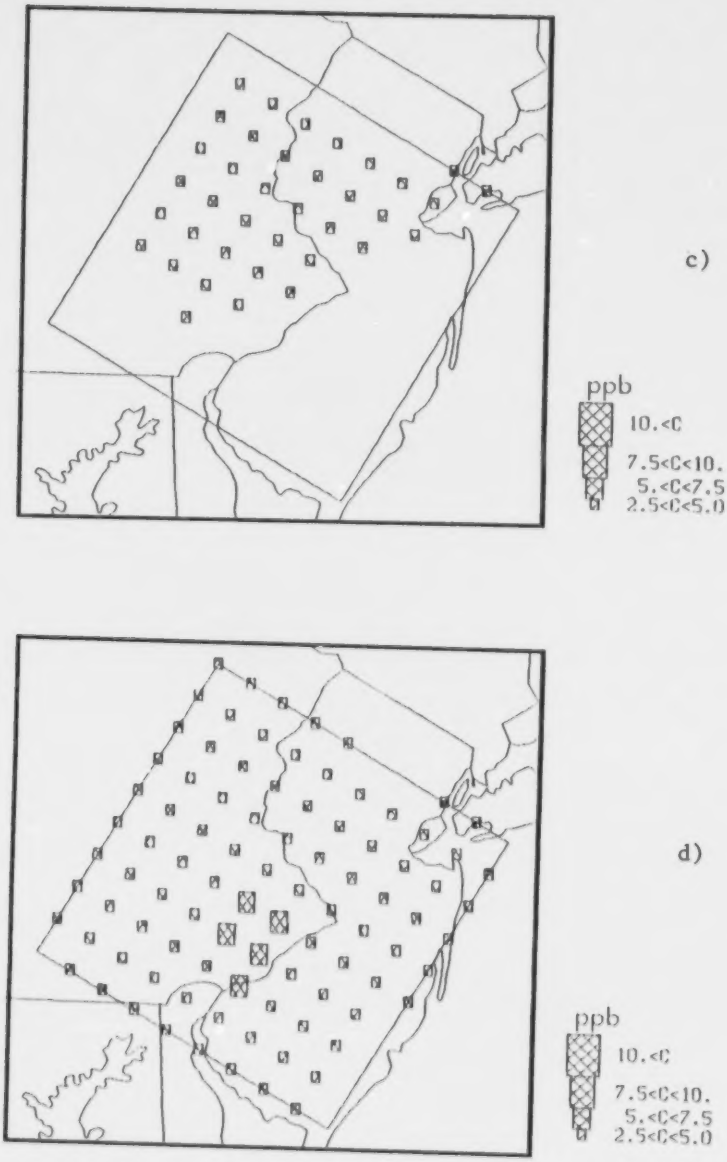

Figure 18. (continued)

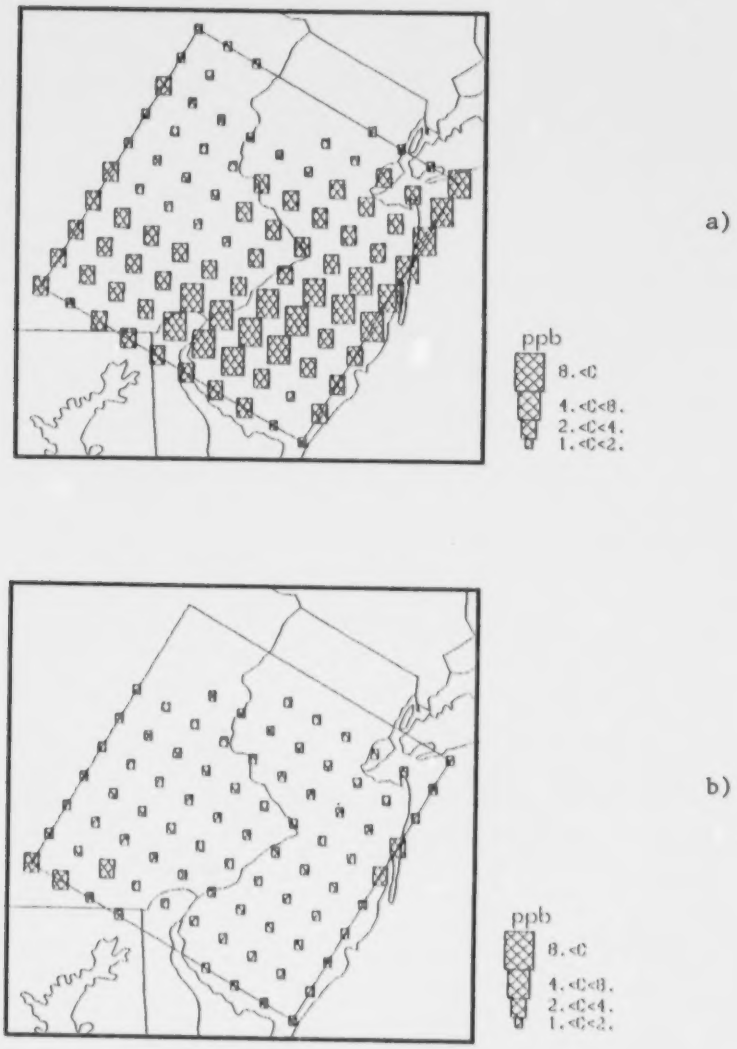

Figure 19. Ground-level gas phase H_2O_2 concentration at a) 2 p.m., b) 4 p.m., c) 2 a.m., and d) 8 a.m.

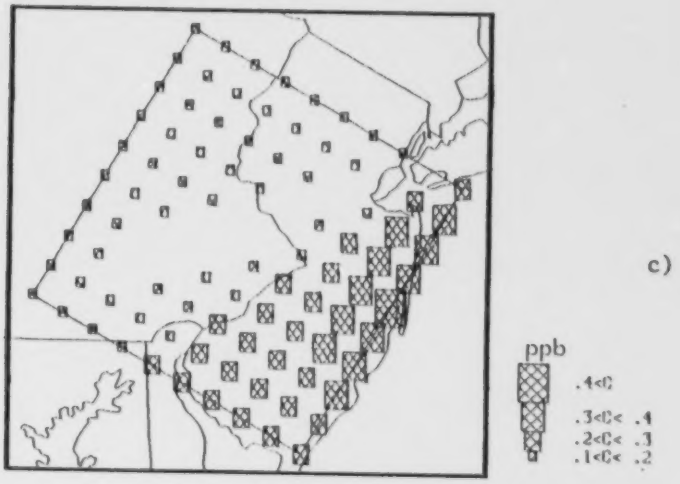

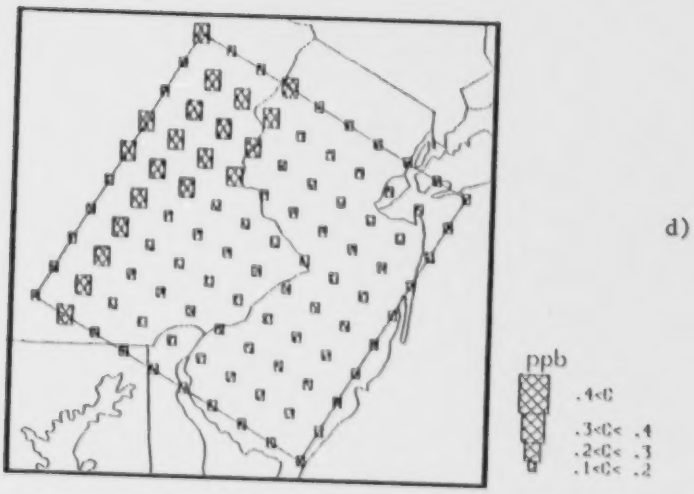

Figure 19. Continued

Figures 20 and 21. The most structure is seen in the nitrate deposition plot. There is high nitrate deposition in the northwest and southwest corners of the domain, reflecting the emissions distribution and the general flow patterns. The sulfate deposition plot shows a much more uniform distribution from east to west. The uniformity in the wet deposition is reflected by the situation that the gas phase concentrations of nitric acid and sulfate in the high source regions are only 20-30% higher than those in the rural areas in spite of the fact that the concentrations of the primary pollutants are 5-10 times higher.

Further details of the deposition at the New Jersey measurement sites and the Pennsylvania sites can be seen by examining the deposition as a function of time at grid points (8,2) and (4,8) (see Figure 5). The time profiles of surface gas phase and rain phase concentrations of selected species are presented for comparison in Figure 22. The New Jersey site is an area of low NO_x and SO_x sources and for the meteorological conditions on May 2nd the wind direction is from the east; thus, relatively clean air is passing to this site through the eastern boundary. Precipitation occurs at this grid point for the first 16 hours of the event. The rain phase concentrations at this grid point show that the soluble pollutants are removed rapidly by the initial rain and that the bulk of the deposition loading occurs in the first hour of the rain event. The liquid phase concentrations of nitrate and H^+ build up beginning at 5:00 LT on May 3rd. This corresponds to the time that the wind shifts to a northeasterly flow transporting polluted air mass from New York.

The Pennsylvania site (grid point (4,8)) is located in a region with high SO_x and NO_x emissions. The site is also downwind of major sources throughout the meteorological conditions of May 2nd 1985. Precipitation began at this site at 17:00 LT May 2nd and continued until 4:00 LT on May 3rd. The time profiles of liquid phase concentrations at this site are also presented in Figure 22. The time profiles are quite different than those at the New Jersey site. The liquid phase concentrations of most species reach maximum values at 19:00 LT. The sulfate and nitrate concentration maximums are about 150μM. The liquid phase concentration profiles of H_2O_2 and bisulfite show opposite trends. The H_2O_2 is high initially and decreases as time progresses. This

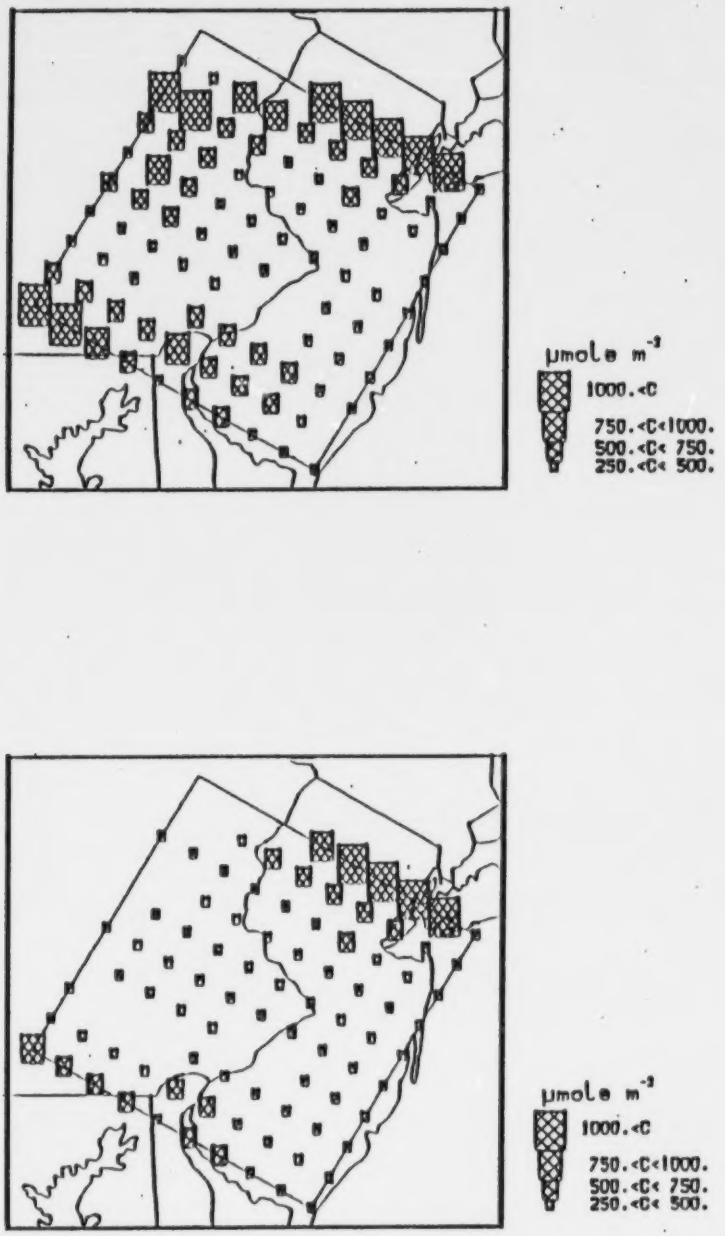

Figure 20. Total 18 hour wet deposition amounts of nitrate (top) and sulfate (bottom).

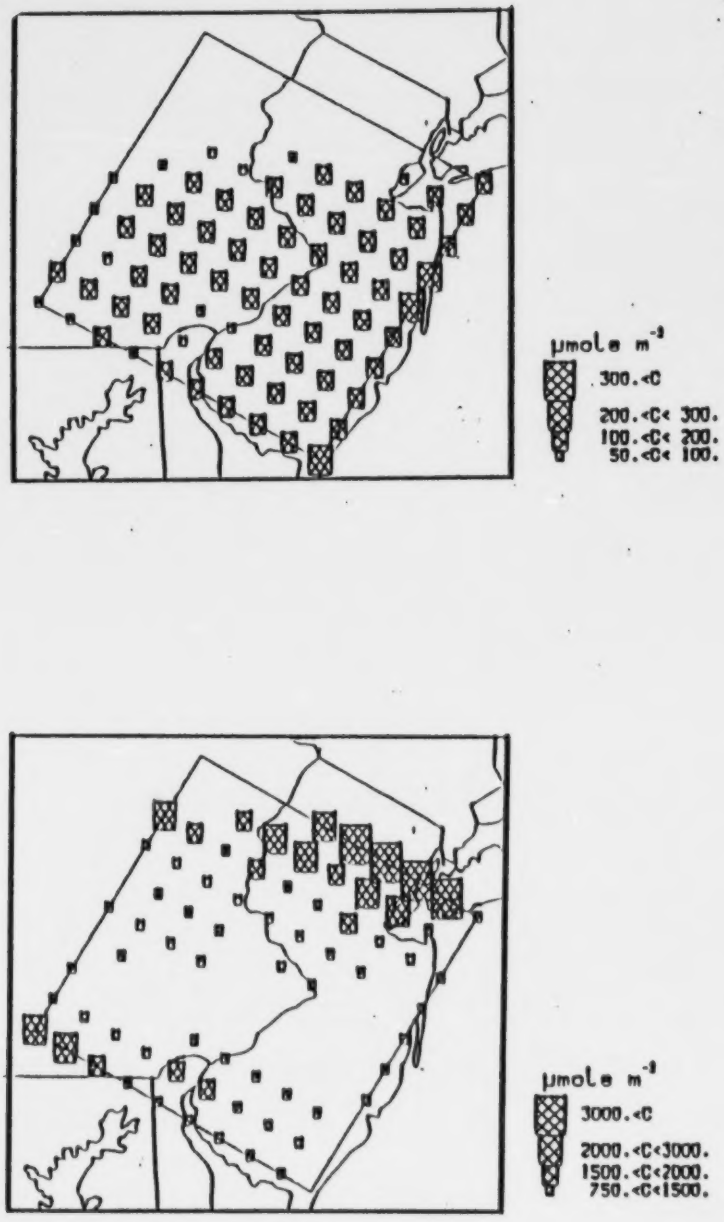

Figure 21. Total 18 hour wet deposition amounts of H_2O_2 (top) and H^+ (bottom) predicted by the fine grid simulation.

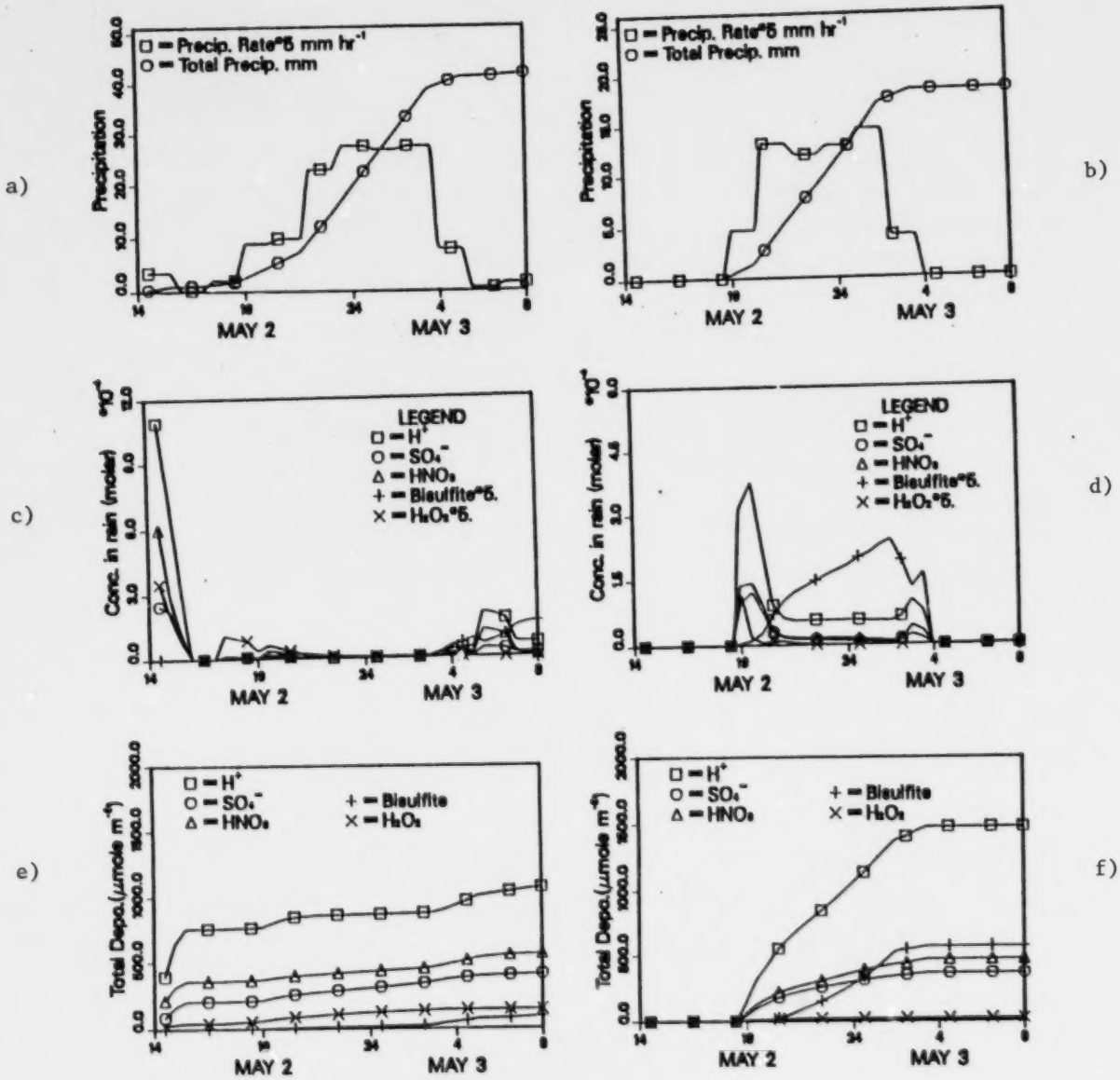

Figure 22. (a) Precipitation field at grid (8,2), (b) precipitation field at grid (4,8), (c) rain water concentrations at grid (8,2), (d) rain water concentrations at grid (4,8), (e) cumulative deposition at grid (8,2), and (f) cumulative deposition at grid (4,8).

indicates that at early times H_2O_2 is present in excess of bisulfite, and the bisulfite is consumed by the reaction with H_2O_2 to produce sulfate. At later times the H_2O_2 is depleted from the system and the bisulfite concentration increases. The gas phase profiles (not shown) indicate that gaseous H_2O_2 is depleted from the area by 22:00, whereas gaseous SO_2 is maintained by local emissions.

The total deposition at the two sites is also plotted. The total H+ deposition is about 1500 $\mu mole/m^2$ at the Pennsylvania site and ~ 1000 $\mu mole/m^2$ at the New Jersey site. The nitrate deposition exceeds the sulfate deposition at each point.

Budget calculations for various processes over the modeling domain for the 18 hour simulation are presented for HNO_3, sulfate and SO_2 in Figure 23. These results provide useful insights into the relative importance of various processes. The SO_2 inventory shows that local emissions during the 18 hour period is equivalent to about 1/3 of the mass of SO_2 initially present. (Furthermore, the net advection (i.e., inflow-outflow) into the region is equivalent to about 1/3 of the amount emitted.) The wet deposition and dry deposition are of equal importance and together are equivalent in magnitude to the emissions. The wet removal processes consist of wet deposition of S(IV) at the surface and the conversion of S(IV) to sulfate in cloud and rain water. As indicated, the importance of liquid phase transformation of S(IV) is much more important than the gas phase reactions of SO_2. The predominant liquid phase reaction for this simulation is the reaction of S(IV) with H_2O_2 to produce sulfate. The inventory for sulfate reveals that the contribution of primary emissions is very small, that wet deposition is much more important than the dry deposition process for this event, that sulfate production by liquid phase processes greatly exceeds that in the gas phase, and that an appreciable fraction is transported out of the model domain. (The net advection term is negative for sulfate). The nitrate inventory is similar to that for sulfate except that the gas phase production of nitric acid dominates. Also, for nitrate the net advection is out of the model domain.

The mass balance calculations for the fine grid simulation are presented along with those for the coarse grid in Table 6. (Please note that the

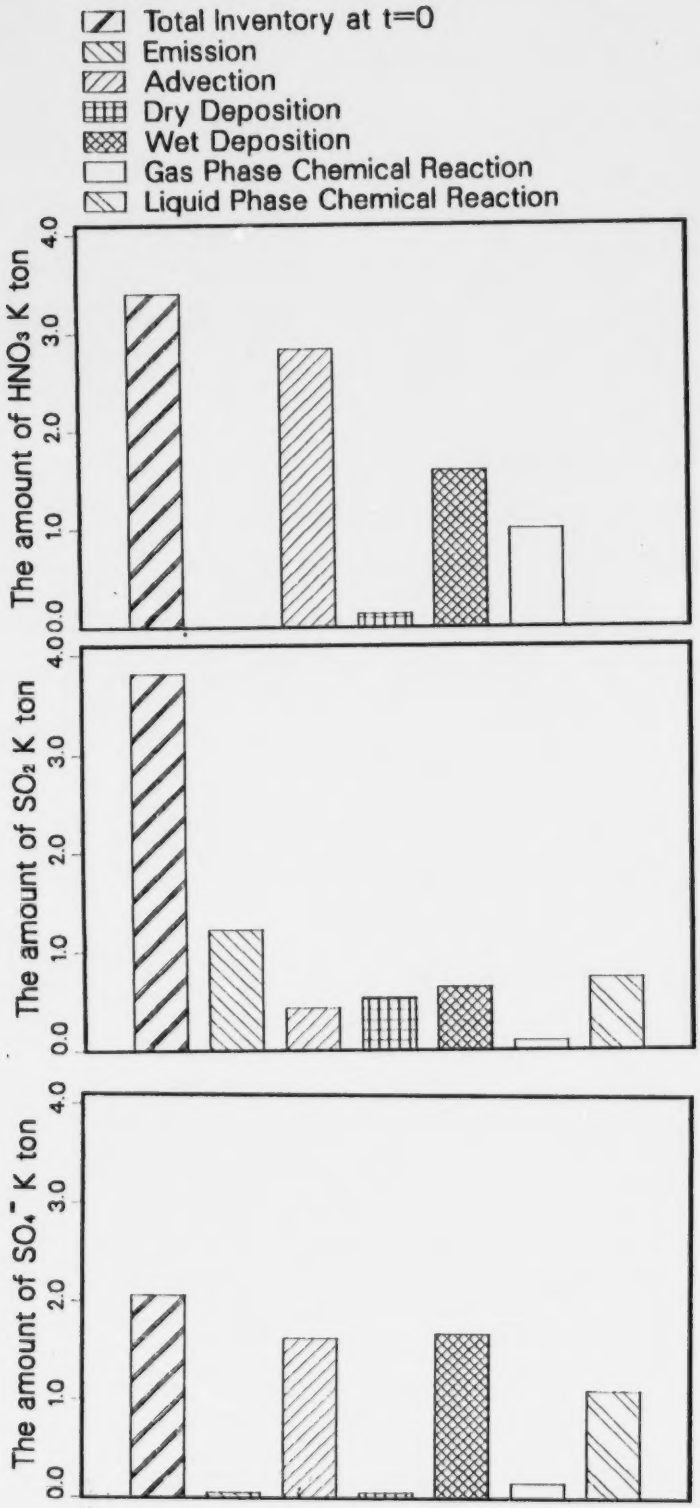

Figure 23. Budget calculations for (a) HNO_3, (b) sulfate and (c) SO_2

Table 6

Budget Calculations of Selected Species for the 18 Hour Simulation for the Coarse and Fine Grid Domains

Coarse Grid

CPU time 17 hours on Prime Computer

(molecules)

	Nitrate	Ammonia	SO_2	SO^{4-}
wet deposited	-2.32E+25	-4.50E+24	-5.60E+24	-1.72E+25
dry deposited	-1.56E+24	-7.62E+23	-6.64E+24	-5.32E+23
emitted	0	3.15E+24	1.33E+25	3.02E+23
gas phase chemical rxn	1.30E+25	-3.40E+23	-8.68E+23	8.68E+23
liquid phase chemical rxn	0	0	-1.38E+25	1.38E+25

Fine Grid

CPU time 4.5 hours on VPS 32

(molecules)

	Nitrate	Ammonia	SO_2	SO^{4-}
wet deposited	-1.51E+25	-1.82E+24	-5.97E+24	-1.05E+25
dry deposited	-1.31E+24	-3.96E+23	-4.98E+24	-3.49E+23
emitted	0	1.36E+24	1.15E+25	3.27E+23
gas phase chemical rxn	9.53E+24	-2.12E+23	-9.58E+23	9.58E+23
liquid phase chemical rxn	0	0	-6.89E+24	6.89E+24

horizontal cross-sectional areas of the 2 grid systems differ by a factor of 1.55 with the coarse grid area being the larger.) In general the same trends are shown. Nitrate wet deposition is larger than dry deposition by a factor of 15, ammonia wet deposition is roughly the same as that for SO_2 and exceeds dry deposition by a factor of 6, dry and wet deposition of SO_2 are of equal importance whereas the liquid phase reactions are 15 times more important than gas phase reactions, and the sulfate wet deposition is 30 times more important than dry deposition. Furthermore, nitrate wet deposition exceeds sulfate wet deposition by 30%.

NESTED GRID CAPABILITIES

The results discussed previously indicate that the deposition on the mesoscale is strongly influenced by the transport of material into the region. In order to better specify the flux of materials into the mesoscale area of interest we are planning to use a regional-scale model simulation to provide boundary conditions for the MesoSTEM model. A one-way nesting of a regional-scale version of STEM-II with the MesoSTEM model is planned. The regional scale grid system is shown in Figure 24. The regional scale study of precipitation scavenging using STEM-II is being conducted for Battelle Pacific Northwest Laboratories in conjunction with the PRECP program. The meteorological fields are being obtained by objective analysis using radiosonde data and gridded precipitation is prepared objectively using a program developed by David Powell at PNL. There are two options available for the regional scale simulations. One option is to use the same detailed version of STEM-II for the regional simulation that is used for the mesoscale simulations. The other option is to use an "engineering" version of STEM-II for the regional simulation. The engineering version of STEM-II has the same numerics and treatment of wet removal processes, but utilizes a simplified chemical mechanism. The engineering model executes about 10-20 times faster than the detailed version of STEM-II. For either option, the regional simulation is done first and output files are used to specify the boundary input files for a separate simulation of STEM-II on the mesoscale.

The engineering version of the model is currently undergoing extensive

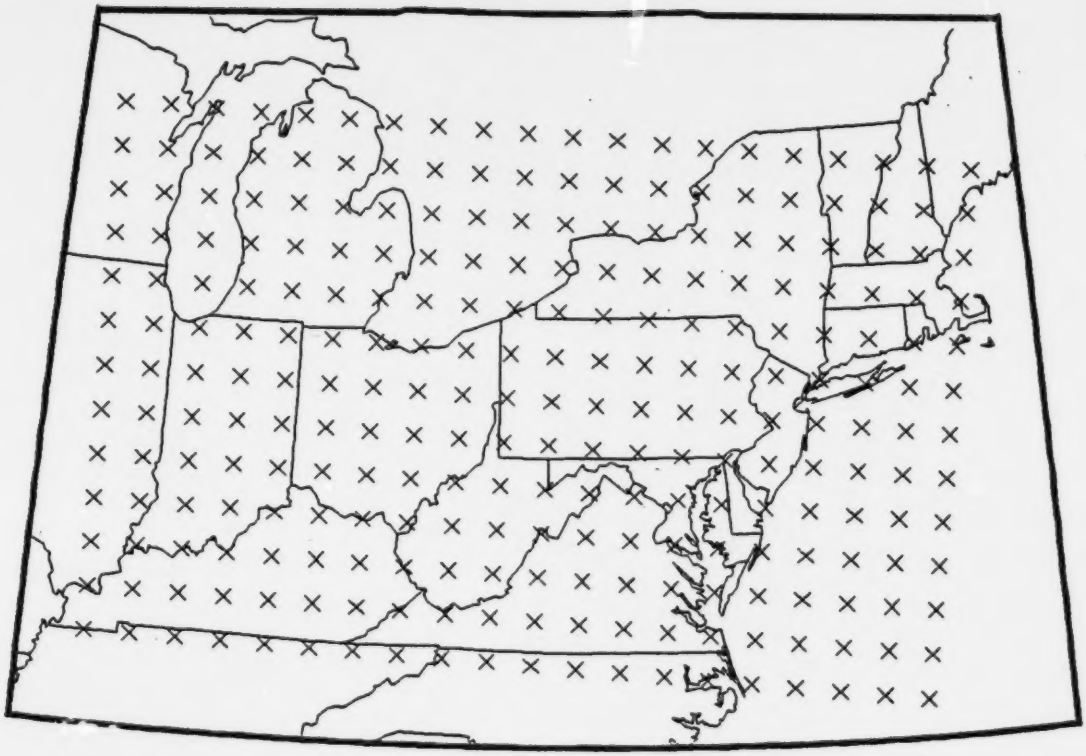

Figure 24. Grid systems for the regional scale simulation

testing. The regional scale meteorological fields will be available by early summer, and regional scale simulations for the May 2nd and 3rd, 1985 conditions from both options will be available this summer.

SIMULATION EXECUTION TIMES

The fine grid simulation utilizing 1400 grid points requires 4.5 CPU hours on the NASA Langley Cyber VPS 32 per 18 hours simulated. The STEM-II plus ASM model was transferred to the VPS 32 machine and optimized. It was found that option - O with the FORTRAN compiler was the best. The following timing profile was obtained for the May 2nd and 3rd simulation.

ion concentration calculation	28%
aqueous phase mass transfer	30%
aqueous phase transport	6%
gas phase reaction	9%
aqueous phase reaction	10%
gas phase transport	<1%
input, output, bookkeeping, print ... traffic control	16%

As indicated 83% of the CPU time is spent performing the chemistry calculations with 58% spent in the ion concentration and the aqueous phase mass transfer. Work on increasing the execution speed must focus on these subroutines. Work was conducted investigating the possibility of using half-word (32 bit) arithmetic. This could speed up the current code by 20 - 30%, with little degradation of the precision of the final results.

5. RELATED ACTIVITIES

There have been several activities carried out during the project period involving the development and applications of the STEM-II model that directly relate and/or are complementary to the Mesoscale Acid Deposition Project (even though they may have been supported to some degree by other sources). These projects are discussed briefly below.

INFLUENCE OF TRANSITION METAL IONS ON SULFATE FORMATION

A one-dimensional version of STEM-II + ASM was used to investigate sulfate production mechanisms in storm systems. This study was conducted to help determine which reactions to include into our diagnostic model studies. This study specifically emphasized the role of transition metal ions (TMI). To evaluate their role, twenty-one TMI reactions involving iron, copper, and manganese were selected from the comprehensive TMI mechanism evaluated by Graedel et al. (1986) and incorporated into the STEM-II model. The results of this coupled chemical cloud-microphysics analysis support the homogeneous, constant pH rain drop results presented by Graedel et al., 1986.

The presence of TMI in the cloud and rain water was shown to affect sulfate production via a number of pathways. The presence of TMI in cloud and rain water reduced the concentration of H_2O_2, increased the concentration of OH, and provided direct catalyzed pathways for S(IV) oxidation. Under high TMI conditions, the Mn-catalyzed pathway was very important for sulfate production. The ground level concentrations of sulfate after 2 hours increased by nearly a factor of 2 under these conditions. The presence of TMI was also shown to reduce the gas phase SO_2 and H_2O_2 profiles and to increase the organic acid production in cloud and rain water.

The role of NO_3 and N_2O_5 in nitrate production in cloud water was also investigated. Under the conditions simulated, solution phase reactions involving NO_3 and N_2O_5 increased the nitrate in solution by about 4% at night. Much higher contributions are expected under lower gaseous HNO_3 conditions. Also gas phase NO_3 and N_2O_5 were shown to slightly increase sulfate production under night time conditions, and the presence of TMI

slightly decreased the nitrate production in solution.

CUMULUS CLOUD SCAVENGING STUDIES

A study on cumulus cloud dynamics was initiated to develop parameterization methods to characterize their effects on regional scales. A summary of this project is presented here and a detailed description is presented in Nair (1987).

The nature and extent of cloud acidification processes are dependent on the physical and transport properties of the wet phase. In the case of cumulus clouds, these properties are the liquid water content, concentration and size distributions of the cloud condensation nuclei, vertical motions, etc. Any chemistry model that simulates cumulus acidification processes should include realistic cumulus parameters so as to yield meaningful results. A one-dimensional kinematic model based on the thermodynamics of PLUVIUS has been formulated to simulate cumulus formation, growth and dissipation.

The updraft/downdraft structure used in the model is based on current knowledge of cumulus cloud properties. Initially, a parabolic vertical velocity profile is introduced to create an updraft parcel which entrains and detrains air laterally. The cloud forms in the upper half of the updraft structure where lateral detrainment occurs, all the entrainment being from below the cloud base. As the updraft velocities increase, the cloud grows and deepens. Downdraft is introduced into the fully developed cloud in such a way that the lateral entrainment into the parcel is from the regions above the cloud top. The cloud is in a laterally detraining region. The cloud dissipates and disappears as the downdraft penetrates and reaches the cloud base.

The liquid water contents (ω) at all levels above cloud base are lower than the values (ω_a) that would be seen in a parcel that rises adiabatically from the cloud base and reaches those levels. The ratio ω/ω_a decreases with height above cloud base. The observed process lapse rate lies between the dry and wet adiabatic lapse rates at cloud levels. Variations were made on the

updraft/downdraft structure, initial moisture and temperature profiles, and CCN concentrations to study their effect on the cloud structure. Even though rain and snow phases are allowed to form in the model, the precipitation levels were negligible.

The model assumes entrainment from more than a single level above the cloud top. Therefore, the Paluch diagram is not expected to give a single point above the cloud-top as the source of in-cloud dilution. However, it is interesting to note that a straight-line fit of the in-cloud points did indicate in some cases a virtual source above the model domain.

The relatively simple one-dimensional cloud model produces cumulus properties that are in good agreement with the observations of other studies. In addition, the model employs an updraft/downdraft structure that is based on the observations of other researchers. Currently, the model is being used along with STEM-II gas and aqueous-phase chemistry to study cumulus acidification.

ACIDIFICATION OF NON-PRECIPITATING CUMULUS CLOUDS

Realistic non-precipitating cumulus clouds were developed using a one-dimensional extension of PLUVIUS to include lateral and top entrainment/detrainment processes. The model clouds show formation, growth, and dissipation life histories typical of cumuli. This cloud model was coupled with comprehensive gas-phase and aqueous-phase chemistry mechanisms to study acidification processes over the complete life cycle of cumuli. Additional details are available in the Ph.D. dissertation of Mr. Shyam Nair (1987.)

These full cumulus cloud runs indicate that the final cloudwater pH primarily depends on the degree of oxidation of S(IV) to S(VI) by H_2O_2, and hence on the background H_2O_2 concentration. Higher background H_2O_2 results in higher acidity. The pH values predicted by a parcel model were generally lower than the cumulus values for similar concentration profiles in the gas-phase. However, the acidity increased with higher concentration of initial H_2O_2. The pH was also seen to increase weakly with increased updraft velocity

in the parcel model.

In these runs, H_2O_2 is the most important oxidant of S(IV) in the aqueous phase. HO_2, OH, Cl_2^- and the intermediate SO_4^- also make significant contributions. O_3 contributes less than 2 percent to the overall oxidation.

First-order rate constants for the conversion of S(IV) and S(VI) increase with increasing concentrations of H_2O_2 in the background and with increasing cloudwater contents in the cumulus runs. The parcel model runs showed the same dependency on initial H_2O_2 and updraft velocity.

H_2O_2 is produced both in the gas and aqueous phases. The gas-phase production is directly linked to the background NO_x concentrations. High background NO_x reacts with HO_2 to produce alternate products, whereas low NO_x frees this pathway and HO_2 is converted to H_2O_2. The diffusion-controlled layer above the clouds clearly shows the formation of H_2O_2 in the gas phase. This is borne out by experimental measurements as well (Alkezweeny, 1985).

Hydroxymethanesulfonate ion constitutes nearly 50 percent of the S(IV) in the aqueous phase. However, nearly all H_2O_2 entering the aqueous phase is consumed in the oxidation of SO_2. This is in agreement with the conclusion of Munger et al. (1986).

Parameterization of cloud properties in the cumulus model is more extensive than in a parcel model. The final cloudwater pH and rate constants show the combined effects of cloudwater content, drop size, updraft velocity, entrainment, detrainment, background conditions, etc. A parcel model is highly simplified, but the results of all models indicate that for background H_2O_2 concentrations of 2 ppb, the rate constants for SO_2 oxidation lie in the range of 5 - 30%/min.

Cumulus clouds behave like giant reactors with entrainment of background air from below and above cloud regions and release of processed air from the sides. Because of these entrainment processes, the contribution of cumulus oxidation to overall oxidation in the atmosphere should not be ignored in any modeling study.

IMPROVED NUMERICAL SCHEMES

With the goal of improving the numerical predictions of STEM-II, a study was initiated to evaluate the sensitivity of the numerical predictions to grid spacings chosen in the discretization of the model region. A detailed discussion is included in Kasibhatla (1987).

The basic step in all numerical schemes for air quality simulations involves discretizing the region of interest with a suitable grid. Difference equations, derived from the original differential equation, are then solved to yield concentration predictions at the node points of the grid. Concentrations at any other location in the grid can be calculated using appropriate techniques. However, one major aspect of the problem has received little attention - namely, the choice of the grid used for the numerical simulation. The grid is often selected without regard to the meteorological conditions or the source distribution. This can, and probably will, result in a lack of sufficient resolution in near-source regions. The common practice in air pollution modeling has been first to choose a grid and then average emissions over the grid element in which the emission points lie. This does not necessarily yield an equivalent source. Serious errors in concentration predictions can occur in areas downwind of the source.

State-of-the-art numerical techniques for solving partial differential equations utilize adaptive grid techniques. In these methods, the mesh is refined based on 'a posteriori' error estimates. However, these techniques have not been used for air pollution simulations since software is available only for certain limiting forms of equations. The aim of this study was to identify parameters that affect the accuracy of numerical solutions of the transport equations involving point sources. Based on these, a grid can be chosen 'a priori' and used for the entire simulation. A two-dimensional finite element model using bilinear elements was used to solve the advection - diffusion problem with an infinite line source.

This study was restricted to two spatial directions, with advection dominating in the x-direction and turbulent diffusion dominating in the z-direction. Numerical results for an inert plume emanating from a single

infinite line source showed that the ratio of the advection time scale to the turbulent diffusion time scale, $\gamma = K_z \Delta x / u \Delta z^2$, should be equal to or greater than one for the most accurate solutions (see Figure 25), where K_z is the eddy diffusivity, Δx is the x-direction grid spacing, u is the wind velocity, and Δt is the z-direction grid spacing. In addition, comparisons between the volume-averaged representation of a point source and the use of an irregular grid for point source representation demonstrated that, near the source, improved results can be obtained by placing a node at the source location.

There are other ways to resolve the conflict between the spatial resolution in the model and the microscale characteristics of point source emissions. Seigneur et al. (1983) embedded a reactive plume submodel into an urban airshed model. In the combined model, a plume released from a large point source was approximated by a plume with constant properties over a given time interval. This allowed for modeling a continuous plume by puffs released at regular intervals from the point source and transported by the mean windflow. While this model is detailed in its description of plume dynamics, it is computationally very expensive.

This study dealt only with inert plumes. The effect of chemical reactions on solution accuracy has yet to be investigated in this context. Inclusion of a first-order chemical reaction is relatively simple. Higher order reactions, however, introduce non-linearity into the equations. In STEM-II (Carmichael et al., 1986), we use an operator-splitting technique to separate the chemical reactions and solve them using time steps different from those used for the transport equations. Incorporation of that algorithm into the model described here and study of the effect on solution accuracy will also be considered. The model described here is being extended to three dimensions, with spatially and temporally varying meteorological conditions, and multiple sources. The effect of linear as well as non-linear chemistry on solution accuracy is being studied also.

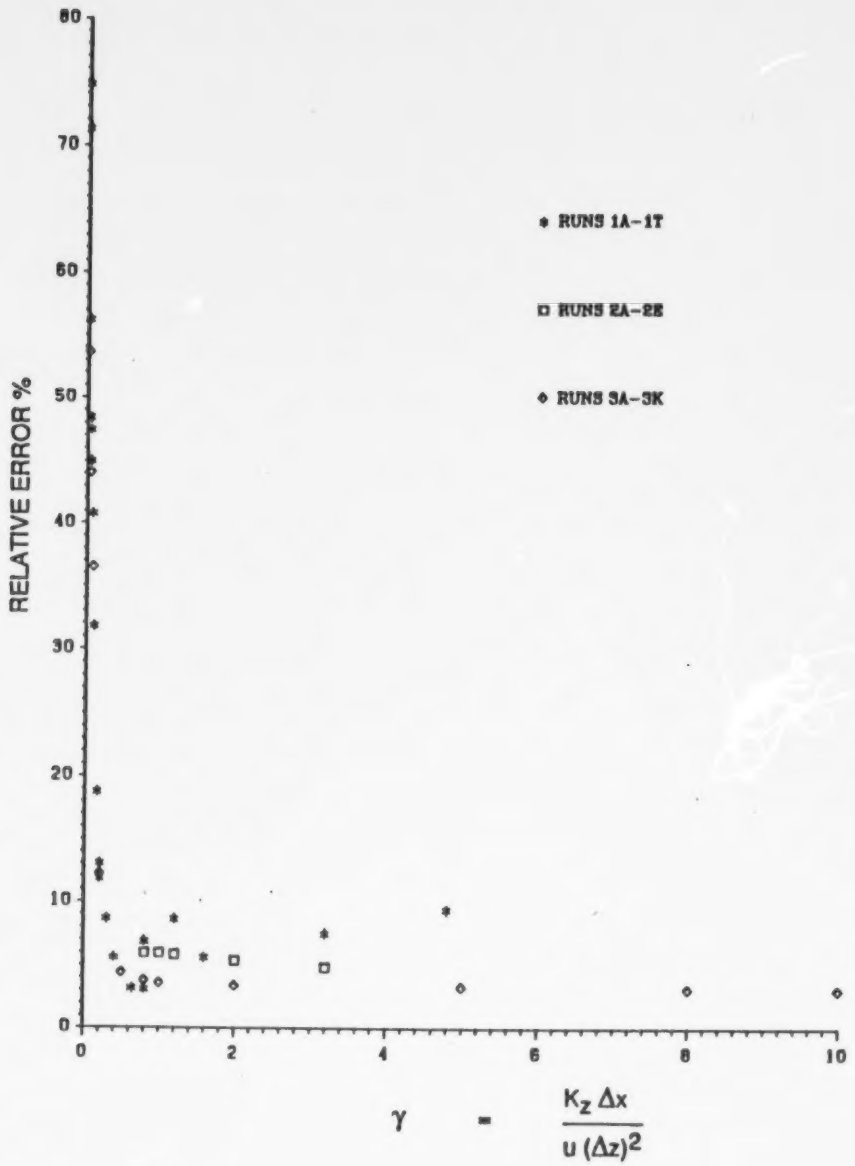

Figure 25. Variation of relative error

EVALUATION OF SOURCE RECEPTOR RELATIONS IN THE STEM MODEL

One important problem with Eulerian models is that it is difficult to assess the influence of one particular source on a particular receptor. However, these source-receptor relations are very important from a policy standpoint. We have been using sensitivity analysis techniques to calculate such relations in the STEM models. Specifically, we have demonstrated the methodology in three-dimensional calculations of the STEM-I model and in the engineering version of STEM-II. The procedure is based on the calculation of the emission sensitivity densities. The influence of a particular source, $E_1(x_1', x_2', x_3', t')$, on the concentration $C_m(x_1, x_2, x_3, t)$ can be represented by the quantity

$$\Omega_{m,1}(x_1,x_2,x_3,t;x_1',x_2',x_3',t') = \frac{\delta C_m(x_1,x_2,x_3,t)}{\delta E_1(x_1',x_2',x_3',t')} \tag{10}$$

where $\Omega_{m,1}$ is called the "emission sensitivity density" and the symbol δ is a functional derivative. Functional derivatives are used instead of partial derivatives because the emissions are distributed spatially and temporally within the model domain. This quantity represents the response of the concentration of the m-th species at position (x_1,x_2,x_3) at the time t to a variation of the emissions of the 1-th species at position (x_1',x_2',x_3') at the time t'. Thus, this quantity contains the important "source-receptor" information. If $\Omega_{m,1}$ is large, then the source of the 1-th species at (x_1',x_2',x_3') and t' has a large influence on the concentration of the m-th species at a receptor located at (x_1,x_2,x_3) at time t. Also, a positive $\Omega_{m,1}$ means that the concentration of the m-th species increases as the emission of the 1-th species increases.

The equations describing the densities for the gas phase are derived by taking the first variation of Eq. (1).

$$\frac{\partial \Omega_{m,1}}{\partial t} + \frac{\partial v_j \Omega_{m,1}}{\partial x_j} = \frac{\partial}{\partial xj} K_{jj} \frac{\partial \Omega_{m,1}}{\partial x_j} + \sum_n \frac{\partial R_m + G_m}{\partial C_n} \Omega_{n,1} \tag{11}$$

$$+ \delta_{m,1} \delta(x_1-x_1') \, \delta(x_2-x_2') \, \delta(x_3-x_3') \, \delta(t-t')$$

Note that even though the species balance equations are non-linear (e.g., Equation 10, the sensitivity density equations are linear. Efficient procedures to calculate these sensitivity densities have been developed (cf, Cho et al. (1987a) and Reuven et al. (1986)).

The response of the concentration at a specific receptor to the perturbation of several species at several locations is represented by

$$\delta C_m(x_1,x_2,x_3,t;\ v_1'\ v_p',t') \sum_{l=1}^{l=q} \sum_{j=1}^{j=p} \int_{v_j} \Omega_{m,l}\delta E_l(x_1',\ x_2',\ x_3',t)dv_j' \quad (12)$$

where p and q are the number of sources and species being perturbed respectively, and v_j' is the local source volume about the point (x_1',x_2',x_3'). If the emissions are perturbed uniformly (i.e., $\delta E_l(x_1',x_2',x_3',t')$ is constant then the individual $\Omega_{m,l}$'s represent the importance of source $E_l(x_1',x_2',x_3')$ at time t, and the relative importance of the individual sources is given by the relative magnitude of the $\Omega_{m,l}$'s.

The use of the emissions sensitivities to quantify source receptor relations is demonstrated using a regional scale application of STEM when we assess the influence of three different SO_2 source regions on the SO_2 concentrations at two receptor locations (see Figure 26). The sensitivity coefficients as a function of time are also presented in Figure 26. The nearby sources affect the SO_2 concentration at a given receptor during the day time, but the influence of the farther upwind source becomes important during the night time. A detailed discussion is presented in Cho et al. (1987b). Currently this work is being extended to include a variety of source response relations of potential interest to field study design and policy evaluation.

INVESTIGATION OF GAS PHASE ACID FORMATION USING SENSITIVITY ANALYSIS

Sensitivity analysis provides a powerful tool for improving both qualitative and quantitative understanding of the chemical mechanisms used in comprehensive air pollution models.. A variety of sensitivity analysis techniques are being used to investigate O_3, OH, HO_2, H_2O_2, sulfate and nitric acid formation in the Atkinson-Lloyd (Atkinson et al., 1982) mechanism used in

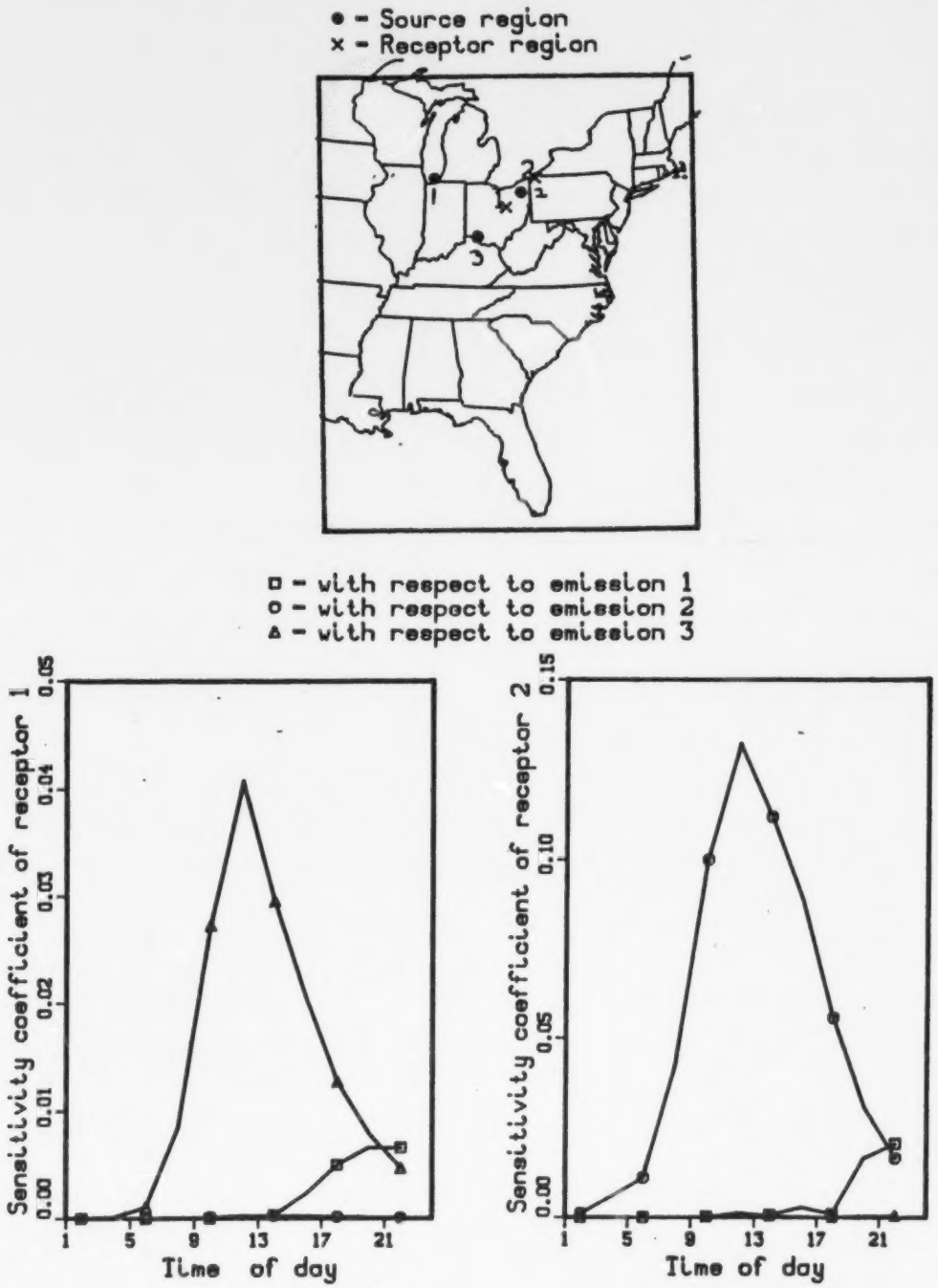

Figure 26. The response of sulfate at the receptors with respect to a positive perturbation of SO_2 in the vicinity of Gary, Cincinnati, and Pittsburgh.

STEM-II. The analysis represents a detailed sensitivity study and makes use of several new techniques. The initial condition and parameter sensitivity coefficients are calculated using the AIM (Analytically Integrated Magnus) method (Kramer, et al., 1981)). The AIM method provides the Green's function surfaces without appreciable additional computational effort. The Green's function surfaces give an overview of the complex interactions among the chemical species in the system. Furthermore, the summation of the Green's function surface by row and the integration of Green's function elements over time yields important lumped system responses. Constrained sensitivity analysis is a very useful tool to investigate the importance of various chemical or physical pathways in determining the concentrations of given chemical species.

These sensitivity tools are being used to probe the general features of the Atkinson-Lloyd mechanism. These techniques provide information that not only confirms our basic understanding of the mechanism, but also quantifies the relationships between various species and the impacts that variations or uncertainties in initial conditions or rate constants have on the calculated responses. Furthermore, sensitivity analysis allows the identification of the important convoluted pathways linking one species to another species and the alternate pathways that may come into importance if a particular path is blocked.

The analysis is emphasizing the production of sulfate, nitric acid, ozone and those species that play an important role in their production (i.e., H_2O_2, OH, HO_2, etc.) Particular attention is given to the role of NO_x and hydrocarbons. For the base case conditions simulated NO_x plays a larger role in the mechanism than hydrocarbons. This was shown both in the initial condition sensitivites and the rate constant sensitivities. The role of organics is also being analyzed in some detail, and the importance of the NO_x to organics ratio and the roles of the individual hydrocarbon species are being quantified. The change of initial conditions have only a slight effect on the shape of the sensitivity curves of O_3, OH and HO_2 with respect to most of the speciated hydrocarbons. However, the time scales are found to change. Many chemical species are shown to play roles as intermediates in

generating O_3 from organics. The aldehydes are found to be the most important intermediates through which organics affect oxidants such as O_3, OH and HO_2 and nitric-organic compounds such as PPN, PAN, El-NO_2. NO_2 is shown to have a negative effect on O_3 due to its role as a sink of OH for the base case simulation. This shows the non-linear characteristics of atmospheric chemistry.

Sensitivity analysis is also being used to evaluate emissions reduction strategies. The effect of various hydrocarbon reduction strategies on O_3 production are being evaluated and the results show that not all strategies are equally effective. For the conditions simulated the strategy of only controlling non-aromatics was the most effective and the control of aromatics alone was the least effective. The proportional response of sulfate to changes in SO_2 concentrations is shown not to be influenced by controls aimed at co-pollutants (i.e., simultaneous SO_2, NO_x, and hydrocarbon controls). Nitric acid production is found not to be directly proportional to changes in NO_x (i.e., a 1% change in NO_x leads to 0.6% response in HNO_3).

6. SUMMARY

The major activities related to the use of the STEM-II model in the Mesoscale Acid Deposition Project have been summarized in this progress report. The installation of the STEM-II model on the NASA Langley Cyber VPS machine and the interface with the MASS model has been completed. The MesoSTEM model framework has been applied to the analysis of the May 2nd and 3rd, 1985 Philadelphia field data. Course grid simulations have been examined and analyzed in detail, and sensitivity runs and a fine mesh simulation have been completed and are currently being analyzed. The coarse and fine mesh simulations, in addition to providing insights into the processes affecting acid deposition in mesoscale precipitation events, will also provide valuable information as to the effect of horizontal and vertical grid resolution on model predictions.

The major efforts for the next project period will be the application of the one-way nested version of the model (to provide boundary conditions for the MesoSTEM application) and the analysis of two additional data sets corresponding to the April 4, 1984 and the December 3, 1983 Philadelphia field studies.

7. REFERENCES

Alkezweeny, A. J., 1985, personal communication.

Atkinson, R., Lloyd, A.C. and Winges, L.. 1982, An updated chemical mechanism for hydrocarbon/NO_x/SO_2 photooxidations suitable for inclusion in atmospheric simulation model, Atmos. Environ., 16:1341.

Balko, J.A. and Peters, L.K., 1983, A modeling study of SO_2 and SO_4 from atmospheric concentration data, Atmos. Environ., 17:1965.

Berry, E.X. and Reinhart, R.L., 1974, An analysis of cloud drop growth by collection, J. of Atmos. Sci., 31:2118.

Carmichael, G.R., Kitada, T. and Peters, L.K., 1983, The effect of in-cloud scavenging on the transport and gas phase reactions of SO_x, NO_z, HC_x, and H_xO_y and O_3compounds, Precipitation Scavenging, Dry Deposition, and Resuspension, edited by Pruppacher, H.R., Semonim, R.G., and Slinn, W.G.N., Elsevier Science, Vol. 1, pp. 675-686.

Carmichael, G.R. and L. K. Peters, 1984a, An Eulerian transport trans-/formation/removal model for SO_2 and sulfate - I. Model Development, Atmos. Environ., 18:937.

Carmichael, G.R. and L. K. Peters, 1984b, The STEM-I model - Model calculation of SO_x transport in the Eastern United States, Atmos. Environ., 18:953.

Carmichael, G.R., Peters, L.K. and Kitada, T., 1986, A second generation model for regional-scale transport/chemistry/deposition, Atmos. Environ., 20:173.

Chameides, W.L., 1984, The photochemistry of a remote marine stratiform cloud, J. Geophys. Res., 89:4739.

Cho, S.Y., Carmichael, G.R., and Rabitz, H., 1987a, Sensitivity analysis of the atmospheric reaction-diffusion equations, Atmos. Environ., in press.

Cho, S.Y., Carmichael, G.R. and Rabitz, H., 1987b, Relations between primary emissions and acid deposition in Eulerian models determined by sensitivity analysis, Atmos. Environ., (to be submitted).

Dronamraju, M., G.R. Carmichael and L. K. Peters, 1987a, An Eulerian transport/chemistry/removal model for SO_2 and Sulfate: III - Comparison with the July 1974 SURE Data Basis, submitted to Atmos. Environ.

Dronamraju, M., Peters, L.K., Carmichael, G.R., and Prasad Kasibhatla, 1987b, Comparison of an Eulerian Transport/Chemistry/Removal Model for SO_2 and Sulfate (STEM-I) with the July 1978 SURE Data Base, submitted to Atmos. Environ.

Easter, R.C. and J. M. Hales, 1984, personal communication.

Forester, C.K., 1977, Higher order monotonic convection difference schemes, J. Comput. Phys, 23:1.

Graedel, T.E., Mandich, M.L. and Weschler, C.J., 1986, Kinetic model studies of atmospheric droplet chemistry 2. Homogeneous transition metal chemistry in rain drops, J. Geophysical Research, 91:5205.

Hales, J.M., 1984, An interim user's manual for the advanced scavenging module (working copy).

Heinrich, J.C., Huyakorn, P.S., Zienkiewicz, O.C. and Mitchell, A.R., 1977, An upwind finite element scheme for two dimensional convective transport equation, Int. J. Num. Meth. Eng., 11:131.

Hong, M-S and G. R. Carmichael, 1986, An investigation of sulfate production in an orgraphic storm using a detailed transport/chemistry model coupled with a detailed cloud scavenging model, Atmos. Environ., 20:1989.

Kaiser, J.A.C., and Hill, R.H., 1976, Irradiance at sea, J. Geophys. Res., 81:395.

Kaplan, M.K., Zack, J.W., Wong, V.C., Tuccillo, J.J., 1982, Initial results from a mesoscale atmospheric simulation system and comparison with the AVE-SESAME I I data set, Monthly Weather Review, 110:1564.

Karamachandani, P.K., and Peters, L.K., 1987, Three dimensional behavior of mixing-limited chemistry in the atmosphere, Atmos. Environ., in press.

Kasibhatla, P.S., 1984, Some aspects of regional scale air pollution modeling, M.S. Thesis, Department of Chemical Engineering, University of Kentucky.

Kasibhatla, P.S., Peters, L.K. and Fairweather, G., 1987, Numerical simulation of transport from an infinite line source: Error analysis, Atmos. Environ., (in press).

Kessler, E., 1969, On the distribution and continuity of water substances in atmospheric circulation, Meteorological Monographs, 52.

Kitada, T., Carmichael, G.R., and Peters, L.K., 1984, Numerical simulation of the transport of chemically reactive species under land- and sea-breeze circulations, J. Clim. Appl. Met, 23:1153.

Kitada, T., Igarashi, K., and M. Owada, 1986, Numerical analysis of air pollution in a combined field of land/sea breeze and mountain/valley wind, J. Clin. & Appl. Meteor, 25:767.

Koch, S.E., Skillman, W.C., Kocin, P.J., Wetzel, P.J., Brill, K.F., Keyser, D.A. and McCumber, M.C., 1985, Synoptic scale forecast skill and systematic errors in the MASS 20 model, Monthly Weather Review, 113:1714.

Koch, S.E., 1985, Ability of a regional-scale model to predict the genesis of intense mesoscale convective systems, Monthly Weather Review, 113:1693.

Kramer, M.A. and Calo, J.M., 1981, An improved computational method for sensitivity analysis, Applied Mathematical Modelling, 5:432.

Lin, Y., Farley, R.D. and Orville, H.D., 1983, Bulk parameterization of the snow field in a cloud, J. Atmos. Sci., 40:1065.

McRae, G.J., Goodin, W.R., and Seinfeld, J.H., 1982, Numerical solution of the atmospheric diffusion equation for chemically reactive flows, J. Comput Phys., 45:1.

Mitchell, A.R., 1969, Computational Methods in Partial Differential Equations, John Wiley, New York.

Munger, A.J., Tiller, C., Hoffman, M.R., 1986, Identification of hydroxymethanesufonic acid in fog water, Science, 231:247.

Nair, S., 1987, Modeling studies on the formation, growth, dissipation and acidification of cumulus cloud, Ph.D. dissertation, Chemical Engineering Department, University of Kentucky.

Preussner, P.R. and Brand, K.P., 1981, Application of a semi-implicit Euler method to mass action kinetics, Chem. Eng. Sci., 10, 1633-1641.

Reuven, Y., Smooke, M.D. and Rabitz, H., 1986, Sensitivity analysis of boundary value problems: Application to non-linear reaction diffusion systems, J. Comp. Phys., 64:27.

Scott, B.C., 1982, Predictions of in-cloud conversion rates of SO_2 based upon a simple kinetic and kinematic storm model, Atmos. Environ., 16:1735.

Seigneur, C., Tesche, T.W., Roth, P.M. and Liu, M.K., 1983, On the treatment of point source emissions in urban air quality modeling, Atmos. Environ., 17:1656.

APPENDIX A. COPIES OF PUBLICATIONS

a) A Second Generation Model for Regional-Scale Transport/Chemistry Deposition, reprinted with permission of Atmospheric Environment.

b) An Evaluation of the Chemical and Physical Process Affecting Sulfate and Nitrate Wet Deposition.

Atmospheric Environment Vol. 20, No. 1, pp. 173–188, 1986
Printed in Great Britain

0004-6981/86 $3.00 + 0.00
© 1986 Pergamon Press Ltd.

A SECOND GENERATION MODEL FOR REGIONAL-SCALE TRANSPORT/CHEMISTRY/DEPOSITION

GREGORY R. CARMICHAEL
Department of Chemical and Materials Engineering, University of Iowa, Iowa City, Iowa 52242, U.S.A.

LEONARD K. PETERS
Department of Chemical Engineering, University of Kentucky, Lexington, Kentucky 40506, U.S.A.

TOSHIHIRO KITADA
School of Regional Planning, Toyohashi University of Technology, Toyohashi 440, Japan

(*First received* 16 *November* 1984 *and in final form* 15 *April* 1985)

Abstract—The regional-scale transport, chemistry and deposition of acidifying compounds, photochemical oxidants, and their precursors are analyzed using a second-generation Eulerian model. The important atmospheric processes are incorporated using chemical, dynamical and thermodynamical parameterizations having sufficient detail to accommodate boundary layer-free troposphere exchange in cloudy and cloud-free environments, and in-cloud and below-cloud wet removal and chemistry. Forty-one species are considered, many of which are also present in the liquid-drop phases. In the regional scale transport, the advected species are NO, NO_2, SO_2, SO_4^{2-}, O_3, HNO_3, NH_3, PAN, H_2O_2, HCHO, alkanes, C_2H_4, other olefins, aromatics, RCHO, ROOH, HNO_2, $RONO_2$ and RO_2NO_2. The model capabilities are illustrated by showing simulations in which non-precipitating clouds are present to absorb gas-phase species, chemically alter these, and then release them to the atmosphere.

Key word index: Regional modeling, acid deposition, Eulerian model, finite element method.

INTRODUCTION

In this paper, a second-generation regional-scale transport/chemistry/deposition model for photochemical oxidants, acidifying compounds, and their precursors is presented. The first-generation model has been discussed previously in some detail (Carmichael and Peters, 1984a, 1984b). In those studies, the regional distribution of SO_2 and sulfate within the lower troposphere (up to approximately 3000 m) was simulated. Concentrations of other relevant species were calculated via pseudo-steady state considerations (for short-lived species such as free radicals) or imposed as constraints on the simulations (for species such as CO). A somewhat elementary SO_2 photochemical oxidation mechanism, based on a 27-reaction scheme, was incorporated into the first-generation model. One of the primary outputs of the chemistry was OH and HO_2 free radical concentrations, which were used to calculate temporally and spatially varying SO_2 conversion rates. Peak conversion rates were in the 1–2%h^{-1} range.

Another major facet of the first-generation model incorporated available data on dry deposition to establish parameterized deposition velocities for SO_2 and sulfate. These were calculated at 3-h intervals from estimates of the aerodynamic and surface resistances based on surface windspeed, roughness, evaporation rate and atmospheric stability. With this procedure, average values for the eastern United States for the 4–10 July 1974 were 0.44 cm s^{-1} and 0.26 cm s^{-1} for SO_2 and sulfate, respectively. These are in excellent agreement with some of the recent suggestions of Wesely and co-workers (cf. Wesely and Shannon, 1984).

The present analysis has greater detail than the first-generation model. Boundary layer-free troposphere exchange in cloud-free and cloudy environments, and in-cloud and below-cloud wet removal and chemistry processes are described more adequately. In the following sections, details of each component of the model are presented.

MODEL DESCRIPTION

Overview

The regional-scale combined transport/chemistry/deposition model is Eulerian and treats 41 chemical species. Nineteen species are advected, while the remaining species are short-lived and are modeled using pseudo-steady state methods. The mathematical analysis consists of partial differential equations for the advected species and additional algebraic equations for the steady-state species. The advected species

Preceding page blank

satisfy

$$\frac{\partial c_i}{\partial t} + \nabla\cdot(\mathbf{v}c_i) = \nabla\cdot\mathbf{K}\cdot\nabla c_i + R_i + S_i - G_i,$$

$$i = 1, \ldots, 19; \quad (1)$$

where c_i is the gas-phase concentration of the ith chemical species, $\mathbf{v}$ is the wind velocity vector, $\mathbf{K}$ is the eddy diffusivity tensor, R_i denotes the chemical reaction term, S_i is the source term, and G_i is used to describe the mass transfer between the gas and condensed phases. The algebraic equations for the gas-phase species assumed to be at steady state are written as

$$R_i(c_1, c_2, \ldots, c_{41}) = 0, \quad i = 20, \ldots, 41. \quad (2)$$

The drop-phase species satisfy the equation

$$\frac{\partial (s_k c_{ik}^d)}{\partial t} + \nabla\cdot(\mathbf{v} - \mathbf{v}_{sk})s_k c_{ik}^d = \nabla\cdot(c_{ik}^d K_k^d\cdot\nabla s_k + R_{ik}^d + G_{ik}^d,$$

$$j = 1, \ldots, m; \quad (3)$$

where s_k denotes the liquid water content of phase k (e.g. cloud water, rain, ice), c_{ik}^d is the concentration of the ith species in the k phase, $\mathbf{v}_{sk}$ is the settling velocity of the hydrometers in phase k, R_{ik}^d represents the chemical reaction term, G_{ik}^d is the mass transfer with the gas phase (i.e. gas dissolution, desorption, condensation evaporation processes, etc.), and m represents the number of transported chemical species in phase k. The eddy diffusivity to describe the turbulent transport for the droplet-phase, K_k^d, depends on the characteristic size of the k phase and is different than the gas-phase eddy diffusivity tensor. Additionally, one should note that $\sum_k G_{ik}^d = G_i$.

The boundary conditions for Equation (1) are as follows:

For inflow (i.e. $\mathbf{n}\cdot\mathbf{v} < 0$),

$$\mathbf{n}\cdot(\mathbf{v}c_{i,b} - \mathbf{K}\cdot\nabla c_i) = \mathbf{F}_c; \quad (4)$$

For outflow (i.e. $\mathbf{n}\cdot\mathbf{v} \geq 0$),

$$[\mathbf{n}\cdot\mathbf{v}c_i - \mathbf{n}\cdot(\mathbf{K}\cdot\nabla c_i)]_{t+\Delta t} = [\mathbf{n}\cdot\mathbf{v}c_i - \mathbf{n}\cdot(\mathbf{K}\cdot\nabla c_i)]_t; \quad (5)$$

At the earth's surface,

$$-\mathbf{n}_b\cdot(\mathbf{K}\cdot\nabla c_i) = Q_i - v_{g_i}c_i. \quad (6)$$

In the above, $\mathbf{n}$ is an outward unit vector normal to the top boundary; $\mathbf{n}_b$ is an inward vector normal to the earth's surface; $c_{i,b}$, Q_i, and v_{g_i} denote the species concentration outside the region, surface emission rate, and deposition velocity of species i, respectively; and $\mathbf{F}_c$ represents a prescribed flux. Stratospheric inputs of NO_x, HNO_3, O_3, etc. can be handled in the model by this formulation. Similar boundary conditions are prescribed for Equation (3).

The analysis utilizes a surface following coordinate system, and the model domain, number of grids, and grid spacing (including non-uniform spacing) can be selected for the particular application. Currently, the height of the region is 8 km, so that boundary layer-free troposphere processes and interactions can be simulated.

Numerics

Simulation of regional transport, chemistry and deposition as described by Equations (1) and (3) requires numerical integration. The method presently used is a combination of the concept of fractional time steps and one-dimensional finite elements. This is referred to as the Locally One-Dimensional, Finite-Element Method (LOD-FEM). The LOD procedures (Mitchell, 1969) split the multi-dimensional partial differential equation into time dependent, one-dimensional problems which are solved sequentially. The time-split equations are of the form

$$\frac{\partial c_i}{\partial t} + L_x c_i = 0, \quad (7)$$

$$\frac{\partial c_i}{\partial t} + L_y c_i = 0, \quad (8)$$

$$\frac{\partial c_i}{\partial t} + L_z c_i = S_i, \quad (9)$$

$$\frac{\partial c_i}{\partial t} = R_i - G_i. \quad (10)$$

L_x, L_y and L_z represent the one-dimensional transport operators; e.g.,

$$L_x c_i = \frac{\partial (uc_i)}{\partial x} - \frac{\partial}{\partial x}\left(K_{xx}\frac{\partial c_i}{\partial x}\right).$$

The equations for the drop phases have the same form. The chemical reaction and mass transfer terms are treated separately becuase these can have time scales much smaller than that for the transport. Splitting out these terms allows different time steps to be specified for the transport and for the chemistry/removal processes.

The transport equations are solved using a Crank–Nicolson Galerkin finite element technique. An upwinding parameter (Heinrich *et al.*, 1977) and spatial filtering, as originally proposed by Forester (1977) and subsequently described by McRae *et al.* (1982), are features included in the analysis. Test calculations are presented in a subsequent section. An important feature of this numerical procedure is that the computer code is structured so that any combination of Equations (7) through to (10) can be used, enabling application to one, two, or three-dimensional time-dependent analysis.

The technique used to integrate the chemistry and mass transfer terms is an adaptation of the semi-implicit Euler method proposed by Preussner and Brand (1981). This method consists of writing Equation (10) in the form

$$\frac{\partial c_i}{\partial t} = -G_i, \quad (11)$$

$$\frac{\partial c_i}{\partial t} = R_i = P_i - D_i c_i. \quad (12)$$

P_i and D_i represent the chemical production and destruction terms. Similar equations can be written for the droplet phases.

$$\frac{\partial c_{ik}^{d}}{\partial t} = G_{ik}^{d} \tag{13}$$

$$\frac{\partial c_{ik}^{d}}{\partial t} = R_{ik}^{d} = P_{ik}^{d} - D_{ik}^{d} c_{ik}^{d}. \tag{14}$$

Over the time step $\Delta t_{j_{chem}}$, Equations (11) to (14) are solved analytically, assuming all other concentrations are constant during the time period. For cases when D_i or D_{ik}^{d} is small (e.g. HNO_3 at night), Equations (12) and (14) are solved by Taylor Series expansion. These procedures have the important properties that c_i and c_{ik}^{d} can never become negative, provided that the reaction rate constants are positive and the intitial values are non-negative. Furthermore, in the limit as $t \to \infty$, the proper steady state concentrations are obtained; i.e.,

$$c_i^{ss} = \frac{P_i}{D_i}. \tag{15}$$

Equations (12) and (14) are used to calculate advected species concentrations only. However, P_i and D_i also contain concentrations of the short-lived gas-phase species (e.g. OH, HO_2) which are calculated using appropriate pseudo-steady state approximations. This procedure results in algebraic equations that depend on the concentrations of the advected species. The calculation procedure to advance from t_j to $t_j + \Delta t_{j_{chem}}$ uses $c_i|_{t_j}$ to calculate the short-lived species concentrations, and then uses these concentrations to advance to $c_i|_{t_j + \Delta t_{j_{chem}}}$ using Equation (12).

The accuracy of this technique depends on the species of interest and $\Delta t_{j_{chem}}$. For long-lived species (e.g. SO_2, CO and alkanes), relatively large $\Delta t_{j_{chem}}$ can be used, but for more reactive species much smaller time steps are required. This pseudo-analytic technique can execute twice as fast as the Gear method for this chemical scheme.

Transport algorithm

The LOD-FEM procedure described previously has been evaluated by several workers including the present authors (cf. Carmichael *et al.*, 1980; Kitada *et al.*, 1983). More recently, Kasibhatla (1984) has evaluated the advection algorithm used in the second-generation model by investigating the accuracy of the solution of the one-dimensional advection equation.

$$\frac{\partial c}{\partial t} + u\frac{\partial c}{\partial x} = 0. \tag{16}$$

Advection of ideal waveforms with a constant wind has been a traditional approach. Kasibhatla's tests were based on advection of triangle, sine and square wave distributions of moderately narrow width. The triangle and square wave tests have very sharp gradients with discontinuous second derivatives at isolated position(s) in the waveform.

Selected results from Kasibhatla's study are shown in Fig. 1 for the three waveforms. These results demonstrate that the Crank–Nicolson Galerkin method, when applied to an advection-dominated problem, gives rise to numerical oscillations, primarily in the wake of the advected waveform. However, the upwinding scheme substantially minimizes this problem. Part of the diffusion that occurs results from filtering of the data. The reduction in peak value of the concentration depends on the shape of the waveform. These results also clearly show the advantages of using the upwinding scheme and the filtering routine. Greater stability of the numerical solution is obtained, and the method is readily applied to high Peclet number situations provided the Courant number ($u\Delta t/\Delta x$) is less than 1. Similar results for multi-dimensional simulations of advection/diffusion have been found also.

In the transport calculations, it is also necessary to recognize that input wind fields used to solve Equation (1) can be derived from either field observation using objective methods or numerical calculation of fluid dynamic equations. Observed wind fields generally do not satisfy exactly the equation of continuity, $\nabla \cdot \mathbf{v} = 0$. This introduces undesirable fictitious production and consumption terms into the numerical solution of Equation (1). For example, calculated concentrations of a conserved species undergoing transport within a flow field derived from a land/sea breeze flow model have shown large deviations due to non-zero divergences (cf. Kitada *et al.*, 1984).

In order to eliminate these effects, a divergence correction formulation is used. This simply subtracts the value of the divergence at each grid point from Equation (1). Thus,

$$\frac{\partial c_i}{\partial t} + \nabla \cdot (\mathbf{v} c_i) - (\nabla \cdot \mathbf{v}) c_i = \nabla \cdot \mathbf{K} \cdot \nabla c_i + R_i + S_i - G_i,$$

$$i = 1, \ldots, 19. \tag{17}$$

The effectiveness of Equation (17) has been demonstrated by Kitada *et al.* (1984).

Chemistry

The chemical pathways controlling regional-scale conversion and oxidation mechanisms involve homogeneous gas-phase reactions, heterogeneous aerosol processes, and aqueous-phase chemistry that occurs in cloud and precipitation drops. Description of these processes is integral to the overall model analysis. The coupling among the chemical processes is illustrated in Fig. 2. These interactions are, for the most part, self explanatory. Each will be discussed in greater detail. In this section, the homogeneous chemistry and treatment of the heterogeneous chemistry are presented. Description of the aqueous-phase chemical processes is reserved for the section on hydrometeor processes.

For the chemistry, the primary concern is with R_i in Equation (1). An equation must be written for each species that is present in the gas phase. Additional

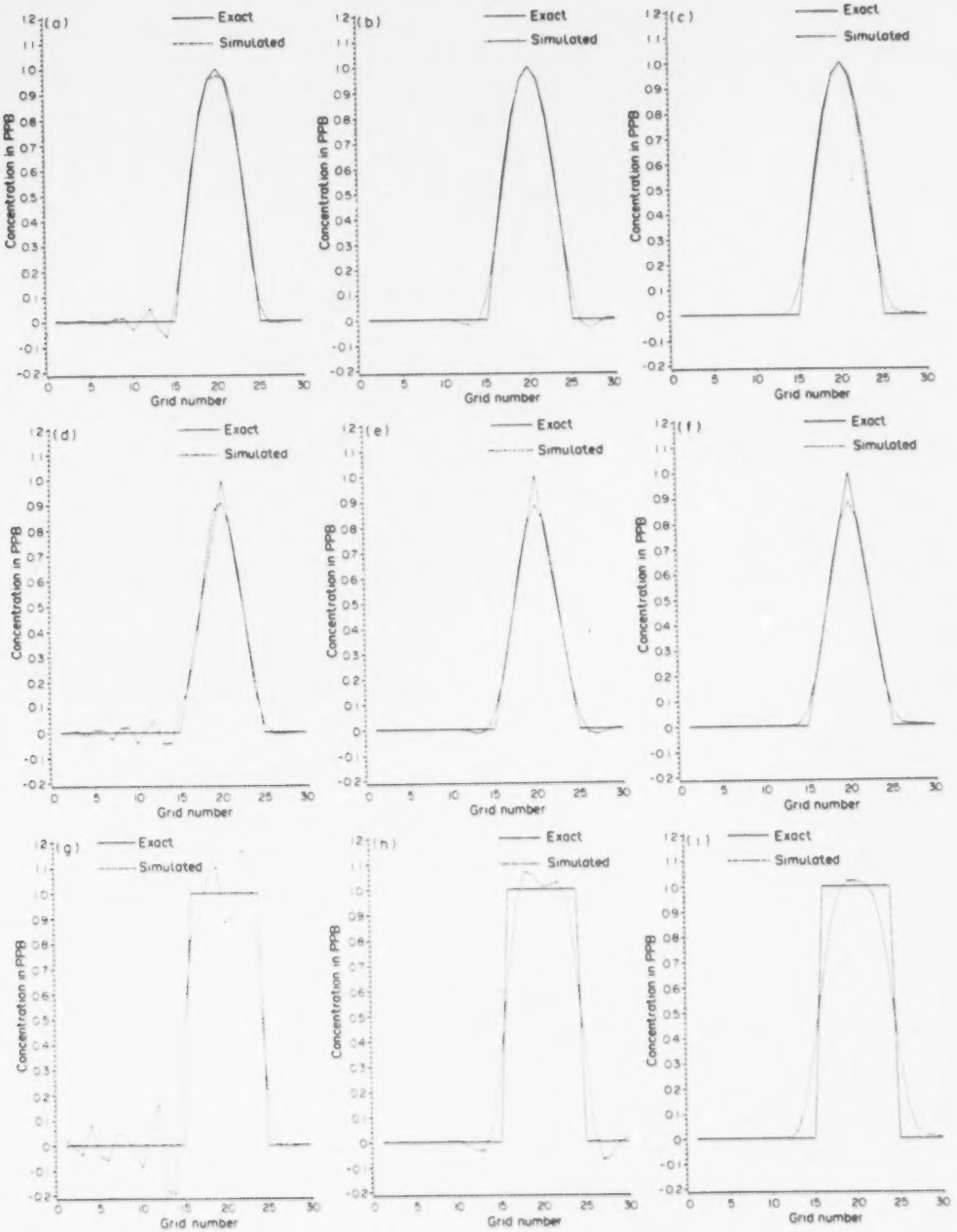

Fig. 1. One-dimensional pure advection test of the Crank–Nicolson Galerkin finite element method with piece-wise linear basis functions. Sine Wave, Triangle Wave, and Square Wave initial wave forms are shown. Plotted are results after 24 h of transport (~ 96 time steps) for the cases without upwinding and without filter (left column), with upwinding and without filter (middle), and with upwinding and filter (right column).

equations for that same species and for other species in the various liquid phases must also be written. Furthermore, if one considers a distribution of drop sizes, then an equation for the species will be required for each drop size. Obviously, all species will not be present in all phases.

Another consideration is the effect of turbulence on limiting the rate of reaction. Even with advanced regional-scale chemical modules, this effect has been ignored for complex reaction mechanisms. There has

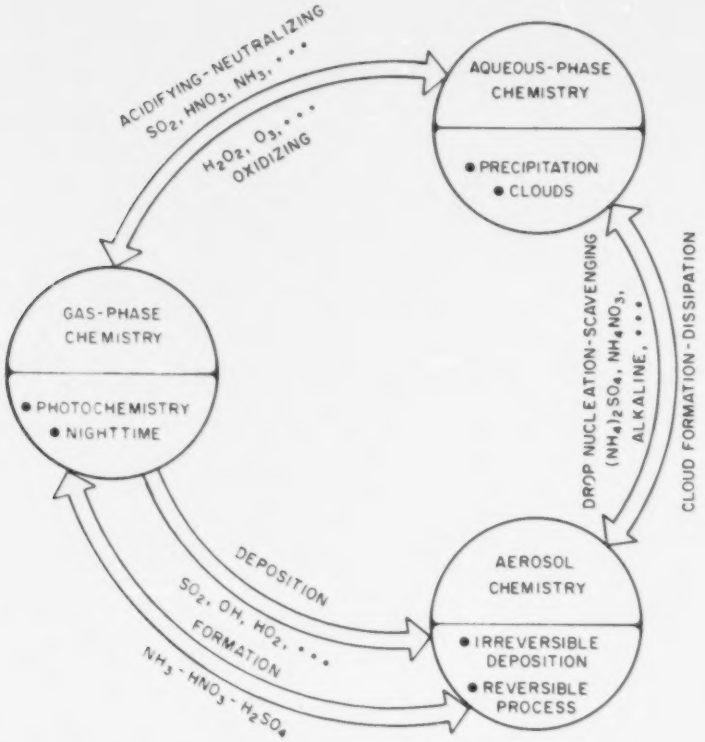

Fig. 2. Schematic of chemical processes treated in the model.

been some research indicating the importance of these effects in the near-source regions (cf. Donaldson and Hilst, 1972; Shu *et al.*, 1978; Carmichael and Peters, 1981; Karamchandani and Peters, 1986). However, these effects have not been included in this chemical module.

Homogeneous gas-phase chemistry. The reaction mechanism listed in Table 1 (adapted from Balko and Peters, 1983) shows the gas-phase chemistry. Very generally, the scheme is based on a lumped hydrocarbon species concept with the following breakdown: alkanes, alkenes (olefins), aromatics, C_2H_4, CH_2O, and higher aldehydes. The philosophy behind this lumping scheme is to divide the hydrocarbons according to reactivity and free radical pathways (Falls *et al.*, 1979). A much finer hydrocarbon breakdown does not seem appropriate, since hydrocarbon emissions data at this time are not much more detailed. Furthermore, this lumping is sufficiently detailed to provide representative free radical initiation, propagation, and termination steps based on current knowledge.

The scheme includes the gas-phase oxidation of SO_2 by both OH and HO_2. This feature provides a base to use the mechanism for plume chemistry, urban air chemistry, and clear air chemistry with some modifications. Reactions (1) through to (56) follow the Falls *et al.* (1979) mechanism, and are primarily responsible for the hydrocarbon/NO_x/O_3 chemistry associated with photochemical smog. Of these reactions, those involving free radicals form the largest part of the mechanism. These species may come about in two ways: (a) formation from more stable species as in Reactions (1), (14), (15), (24), (34) and (39) which are initiation reactions; or (b) formation from existing free radicals, Reactions (16), (17), (21), (29), (30), (37), (38), (40), (41), (42) and (43), which are chain propagating. Free radicals are consumed by Reactions (4), (5), (6), (18), (19), (22), (23), (26), (27), (28), (45) and (47) through to (50). These radicals terminate the free radical chain and form stable end products.

Some recent evidence indicates that the O_3–olefin reaction may have significant implications in night-time atmospheric chemistry. The Criegee mechanism has been advanced as the predominant pathway for this reaction. An important by-product of this mechanism is the stable intermediate RCHOO and possibly OH and HO_2 radicals. Calvert *et al.* (1978) have shown that RCHOO may react to a limited extent with SO_2. At night-time in high hydrocarbon/NO_x situations (e.g. aged plumes), the O_3–olefin reaction can occur at an appreciable rate. This provides not only RCHOO but also the OH and HO_2 necessary for significant homogeneous gas-phase oxidation of SO_2. This can then occur without direct photochemical initiation.

Table 1. Reactions used in the gas-phase chemistry model (after Balko and Peters, 1983)

	Reaction	Rate constant*
1.	$NO_2 + v \rightarrow NO + O(^3P)$	variable
2.	$O(^3P) + O_2 + M \rightarrow O_3 + M$	$6.2 \times 10^{-34} (T/300)^{-2}$
3.	$O_3 + NO \rightarrow NO_2 + O_2$	$2.3 \times 10^{-12} \exp(-1450/T)$
4.	$NO_2 + O(^3P) \rightarrow NO + O_2$	9.3×10^{-12}
5.	$NO_2 + O(^3P) + M \rightarrow NO_3 + M$	$9.0 \times 10^{-32} (T/300)^{-2}$
6.	$NO + O(^3P) + M \rightarrow NO_2 + M$	$1.2 \times 10^{-31} (T/300)^{-1.8}$
7.	$NO_2 + O_3 \rightarrow NO_3 + O_2$	$1.2 \times 10^{-13} \exp(-2450/T)$
8.	$NO_3 + NO \rightarrow 2NO_2$	2.0×10^{-11}
9.	$NO_3 + NO_2 + M \rightarrow N_2O_5 + M$	$1.4 \times 10^{-30} (T/300)^{-2.8}$
10.	$N_2O_5 + M \rightarrow NO_2 + NO_3 + M$	$8.8 \times 10^{-6} \exp(-9700/T)$
11.	$N_2O_5 + H_2O \rightarrow 2HONO_2$	1.0×10^{-20}
12.	$NO + NO_2 + H_2O \rightarrow 2HONO$	6.0×10^{-38}
13.	$HONO + HONO \rightarrow NO + NO_2 + H_2O$	9.5×10^{-19}
14.	$O_3 + hv \rightarrow O_2 + O(^1D)$	variable
15.	$O_3 + hv \rightarrow O_2 + O(^3P)$	variable
16.	$O(^1D) + M \rightarrow O(^3P) + M$	$2.0 \times 10^{-11} \exp(107/T)$
17.	$O(^1D) + H_2O \rightarrow 2OH$	2.3×10^{-10}
18.	$HO_2 + NO_2 \rightarrow HONO + O_2$	3.0×10^{-15}
19.	$HO_2 + NO_2 + M \rightarrow HO_2NO_2 + M$	$2.1 \times 10^{-31} (T/300)^{-5}$
20.	$HO_2NO_2 \rightarrow HO_2 + NO_2$	$2.87 \times 10^{13} \exp(-10015/T)$
21.	$HO_2 + NO \rightarrow NO_2 + OH$	$4.3 \times 10^{-12} \exp(200/T)$
22.	$OH + NO + M \rightarrow HONO + M$	$6.7 \times 10^{-31} (T/300)^{-3.3}$
23.	$OH + NO_2 + M \rightarrow HONO_2 + M$	$2.6 \times 10^{-30} (T/300)^{-2.9}$
24.	$HONO + hv \rightarrow OH + NO$	variable
25.	$CO + OH \xrightarrow{O_2} CO_2 + HO_2$	$1.35 \times 10^{-13} (1 + P_{atm})$
26.	$OH + HONO \rightarrow H_2O + NO_2$	6.6×10^{-12}
27.	$HO_2 + HO_2 \rightarrow H_2O_2 + O_2$	2.5×10^{-12}
28.	$OH + HO_2 \rightarrow H_2O + O_2$	4.0×10^{-11}
29.	$OH + O_3 \rightarrow HO_2 + O_2$	$1.6 \times 10^{-12} \exp(-940/T)$
30.	$HO_2 + O_3 \rightarrow OH + 2O_2$	$1.1 \times 10^{-14} \exp(-580/T)$
31.	$HCHO + hv \xrightarrow{O_2} HO_2 + HCO$	variable
32.	$HCHO + hv \rightarrow H_2 + CO$	variable
33.	$HCHO + OH \rightarrow HCO + H_2O$	1.0×10^{-11}
34.	$HCO + O_2 \rightarrow HO_2 + CO$	5.0×10^{-12}
35.	$RCHO + hv \xrightarrow{O_2} RO_2 + HCO$	variable
36.	$RCHO + OH \rightarrow RCO_3 + H_2O$	1.42×10^{-11}
37.	$OL + OH \rightarrow RO_2$	$4.11 \times 10^{-12} \exp(544/T)$
38.	$OL + O(^3P) \rightarrow RO_2 + RCO_3$	$4.11 \times 10^{-12} \exp(-38/T)$
39.	$OL + O_3 \rightarrow 0.5\delta HCHO + (1 - 0.5\delta)RCHO + 0.5(\varepsilon)(\zeta + 0.5\eta)RO_2 + 0.25(\varepsilon)(\zeta + \eta)HO_2 + 0.25(\varepsilon\zeta)OH + 0.25(\varepsilon\eta)RO + 0.25(\varepsilon\eta)HCO + 0.5(1 - \varepsilon)RCHOO$	$6.12 \times 10^{-15} \exp(-1900/T)$
40.	$ALK + OH \rightarrow RO_2$	$1.77 \times 10^{-11} \exp(-560/T)$
41.	$ALK + O(^3P) + RO_2 + OH$	$4.82 \times 10^{-11} \exp(-2900/T)$ $8.83 \times 10^{-11} \exp(-2250/T)$
42.	$C_2H_4 + OH \rightarrow RO_2$	$2.2 \times 10^{-12} \exp(385/T)$
43.	$C_2H_4 + O(^3P) \rightarrow RO_2 + HCO$	$5.5 \times 10^{-12} \exp(-565/T)$
44.	$RO \rightarrow \alpha HO_2 + (1 - \alpha)RO_2 + \beta HCHO + \gamma RCHO$	3340
45.	$NO + RO \rightarrow RONO$	3.33×10^{-10}
46.	$RONO + hv \rightarrow RO + NO$	variable
47.	$NO_2 + RO \rightarrow RONO_2$	1.05×10^{-11}
48.	$NO_2 + RO \rightarrow RCHO + HONO$	9.17×10^{-13}
49.	$NO_2 + RO_2 \rightarrow RO_2NO_2$	3.73×10^{-12}
50.	$NO_2 + RO_2 \rightarrow RCHO + HONO_2$	3.73×10^{-15}
51.	$RO_2NO_2 \rightarrow NO_2 + RO_2$	8.33×10^{-3}
52.	$NO + RO_2 \rightarrow NO_2 + RO$	8.15×10^{-12}
53.	$NO + RCO_3 \rightarrow NO_2 + RO_2$	2.58×10^{-12}

Table 1. (*Contd.*)

Reaction	Rate constant*
54. $NO_2 + RCO_3 \rightarrow PAN$	1.41×10^{-12}
55. $PAN \rightarrow NO_2 + RCO_3$	$7.95 \times 10^{14} \exp(-12516/T)$
56. $ARO + OH \rightarrow RO_2 + RCHO$	1.67×10^{-11}
57. $SO_2 + HO_2 \rightarrow OH + SO_3$	1×10^{-18}
58. $SO_2 + OH + M \rightarrow HSO_3 + M$	$3.0 \times 10^{-31} (T/300)^{-2.9}$
or 58. $SO_2 + OH + M \xrightarrow[O_2]{H_2O} H_2SO_4 + HO_2 + M$	$3.69 \times 10^{-4} \exp(1007/T)$
59. $SO_2 + O(^3P) + M \rightarrow SO_3 + M$	$4.0 \times 10^{-32} \exp(-1000/T)$
60. $SO_2 + RO_2 \rightarrow RO + SO_3$	5.3×10^{-15}
61. $SO_2 + RO \rightarrow RSO_3$	6.04×10^{-15}
62. $SO_2 + RCHOO \rightarrow RCHO + SO_3$	4.3×10^{-15}
63. $SO_2 \rightarrow$ particle	3.0×10^{-6}
64. $SO_3 + H_2O \rightarrow H_2SO_4$ (Part.)	9.1×10^{-13}
65. $HSO_3 + O_2 \rightarrow HSO_5$	1.7×10^{-12}
66. $HSO_5 + H_2O \rightarrow HSO_5 \cdot H_2O$ (Part.)	2.51×10^{-13}
67. $RSO_3 + O_2 \rightarrow RSO_5$	8.89×10^{-15}
68. $RSO_5 + H_2O \rightarrow RSO_5 \cdot H_2O$ (Part.)	1.3×10^{-15}
69. $RCHOO + H_2O \rightarrow RCOOH + H_2O$	7.6×10^{-16}
70. $NH_3 + HNO_3 \xrightarrow{M} NH_4NO_3$	1.95×10^{-17}

* Rate constants are in molecules-cm^{-3}-s units; T is temperature in Kelvin.

Results presented by Balko and Peters (1983) and Kasibhatla (1984) indicate the potential importance of this chemistry at night-time.

NO_x chemistry may also be important at night-time in producing acidifying compounds (cf. Platt *et al.*, 1980a, b). For example, residual O_3 at night-time can oxidize NO_2 according to Reaction (7). This and the following additional reactions represent a night-time source of HNO_2 and HNO_3 (cf., Stockwell and Calvert, 1983a); i.e.

$$NO_2 + O_3 \rightarrow NO_3 + O_2,$$

$$NO_3 + NO \rightarrow 2NO_2,$$

$$NO_3 + NO_2 \rightarrow N_2O_5,$$

$$N_2O_5 \rightarrow NO_2 + NO_3,$$

$$N_2O_5 + H_2O \rightarrow 2HNO_3,$$

$$NO_2 + HO_2 \rightarrow HNO_2 + O_2.$$

These considerations and the foregoing discussion on the O_3–olefin reaction indicate that high hydrocarbon/NO_x ratios may lead to SO_2 oxidation and H_2SO_4 formation at night-time, whereas lower hydrocarbon/NO_x ratios may lead to NO_3, HNO_2 and HNO_3 formation at night-time.

Oxidation of SO_2 to H_2SO_4 and other sulfate species in the gas phase is predominantly by reaction with free radicals. As already noted, the two most important radicals appear to be OH [Reaction (58)] and HO_2 [Reaction (57)], of which OH seems to be considerably more important. Direct photo-oxidation of SO_2 is decidedly unimportant. It is rather well agreed that the fate of SO_3 from Reaction (57) is near instantaneous reaction with H_2O to form H_2SO_4. The fate of HSO_3 from Reaction (58) is considerably less certain, and the steps shown [Reactions (65) and (66)] have been suggested by Davis *et al.* (1979) and others. However, a recent model study by Stockwell and Calvert (1983b) indicates that a more suitable fate for the HSO_5 formed in Reaction (65) may be decomposition into SO_3 and HO_2. This suggestion is important from two aspects. First, SO_3 is formed directly; and secondly, the reaction is not chain terminating, since HO_2 is produced and can participate in other reactions. However, simulations representative of rather polluted air mass concentration levels using this overall scheme have not shown substantial differences.

The gas-phase chemistry described in Table 1 has been evaluated and shows reasonable agreement with some field experiments. Balko and Peters (1983) modeled the August 1975 field experiments conducted within the urban St. Louis plume (Alkezweeny and Powell, 1977). The St. Louis plume is characterized by relatively high hydrocarbon/NO_x ratios and substantial SO_2 concentrations. Figure 3 shows the ratio of SO_2 to total sulfur as a function of time for both observed and simulated values. In both cases, surprisingly high conversion rates (10–14 %h^{-1}) were reported. This shows that, in the presence of high hydrocarbon/NO_x ratios, high gas-phase conversion rates can be predicted.

Heterogeneous chemistry. The two aspects illustrated in Fig. 2 for aerosol processes are direct, irreversible deposition of species on atmospheric particles and interactions between the aerosol com-

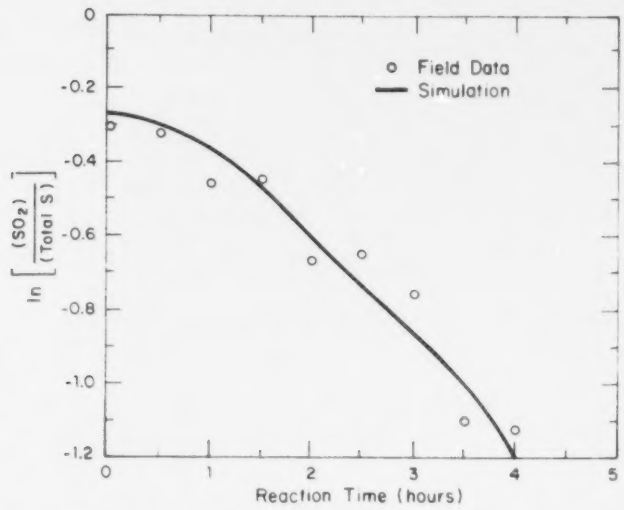

Fig. 3. Comparison of predicted SO_2/(total sulfur) ratios using the model chemistry with observations of the urban St. Louis plume.

position and the gas-phase concentrations of NH_3, HNO_3 and H_2SO_4.

The first process, irreversible deposition, has been considered by several authors including Luther and Peters (1982) and Thompson and Heikes (1982). While these processes obviously affect the composition of the aerosol phase, it is equally or more important to note that the gas-phase composition can also be substantially affected, leading to an apparent irreversible loss of the species from the gas phase. The analysis of Luther and Peters (1982) has been adopted in this study, and treats the mass exchange between the gas phase and aerosol phase by kinetic theory for very small particles and by continuum theory for the larger particles. In either case, characterization of the physico–chemical interactions is only approximately known, leading to some uncertainties.

For kinetic theory a principal limitation is knowledge of the accommodation coefficient, while for continuum mass transfer the limitation is related to solubility, equilibrium distribution coefficient, or adsorption isotherm between the aerosol and gas phases. If one assumes an accommodation coefficient of unity, heterogeneous loss constants on the order of $10^{-4}\,s^{-1}$ are estimated, indicating that heterogeneous rates could dominate the known homogeneous processes. One of the more striking examples is for HNO_3, where the homogeneous gas-phase loss processes have a rate constant on the order of 10^{-6}–$10^{-7}\,s^{-1}$, compared to $10^{-4}\,s^{-1}$ or higher for heterogeneous processes. Other differences, although less substantial, are also noted for HCHO and H_2O_2. Some typical values are shown in Table 2. It seems that more laboratory data will be forthcoming during the next 2–3 years to better quantify these interactions.

One example of the importance of deposition onto aerosol surfaces is presented in Fig. 4. Model results comparing the predicted photostationary state parameter under conditions where heterogeneous removal is included or is ignored are compared to the measured values of Shetter *et al.* (1983). Although the actual field study conditions (i.e. the dynamics, upwind sources, etc.) have not been simulated, the results do indicate that the observed values fall within the variability introduced by the inclusion of heterogeneous removal. These results also suggest that the relative importance of heterogeneous removal may vary diurnally, with heterogeneous removal having minimum influence during the mid-afternoon period. This diurnal behavior may be coupled to those aerosol processes and meteorological factors that determine whether the aerosol is a solid or a liquid (e.g. relative humidity, temperature, etc.).

A subset of the aerosol chemistry that has been

Table 2. Typical calculated heterogeneous loss constants for aerosol–gas interactions*

Species	$k_{het}\ (s^{-1})$
NO	1.4×10^{-8}
O_3	6.7×10^{-8}
OH	1.1×10^{-3}
H_2O_2	6.2×10^{-4}
HNO_3	6.5×10^{-4}
NO_3	6.7×10^{-4}
O_2	7.0×10^{-9}
NO_2	7.6×10^{-4}

*These values are based on the aerosol size distribution of Junge (1963) with a surface area of $5.2\,\mu m^2\,cm^{-3}$ and an accommodation coefficient of unity.

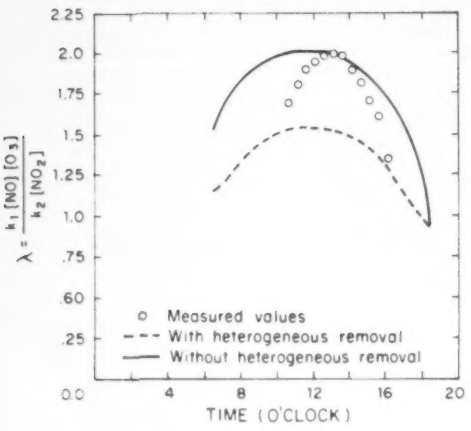

Fig. 4. Model simulation of the effect of heterogeneous removal on the predicted photostationary state parameter. Also shown are the observations of Shetter *et al.* (1983).

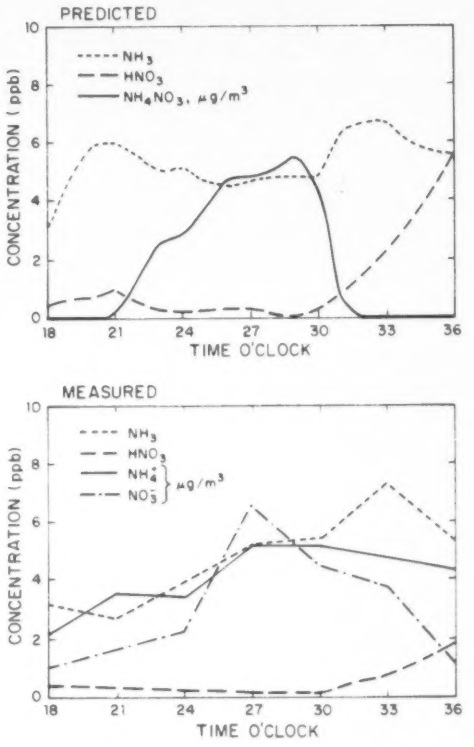

Fig. 5. Simulation of the model using the aerosol equilibrium assumption for the ammonium nitrate system. Predictions and measurements are shown for 29 and 30 July 1983, at Nagano Prefecture, Japan.

reasonably well studied is the NH_3–HNO_3–H_2SO_4–NH_4NO_3–$(NH_4)_2SO_4$ system. Stelson *et al.* (1979) originally suggested that an equilibrium relationship may exist among NH_3, HNO_3 and particulate NH_4NO_3. This has been generalized to aqueous solutions of nitrate, sulfate and ammonium (Stelson and Seinfeld, 1982a, b). The relevant point in terms of the chemistry is that computing such equilibrium interactions requires the NH_3 concentration, production rates of H_2SO_4 and HNO_3, temperature, and relative humidity. All of these variables are available from a gas-phase chemistry scheme like that shown in Table 1. Russell *et al.* (1983) have performed some comparisons with such an approach on an urban scale and have shown variable success.

This aerosol equilibrium approach has also been incorporated into the second generation model. Ground level NH_3, HNO_3, and aerosol NH_4^+ and NO_3^- measured at Nagano Prefecture, Japan on 29 and 30 July 1983 are compared with predicted values in Fig. 5. The predicted results compare favorably with the measurements. Conditions of high relative humidity and low temperature at night are shown to favor NH_4NO_3 aerosol formation.

Hydrometeor processes

Hydrometeors in the form of clouds and precipitation provide transport/chemical processes that can substantially affect the distribution of trace species in the atmosphere. The second-generation model is structured to treat these processes in detail. The chemical/physical interactions involving hydrometeors and the gas and aerosol phases are shown schematically in Fig. 2.

The effects of hydrometeors on the gas-phase concentrations are incorporated through G_i in Equation (1), and the droplet phase mass balance equation given by Equation (3). The mass exchange between the gas phase and droplet phases can be treated in various degrees of sophistication, ranging from highly parameterized schemes to detailed microphysical analyses.

The mass transfer rates between the gas phase and droplets are calculated as

$$G_{ik}^{d} = \int_r 4\pi r^2 k_{g_i}(r) n(r) (c_i - H_i c_{ik}^{d}) \, dr, \qquad (18)$$

where r represents the drop radius, $n(r)$ the number of droplets per unit volume of radius r, H_i is the Henry's Law constant, and k_{g_i} is the mass transfer coefficient. The chemistry occurring in the aqueous phases is still highly uncertain. However, the model is structured so that aqueous-phase chemistry can be treated in various degrees of detail, ranging from pseudo first-order processes to a comprehensive mechanism including free radical reactions. The mechanism used in current applications is that discussed by Adewuyi *et al.* (1984). The oxidation reactions are shown in Table 3. In addition to these reactions, expressions involving the dissociation phenomena and interfacial equilibrium relationships are also included.

The effect of clouds on the solar flux values is also included in the analysis. Currently, the effects of clouds on the photon flux are included in the calculation through use of the following empirical correlation

Table 3. Cloudwater oxidation reactions

	Reaction rate constants 25°C ($M^{-1}S^{-1}$)
$O_3 + HSO_3^- \rightarrow HSO_4^- + O_2$	3.1×10^5
$O_3 + SO_3^{2-} \rightarrow SO_4^{2-} + O_2$	2.2×10^9
$H_2O_2 + HSO_3^- \rightarrow HSO_4^-$	5.2×10^7
$HSO_4^- + OH \rightarrow SO_4^- + H_2O$	1.0×10^6
$SO_4^- + Cl^- \rightarrow SO_4^{2-} + Cl$	2.0×10^8
$OH + HSO_3^- \rightarrow 0.5\,SO_4 + 0.5\,SO_4^- + OH$	9.5×10^9
$CH_2(OH)_2 + OH \rightarrow CH(OH)_2 + H_2O$	2.0×10^9
$CH(OH)_2 + O_2 \rightarrow HO_2 + HCOOH\,(aq)$	4.5×10^9
$HCOO^- + OH \rightarrow H_2O + CO_2 + HO_2$	3.0×10^9
$OH + H_2O_2 \rightarrow HO_2 + H_2O$	45×10^7
$O_2^- + HO_2 \rightarrow HO_2^- + O_2$	8.5×10^7
$O_2^- + HCO_3 \rightarrow HO_2^- + CO_3^-$	1.5×10^6
$CO_3^- + O_2^- \rightarrow CO_3^{2-} + O_2$	4.0×10^8
$CO_3^- + H_2O_2 \rightarrow CO_3^{2-} + H_2O_2^+$	
$OH + Cl^- + H^+ \rightarrow Cl$	2.0×10^{10}
$Cl_2^- + HO_2 \rightarrow 2Cl^- + H^+ + O_2$	4.5×10^9
$O_2^- + O_3 \xrightarrow{H^+} OH + 2O_2$	1.0×10^9
$CH_2(OH)O^- + H_2O_2 \rightarrow H_2COOH + OH^- + OH$	5.3
$HCHO + HSO_3^- \rightarrow CH_2(OH)SO_3^-$	2.4×10^{-1}

relating photon flux to cloud cover (Kaiser and Hill, 1976),

$$F = F_c(1 - AC^{1.75}), \tag{19}$$

where F_c is the photon flux for clear sky, and C is the cloud cover fraction. A is a constant dependent on cloud type, which has a value of 0.55 for fair weather cumulus or patches of cirrus or cumulus clouds. Also, the increase of photon flux due to cloud albedo is included by multiplying the clear sky flux at grid points directly above the cloud level by a factor of 1.3.

Simulations illustrating the importance of some of these processes are presented in a subsequent section.

Model inputs

The model requires source distributions, initial conditions, and meteorological data for input, and is structured to handle spatial and temporal variations in all inputs. The meteorological inputs are treated externally to the transport/chemistry/deposition calculations. Thus, the model can be executed with representative hypothetical inputs, with data determined from objective analysis of observations, or with values derived by meteorological models.

Currently, the diurnal boundary layer is described using the one-dimensional boundary layer model developed by Yamada and Mellor (1975). However, this is not necessary since it is not integral to the model. The dry deposition velocities are calculated from estimates of the aerodynamic and surface resistances and can vary both temporally and spatially. The aerodynamic resistance is estimated using the turbulence length scales calculated in the boundary layer model. The surface resistances are calculated based on the chemical and physical properties of the deposited species [see Carmichael and Peters (1984a) for more details].

MODEL SIMULATIONS

The analysis is being used for a variety of simulation applications. Some of these are (a) transport of SO_2/NO_x/hydrocarbon urban plumes to the background troposphere (Balko and Peters, 1983); (b) sulfate, nitrate, and oxidant formation in the presence of a land/sea breeze (Kitada *et al.*, 1984); (c) effects of in-cloud scavenging on homogeneous gas-phase chemistry (Carmichael *et al.*, 1983); (d) effects of cloud processes (i.e. in-cloud chemistry and transport) on the distribution of trace gases (Hong and Carmichael, 1983); and (e) regional-scale transport of SO_2 and sulfate in the eastern United States. In this section, illustrative results further demonstrating the model's features are discussed. Detailed analyses of the simulation results can be found in the papers cited.

The first illustration is a simulation using two-dimensional flow fields, liquid water content, and temperature fields generated by the convective cloud model of Orville and co-workers (cf. Orville and Kopp, 1977). The meteorological fields and predicted pollutant profiles are presented in Figs 6 and 7. The evolution of the predicted NH_3 concentration (in the hypothetical situation of no cloud removal) shows the rapid vertical transport through the convective cell and the slow downward transport associated with the subsiding air. At later times the horizontal transport of the upper air mass is clearly shown. The contours of

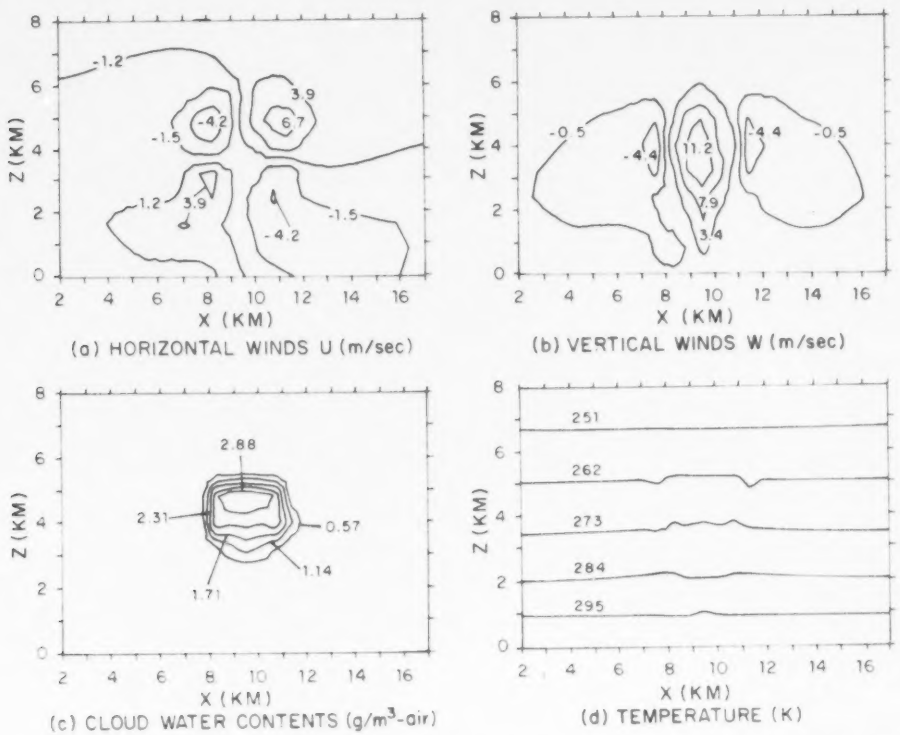

Fig. 6. Meteorological fields used in a 2-dimensional model simulation of a convective cloud. The meteorological inputs are from the model of Orville (cf. Orville and Kopp, 1977).

NH_3 when heterogeneous removal is included show the effectiveness of clouds in removing soluble species from the ingested air.

Complex coupling between gas-phase and cloud-phase processes is further illustrated with a one-dimensional model simulation where a non-precipitating cloud appears at 2 km elevation at 10:00 and disappears at 19:45. Results with a simulation having a surface source are shown in Figs 8 and 9. The aqueous-phase chemistry used in this simulation is that listed in Table 3. The surface source strengths used for NO, NO_2, SO_2, alkanes, C_2H_4, olefins and aromatics were 1.8, 0.2, 1.5, 3.0, 2.4, 1.0, 1.0, and 1.0 ($\times 10^{11}$) molecules cm^{-2}-s, respectively.

Time series plots of SO_2 and H_2O_2 are plotted as a function of time in Fig. 8. As shown, the H_2O_2 concentration decreases as the HSO_3^- concentration increases. This reflects the rapid uptake of H_2O_2 and inability of photochemical production of H_2O_2 to keep pace with its liquid phase destruction by the reaction with HSO_3^-.

The vertical profiles of gas-phase sulfate are shown in Fig. 9. The relative importance of the in-cloud and the gas-phase production processes are illustrated. The sharp increase in gas-phase sulfate after 19:00 is due to injection of sulfate that was generated in the cloud into the gas phase when the cloud evaporated. Nearly 70% of the sulfate in the air mass is formed by in-cloud processes. Under the conditions simulated, the sulfate formation is dominated by the HSO_3^- reaction with H_2O_2 (about 15% of the H_2O_2 was generated in-cloud).

Similar interactions between the gas phase and cloud phase are shown in a two-dimensional simulation where a cloud is transported within a uniform wind field over a surface source region and then evaporated (see Fig. 10). In this simulation, the equation for cloud-phase sulfate is described by Equation (3) with $R_i - G_i = 2.8 \times 10^{-5} c_{SO_2}$. Predicted sulfate concentrations at cloud-level in the gas phase and the cloud phase are also presented in Fig. 10. The in-cloud sulfate concentrations increase as the cloud travels over the source region. The relative concentrations of sulfate in the gas phase and in the cloud phase illustrate the significance of in-cloud sulfate production. These simulation results also clearly show evaporation of the cloud, causing a sudden increase in gas-phase sulfate. The decrease in gas-phase sulfate after evaporation is due to diffusion processes. The sulfate concentration predicted for the case where there are no clouds is also presented for comparison.

The effect of clouds on the photon flux is shown clearly in the OH contour plots in Fig. 11. The OH concentrations are significantly lower below cloud,

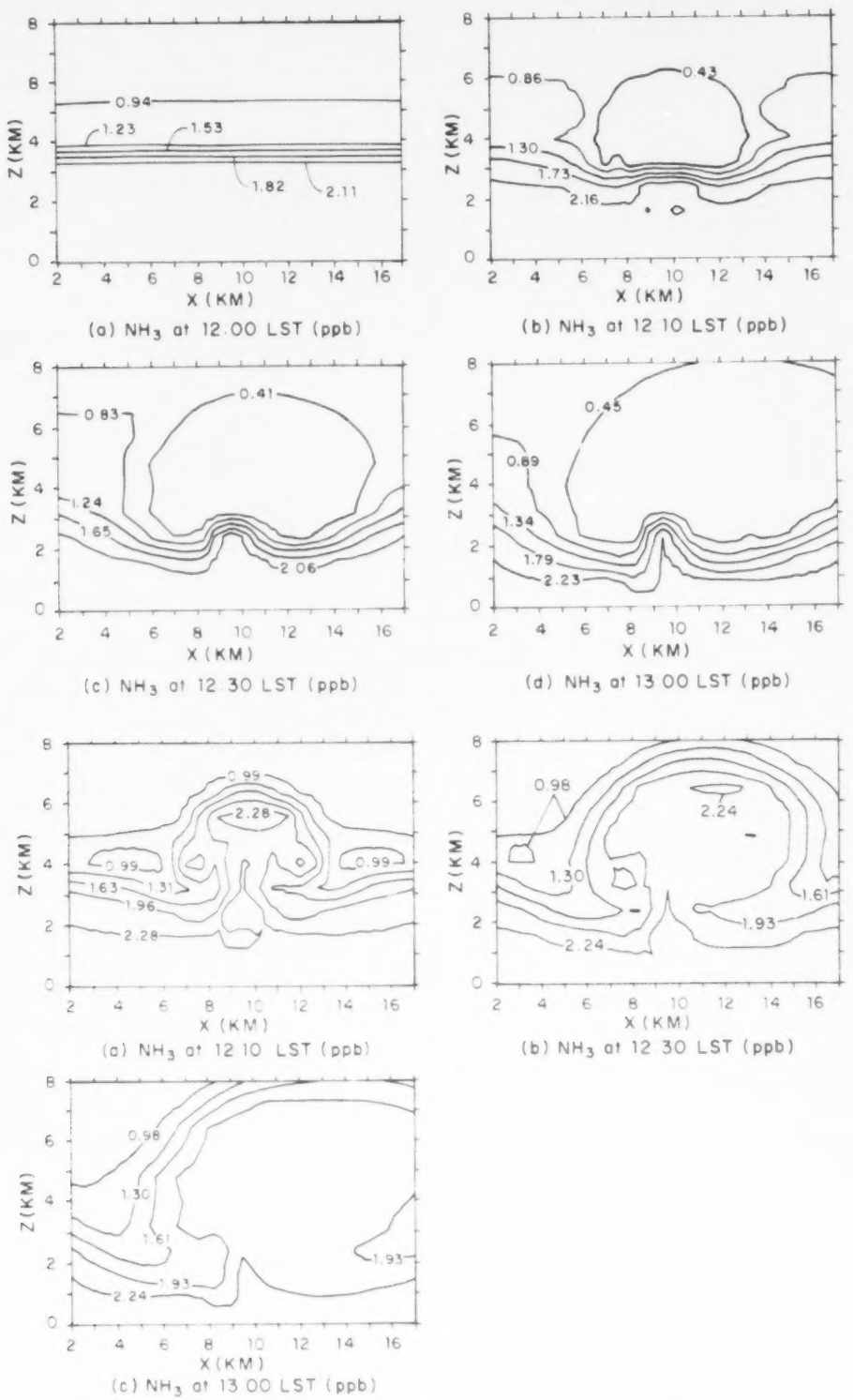

Fig. 7. Predicted NH_3 concentration fields for the case where in-cloud removal is included in the calculation (the upper sequence) and where the in-cloud removal is neglected (i.e. for an insoluble species).

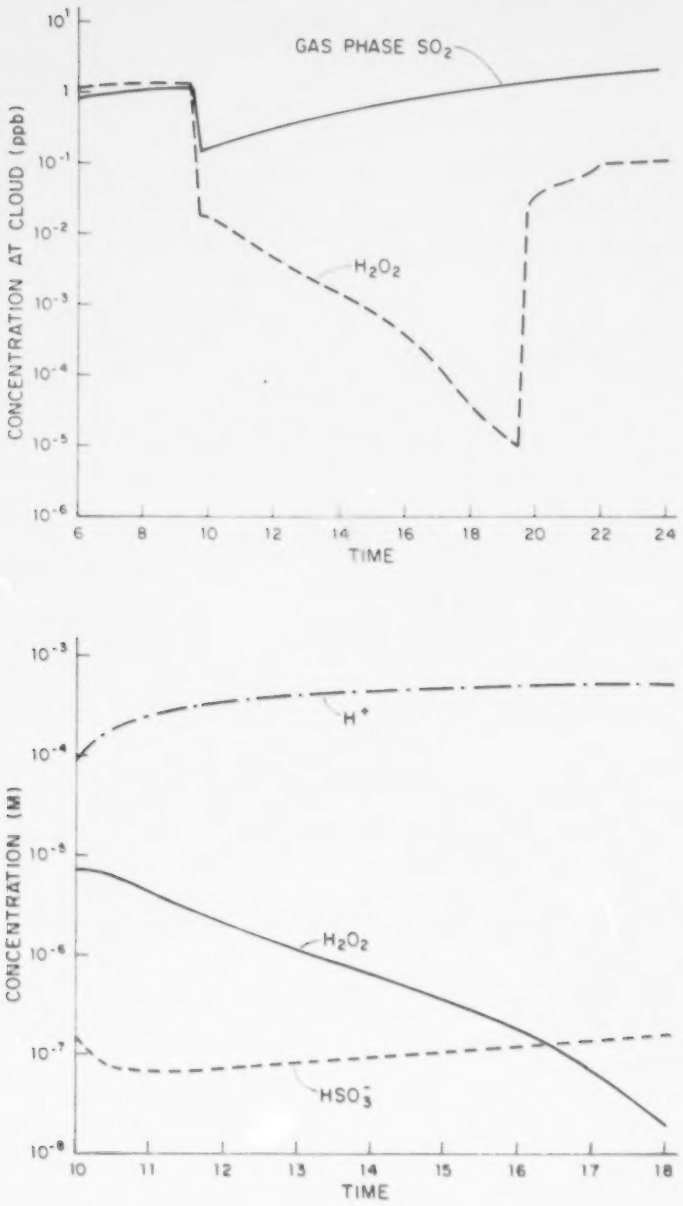

Fig. 8. Predicted cloud-level gas phase SO_2 and H_2O_2 concentrations (upper figure) and cloudwater H^+, HSO_3^-, and H_2O_2 concentrations (lower figure) for a simulation when a non-precipitating cloud forms at 10:00 and disappears at 19:45.

and this area of reduced concentration moves with the cloud transport.

SUMMARY

Model analysis of atmospheric processes can play an important role in understanding the impact of different sources on regional-scale air quality. A second-generation Eulerian model, primarily directed at analyzing regional-scale transport and deposition of O_3, SO_x, NO_x, and other trace gas species, has been presented. The major advances relative to the initial regional-scale model are improved chemistry, incorporation of wet deposition and heterogeneous chemical processes and improved numerics.

The model and its components have, thus far, been

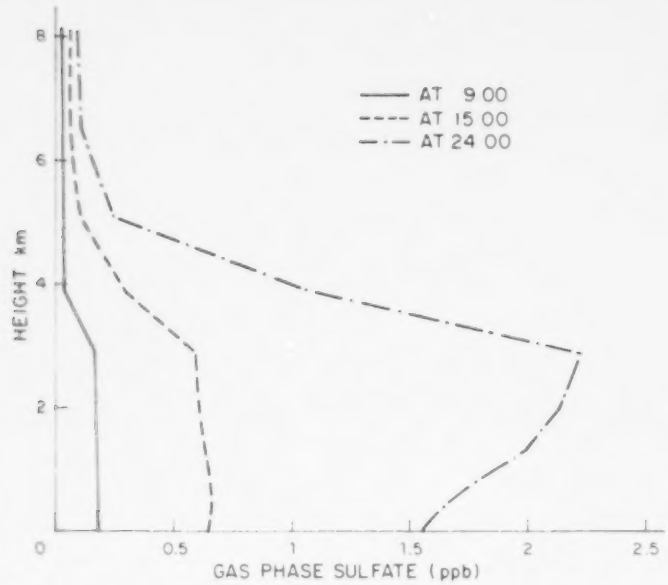

Fig. 9. Predicted sulfate profiles before cloud formation (9:00) and after the cloud disappears (24:00).

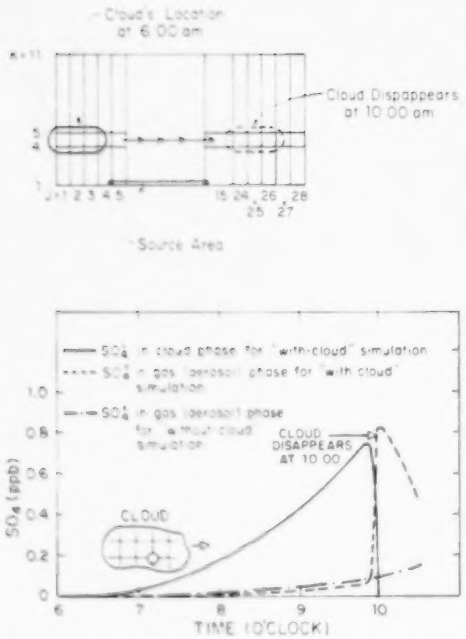

Fig. 10. Schematic of a 2-dimensional model simulation (upper figure) and the predicted cloud water and interstitial cloud air sulfate as a function of time for the sampling point indicated.

used for a variety of simulation applications. Some of these are (a) transport of SO_2/NO_x/hydrocarbon urban plumes to the background troposphere (Balko and Peters, 1983); (b) sulfate and nitrate formation in the presence of a land/sea breeze (Kitada *et al.*, 1984); (c) effects of in-cloud and below-cloud scavenging on homogeneous gas-phase chemistry (Carmichael *et al.*, 1983); and (d) detailed analysis of mixing-limited chemical reaction of NO emissions (Karamchandani and Peters, 1986). The model is also being used to analyze field data, to evaluate emission control strategies, and to investigate local flow situations.

Current development work is emphasizing subgrid-scale parameterization of chemical reactions and cloud processes.

Acknowledgements—This research was supported in part by the National Aeronautics and Space Administration under Research Grant NAG 1-36, and the National Acid Precipitation Assessment Program by the U.S. Environmental Protection Agency through the Battelle Pacific Northwest Laboratories. Several individuals, especially J. A. Balko, S-Y. Cho, P. S. Kasibhatla and S-G. Shim were instrumental in performing some of the simulations.

REFERENCES

Adewuyi Y-G., Cho S-Y., Tsay R-F. and Carmichael G. R. (1984) Importance of formaldehyde in cloud chemistry. *Atmospheric Environment* **18**, 2413-2420.

Alkezweeny A. J. and Powell D. C. (1977) Estimation of transformation rate of SO_2 and SO_4 from atmospheric concentration data. *Atmospheric Environment* **11**, 179-182.

Balko J. A. and Peters L. K. (1983) A modeling study of SO_x-NO_x-hydrocarbon plumes and their transport to the background troposphere. *Atmospheric Environment* **17**, 1965-1978.

Calvert J. G., Su F., Bottenheim J. W. and Strauss O. P. (1978)

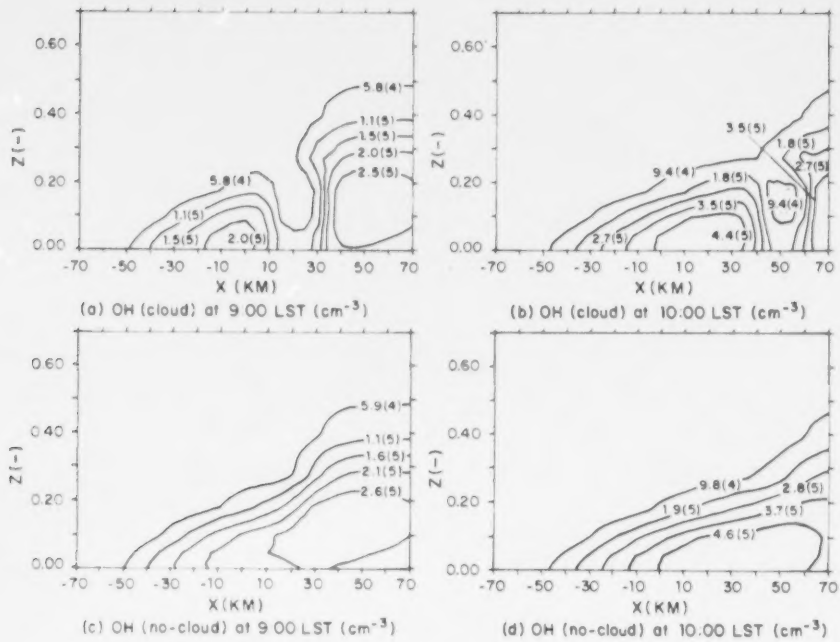

Fig. 11. Predicted OH concentration (radicals cm^{-3}) fields for the case where the cloud is present [(a) and (b)] and for the no-cloud case [(c) and (d)]. Simulation conditions are those in Fig. 10.

Mechanism of the homogeneous oxidation of sulfur dioxide in the troposphere. *Atmospheric Environment* **12**, 197–226.

Carmichael G. R., Kitada T. and Peters L. K. (1983) The effect of in-cloud scavenging on the transport and gas phase reactions of SO_x, NO_x, HC_x, H_2O_y, and O_3 compounds. *Precipitation Scavenging, Dry Deposition, and Resuspension*, (edited by Pruppacher H. R., Semonim R. G. and Slinn W. G. N.) Elsevier Science, Vol. 1, pp. 675–686.

Carmichael G. R. and Peters L. K. (1981) Application of the mixing-reaction in series model to NO_x–O_3 plume chemistry. *Atmospheric Environment* **15**, 1069–1074.

Carmichael G. R. and Peters L. K. (1984a) An Eulerian transport/transformation/removal model for SO_2 and sulfate—I. Model development. *Atmospheric Environment* **18**, 937–952.

Carmichael G. R. and Peters L. K. (1984b) An Eulerian transport/transformation/removal model for SO_2 and sulfate—II. Model calculation of SO_x transport in the eastern United States. *Atmospheric Environment* **18**, 953–967.

Davis D. D., Ravishankara A. R. and Fischer S. (1979) SO_2 oxidation via the hydroxyl radical: atmospheric fate of HSO_x radicals. *Geophys. Res. Lett.* **6**, 113–116.

Donaldson C. D. and Hilst G. R. (1972) Effect of inhomogeneous mixing on atmospheric photochemical reactions. *Envir. Sci. Technol.* **6**, 812–816.

Falls A. H., McRae G. J. and Seinfeld J. H. (1979) Sensitivity and uncertainty of reaction mechanisms for photochemical air pollution. *Int. J. Chem. Kinet.* **11**, 1137–1162.

Forester C. K. (1977) Higher order monotonic convection difference schemes. *J. Comput. Phys.* **23**, 1–22.

Heinrich J. C., Huyakorn P. S., Zienkiewicz O. C. and Mitchell A. R. (1977) An 'upwind' finite element scheme for two dimensional convective transport equation. *Int. J. Num. Meth. Eng.* **11**, 131–143.

Hong M. S. and Carmichael G. R. (1983) An investigation of sulfate production in clouds using a flow-through chemical reactor model approach. *J. geophys. Res.* **88**, 10733–10743.

Junge C. E. (1963) *Air Chemistry and Radioactivity*, p. 382. Academic Press, New York.

Kaiser J. A. C. and Hill R. H. (1976) Irradiance at sea. *J. geophys. Res.* **81**, 395–398.

Karamachandani P. K. and Peters L. K. (1986) Three-dimensional behavior of mixing-limited chemistry in the atmosphere. *Atmospheric Environment* (submitted for publication).

Kasibhatla P. S. (1984) Some aspects of regional scale air pollution modeling. M.S. Thesis, Department of Chemical Engineering, University of Kentucky.

Kitada T., Carmichael G. R. and Peters L. K. (1983) The locally-one-dimensional, finite element method (LOD-FEM) for atmospheric transport/chemistry calculations. *Proceedings of the Third International Conference on Numerical Methods in Engineering*, Paris, France, March.

Kitada T., Carmichael G. R. and Peters L. K. (1984) Numerical simulation of the transport of chemically reactive species under land- and sea-breeze circulations. *J. Clim. appl. Met.* **23**, 1153–1172.

Luther C. J. and Peters L. K. (1982) The possible role of heterogeneous aerosol processes in the chemistry of CH_4 and CO in the troposphere. In *Heterogeneous Atmospheric Chemistry*, (edited by Schryer D. R.), pp. 264–273. Geophysical Monograph 26, American Geophysical Union, Washington.

McRae G. J., Goodin W. R. and Seinfeld J. H. (1982) Numerical solution of the atmospheric diffusion equation for chemically reactive flows. *J. Comput. Phys.* **45**, 1–42.

Mitchell A. R. (1969) *Computational Methods in Partial Differential Equations*. John Wiley, New York.

Mitsumoto S., Ueda H. and Ozoe H. (1983) A laboratory experiment on the dynamics of the land and sea breeze. *J. atmos. Sci.* **40**, 1228–1240.

Orville H. D. and Kopp F. J. (1977) Numerical simulation of the life history of a hailstorm. *J. atmos. Sci.* **34**, 1596–1618.

Platt U., Perner D., Harris G. W., Winer A. M. and Pitts J. N. Jr. (1980a) Observations of nitrous acid in an urban atmosphere by differential optical absorption. *Nature, Lond.* **285**, 312–314.

Platt U., Perner D., Winer A. M., Harris G. W. and Pitts J. N., Jr. (1980b) Detection of NO_3 in the polluted troposphere by differential optical absorption. *Geophys. Res. Lett.* **7**, 89–92.

Preussner P. R. and Brand K. P. (1981) Application of a semi-implicit Euler method to mass action kinetics. *Chem. Eng. Sci.* **10**, 1633–1641.

Russell A. G., McRae G. J. and Cass G. R. (1983) Mathematical modeling of the formation and transport of ammonium nitrate aerosol. *Atmospheric Environment* **17**, 949–964.

Shetter R. E., Stedman D. H. and West D. H. (1983) The NO NO_2 O_3 photostationary state in Claremont, California. *J. Air Poll. Control Assoc.* **33**, 212–214.

Shu W. R., Lamb R. G. and Seinfeld J. H. (1978) A model of second-order chemical reactions in turbulent fluid—Part II. Application to atmospheric plumes. *Atmospheric Environment* **12**, 1695–1704.

Stelson A. W., Friedlander S. K. and Seinfeld J. H. (1979) A note on the equilibrium relationship between ammonia and nitric acid and particulate ammonium nitrate. *Atmospheric Environment* **13**, 369–371.

Stelson A. W. and Seinfeld J. H. (1982a) Relative humidity and temperature dependence of the ammonium nitrate dissociation constant. *Atmospheric Environment* **16**, 983–992.

Stelson A. W. and Seinfeld J. H. (1982b) Relative humidity and pH dependence of the vapor pressure of ammonium nitrate–nitric acid solutions at 25°C. *Atmospheric Environment* **16**, 993–1000.

Stockwell W. R. and Calvert J. G. (1983a) The mechanism of NO_3 and HONO formation in the night-time chemistry of the urban atmosphere. *J. geophys. Res.* **88**, 6673–6682.

Stockwell W. R. and Calvert J. G. (1983b) The mechanism of the HO–SO_2 reaction. *Atmospheric Environment* **17**, 2231–2235.

Thompson A. M. and Heikes B. G. (1982) Heterogeneous chemistry: effect on NO_3 in the unpolluted atmosphere. *Second Symposium, Composition of the Nonurban Troposphere*. pp. 134–136. American Meteorological Society, Boston.

Wesely M. L. and Shannon J. D. (1984) Improved estimates of sulfate dry deposition in eastern North America. *Entir. Prog.* **3**, 78–81.

Yamada T. and Mellor G. L. (1975) A simulation of the Wangara atmospheric boundary layer data. *J. atmos. Sci.* **32**, 2309–2329.

AN EVALUATION OF THE CHEMICAL AND PHYSICAL PROCESSES AFFECTING SULFATE AND NITRATE WET DEPOSITION

Shang G. Shim, Young S. Chang, Seog Y. Cho and
Gregory R. Carmichael
Department of Chemical and Materials Engineering
University of Iowa, Iowa City, IA 52242, USA

INTRODUCTION

The assessment of the effect of a reduction in primary emissions of SO_x, NO_x, and hydrocarbons on the pH of rain, on the ambient sulfate and nitrate levels, and on the total deposition amounts of sulfates and nitrates is currently one of the most important environmental challenges. However, the relationships between the emissions and the resultant distribution of acids and acidic precursors are difficult to determine because of the number and nature of the processes that occur. For example, the convective and diffusive processes, the in-cloud meteorology and chemistry, the homogeneous gas phase chemistry, and the deposition processes all influence the source receptor relationships.

In order to better understand these complex relationships a detailed combined transport/chemistry/removal model (referred to as STEM-II) has been developed by Carmichael et al., 1986. In this paper the wet deposition of sulfate and nitrates are investigated using the STEM-II model. The discussion includes an evaluation of the various chemical and physical processes contributing to sulfate and nitrate concentrations in hydrometeors and the diagnostic analysis of the primary processes in a mesoscale deposition event that occurred in the Philadelphia area on May 2nd 1985.

DESCRIPTION OF STEM-II MODEL

The STEM-II model (Carmichael et al., 1986) is an Eulerian combined

transport/chemistry/removal model which treats chemical species in the gas, cloud, rain and snow phases. Thirty-nine species are advected, while twenty-one species are short-lived and are modeled using pseudo-steady state methods. The advected species satisfy the folowing equations

Gas Phase:

$$\frac{\partial C_i}{\partial t} + \frac{\partial (U_j C_i)}{\partial x_j} = \frac{\partial}{\partial x_j}\left[K_{jj} \frac{\partial C_i}{\partial x_j}\right] + R_i + S_i + G_i \qquad i=1,\ldots,39 \qquad (1)$$

Cloud, Rain and Snow Phases:

$$\frac{\partial (S_m C_{im})}{\partial t} + \frac{\partial}{\partial x_j}(U_j - V_{sm})\, S_m C_{im} = \frac{\partial}{\partial x_j}\left(K_{jjm} C_{im} \frac{\partial S_m}{\partial x_j} + R\right)_{im} + G_{im} \qquad (2)$$

$i=1,\ldots,39$ m = 1 for cloud ($V_{sm}=0$)
= 2 for rain
= 3 for snow

where C_i's denote the concentrations,
U_j's are velocity components,
S's are the liquid water contents,
V_s's are the setting velocities of the hydrometeors,
K_{jj}'s are the eddy diffusivities, and
R_i, G_i and S_i are the rates of chemical reaction, mass transfer, and emissions, respectively.

The STEM-II model is structured to treat in detail wet removal processes. The physical processes of nucleation, accretion, autoconversion, and riming are included in the model analysis. In this model, the in-cloud scavenging of sulfate aerosol is presumed to occur totally by nucleation. Both cloud and aerosol size distributions are assumed to be monodispersed. Once the cloud forms, the number of sulfate aerosols activated and dissolved to form aqueous sulfate is assumed to be the same as the number concentration

of cloud droplets. Rain drops are also assumed to be monodispersed. Secondary sulfate is treated in the same way as primary sulfate and is allowed to be reinjected into the gas phase as hydrometeors evaporate.

The cloud parameters are calculated by the ASM cloud scavenging model (Hales, 1984). The ASM model treats the cloud microphysics and calculates the cloud and precipitation distributions, and interconversion rates. ASM calculates a self consistent and realistic meteorological data set of the simulated storm. The precipitation-formation processes are treated in a parameterized fashion. The parameterizations of rain-formation are adapted from Berry and Reinhardt (1974), Scott (1982), Kessler (1969), and Lin et al., (1983). The snow-formation is parameterized based on schemes similar to that developed by Lin et al., (1983) and Scott (1982). The scheme lumps water into four categories: water vapor, cloud water, rain and snow. The cloud related parameters calculated in ASM are transferred to the STEM-II model where the transport/chemistry/removal of pollutants is calculated.

For the gas phase, the new reaction mechanism of Atkinson and Lloyd (1982) which includes 81 reactions and 60 chemical species, is used. Of these species, 39 long-lived species are advected while the remaining 21 short-lived species such as free radicals are modeled using Pseudo Steady State Approximation.

In addition, for the liquid phase, 16 dissociation expressions, 33 chemical reactions and 22 ionic species based on the work of Chameides et al., (1984) are included in the STEM-II code. Detailed solution equilibria and chemical kinetics are solved using a modified semi-implicit method while satisfying the electrical-neutrality constraint. Also, the mass transfer associated with absorption into, and desorption from droplets is included.

The effect of clouds on the solar flux values is also included in this analysis. The following empirical correlation relating photon flux to cloud cover (Kaiser and Hill, 1976) is employed.

$$F = F_c(1 - AC^{1.75}) \qquad (3)$$

where F_c is the photon flux for clear sky, C is the cloud cover fraction, and A is a constant dependent on cloud type.

The numerical integration of the model equations makes use of the concept of fractional time steps and one-dimensional finite elements; referred to as the Locally One-Dimensional Finite Element Method (LOD-FEM). The transport equations are solved using a modified Galerkin FEM with asymmetric weighting functions and the Crank-Nicolson method for time. The chemistry equations are solved using a modification of the semi-implicit Eulerian method. Details of the numerics used in the model are found in Carmichael et al. (1986).

RESULTS AND DISCUSSION

The STEM-II model is being used to analyze field data collected in the U.S.E.P.A. Mesoscale Acid Deposition Study. The purpose of the study is to assess the importance of local emissions on the wet deposition loadings at receptors located within 200-300 km of urban centers. Discussions here will focus on the analysis of the May 2nd field study conducted in the Philadelphia area.

The modeling domain used for this analysis is shown in Figure 1. Two different grid systems are being used: a coarse grid with horizontal grid spacings of ~ 56 km; and a fine grid with horizontal spacings of 20 km. The vertical domain is the same in each system with 14 vertical grids non-uniformly spaced between the surface and a height of 6 km. The wind, temperature, and surface precipitation fields predicted by the dynamic meteorological model MASS (cf, Kaplan et al., 1982) were used as inputs to the STEM-II model. The predicted preicipitation fields were used as inputs to the ASM cloud model to generate the microphysical parameters for the wet removal calculations.

The emissions fields for the simultations were based on Version 5.2 of the U.S.E.P.A. inventory which includes SO_x, NO_x, and speciated hydrocarbons. Point sources of SO_2 and NO_x in the region are shown in Figure 2. As shown, the Pennsylvania side of the domain (the west half of the region) has many sources, while the New Jersey side (the east half of the region) is a relatively low source region.

The May 2nd event was an example of a slow moving frontal system which produced very heavy precipitation in the study area. The flow field in the modeling region at 14:00 LT (local time) was generally from the east and

gradually shifted from the northeast at 22:00 LT. The wind speeds were high throughout the period with horizontal winds of 15 m/s. The precipitation came from the south and reached Philadelphia at 15:50 LT.

The measured wet deposition loadings of nitrate and sulfate are shown in Figure 3. The general features show that for both species the loadings were higher on the Pennsylvania side. Furthermore, the nitrate loadings were slightly higher than those for sulfate on the New Jersey side.

Coarse grid model predictions are presented in Figure 4. The results are for an 18 hr period corresponding to 14:00 May 2nd to 8:00 May 3rd, 1985. The model was initialized by starting with remote conditions and then seasoning under no-flow conditions with real emissions for a period of 2-3 days. The chemical composition of the air masses transported into the model region (through the eastern and northern boundaries) was estimated by performing 1-dimensional model calculations reflecting the air mass histories. For example, the air entering through the eastern boundary has relatively low concentrations reflecting that it originated from the south and traveled along a wet trajectory, whereas the air mass entering the northern boundary has high concentrations of pollutants reflecting the high sources regions upwind in New York.

Predicted total 18 hr wet deposition loadings of selected species are presented in Figure 4. The sulfate and nitrate loadings show similar general features. The deposition values are much higher in the western part of the region and the nitrate values are somewhat higher than the sulfate levels. The regions of deposition loadings greater than 1000 μ mole m^{-2} are found downwind of the major sources (recall the flow is originally from the east and later from the northeast).

The deposition loadings of bisulfite and H_2O_2 are also presented. The bisulfite loadings are from 3-5 times lower than those for sulfate. The general pattern for bisulfite and H_2O_2 appear to be anticorrelated with high bisulfite and low H_2O_2 loadings occurring in the north and west regions and low bisulfite and high H_2O_2 loadings in the south and east regions. The pattern of the H_2O_2 loadings is quite similar to that for the total predicted precipitation loading.

The predicted deposition loadings are in good agreement with the measured

values (see Figure 3). The average predicted values of sulfate and nitrate in the areas of measurements on the Pennsylvania and the New Jersey side are 417 and 305 for sulfate, and 623 and 374 $\mu M/m^2$ for nitrate, respectively.

Further details of the deposition at the New Jersey measurement sites and the Pennsylvania sites can be seen by examining the deposition as a function of time at grid points (2,4) and (4,2) (see Figure 1). The time profiles of surface gas phase and rain phase concentrations of selected species are presented for comparison in Figure 5. The New Jersey site is an area of low NO_x and SO_x sources and for the meteorological conditions on May 2nd the wind direction is from the east; thus, relatively clean air is passing to this site through the eastern boundary. Precipitation occurs at this grid point for the first 16 hours of the event. The rain phase concentrations at this grid point show that the soluble pollutants are removed rapidly by the initial rain and that the bulk of the deposition loading occurs in the first hour of the rain event. The liquid phase concentration of H_2O_2 builds up beginning 1:00 LT on May 3rd. This corresponds to the time that the wind shifts to a northeasternly flow transporting polluted air mass reaching this site.

The Pennsylvania site (grid point (2,4)) is located in a region with high SO_x and NO_x emissions. The site is also downwind of major sources throughout the meteorological conditions of May 2nd 1985. Precipitation began at this site at 17:00 LT May 2nd and continued until 4:00 LT on May 3rd. The time profiles of gas and liquid phase concentrations at this site are also presented in Figure 5. The time profiles are quite different than those at the New Jersey site. The liquid phase concentrations of most species reach maximum values at 19:00 LT. The nitrate concentration maximum is ~ 200μM while that of sulfate is~ 100μM. The liquid phase concentration profiles of H_2O_2 and bisulfite show opposite trends. The H_2O_2 is high initially and decreases as time progresses. This indicates that at early times H_2O_2 is present in excess of bisulfite, and the bisulfite is consumed by the reaction with H_2O_2 to produce sulfate. At later times the H_2O_2 is depleted from the system and the bisulfite concentration increases. The gas phase profiles (not shown) indicate that gaseous H_2O_2 is depleted from the area by 22:00, whereas gaseous SO_2 is maintained by local emissions.

The mass balance inventories for the 18 hour simulation are presented for HNO_3, sulfate and SO_2 in Figure 6. These results useful insights into the

relative importance of various processes. The SO_2 inventory shows that local emissions during the 18 hour period is equivalent to about 1/3 of the mass of SO_2 initially present. (Furthermore, the net advection into the region is equivalent to the amount emitted). The wet deposition and dry deposition are of equal importance and together are equivalent in magnitude to the emissions. The wet removal processes consists of wet deposition of S(IV) at the surface and the conversion of S(IV) to sulfate in cloud and rain water. As indicated the importance of liquid phase consumption of S(IV) is much more important than the gas phase destruction reactions of SO_2. The predominant liquid phase reaction for this simulation is the reaction of S(IV) with H_2O_2 to produce sulfate. The inventory for sulfate reveals that the contribution of primary emissions is very small, that wet deposition is much more important than the dry deposition process for this event, and that sulfate production by liquid phase processes greatly exceeds that in the gas phase. The nitrate inventory is similar to that for sulfate except that there were no liquid phase production or consumption reactions involving nitrate included in the analysis.

ACKNOWLEDGEMENTS

This work was supported in part by funds provided by the U.S. Environmental Protection Agency's Meso-scale Acid Deposition Program through contract with NASA/Langley, through a grant from the Electric Power Research Institute, and by the D.O.E. PRECIP program through subscontract with the Battelle Pacific Northwest Laboratory.

REFERENCES

Atkinson, R., Lloyd, A.C. and Winges, L.. 1982, An updated chemical mechanism for hydrocarbon/NO_x/SO_2 photooxidations suitable for inclusion in atmospheric simulation model, Atmos. Environ., 16:1341.

Berry, E.X. and Reinhart, R.L., 1974, An analysis of cloud drop growth by collection, J. of Atmos. Sci., 31:2118.

Carmichael, G.R., Peters, L.K. and Kitada, T., 1986, A second generation model for regional-scale transport/chemistry/deposition, Atmos. Environ., 20:173.

Chameides, W.L., 1984, The photochemistry of a remote marine stratiform cloud, J. Geophys. Res., 89:4739.

Hales, J.M., 1984, An interim user's manual for the advanced scavenging module (working copy).

Kaplan, M. K., Zack, J.W., Wong, V.C., Tuccillo, J.J., 1982, Initial results from a mesoscale atmospheric simulation system and comparison with the AVE-SESAME I I data set, Monthly Weather Review, 110:1564.

Kessler, E., 1969, On the distribution and continuity of water substances in atmospheric circulation, Meteorological Monographs, 52.

Lin, Y., Farley, R.D. and Orville, H.D., 1983, Bulk parameterization of the snow field in a cloud, J. Atmos. Sci., 40:1065.

Scott, B.C., 1982, Predictions of in-cloud conversion rates of SO_2 based upon a simple kinetic and kinematic storm model, Atmos. Environ., 16:1735.

Figure 1. Philadelphia mesoscale acid deposition study domain. The shaded regions denote the areas where the monitoring stations were deployed. The large slanted square represents the modeling region.

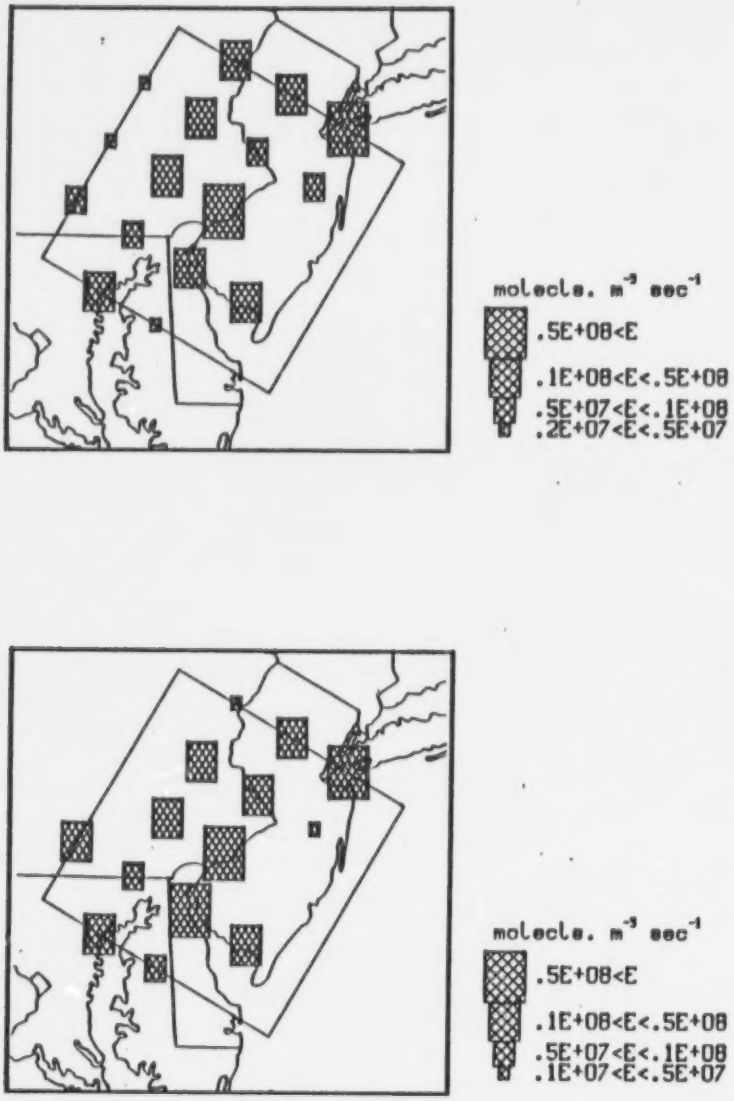

Figure 2. The point source emissions of (a) NO and (b) SO_2 at the surface.

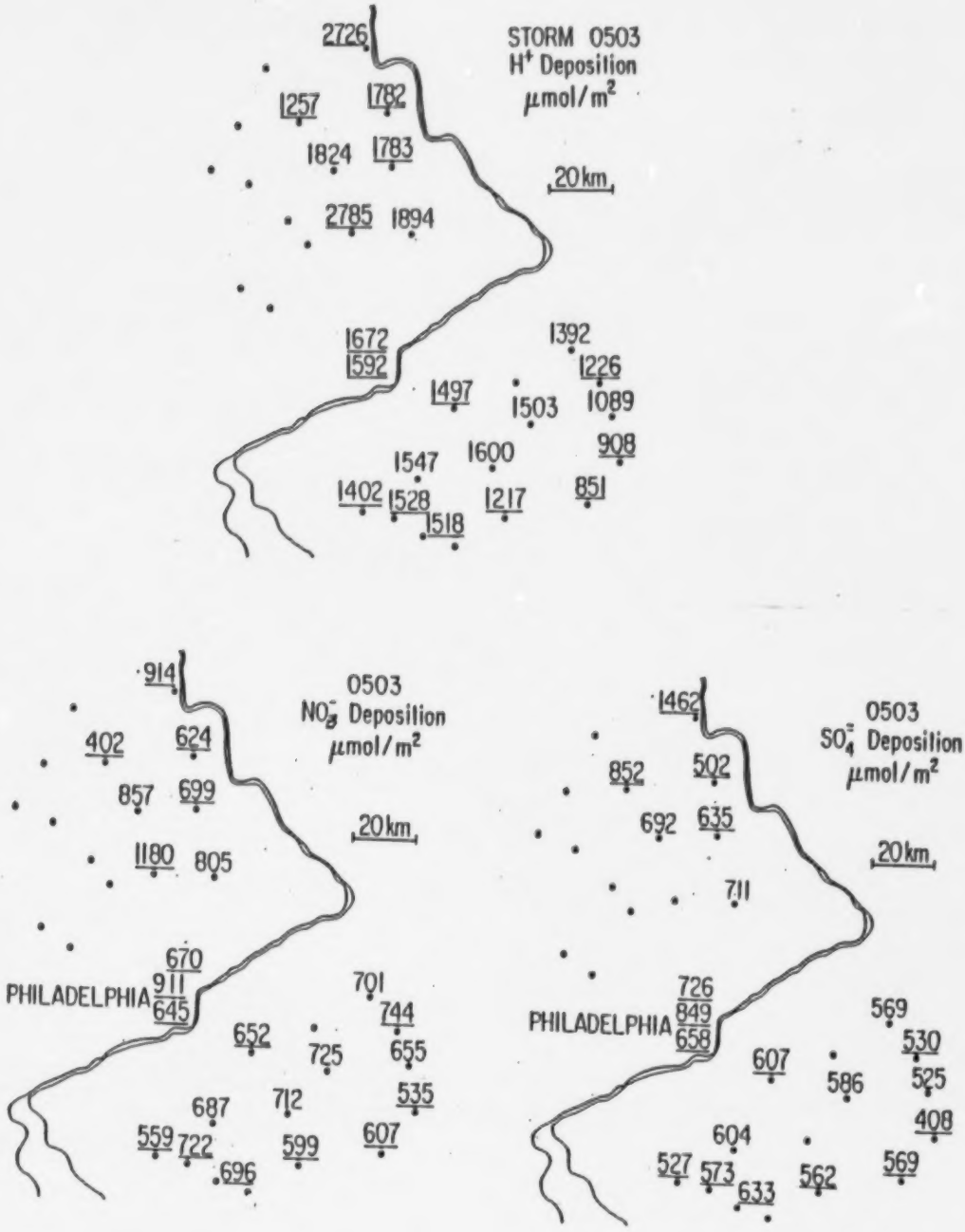

Figure 3. Measured total deposition of (a) H^+, (b) HNO_3 and (c) $SO_4^=$.

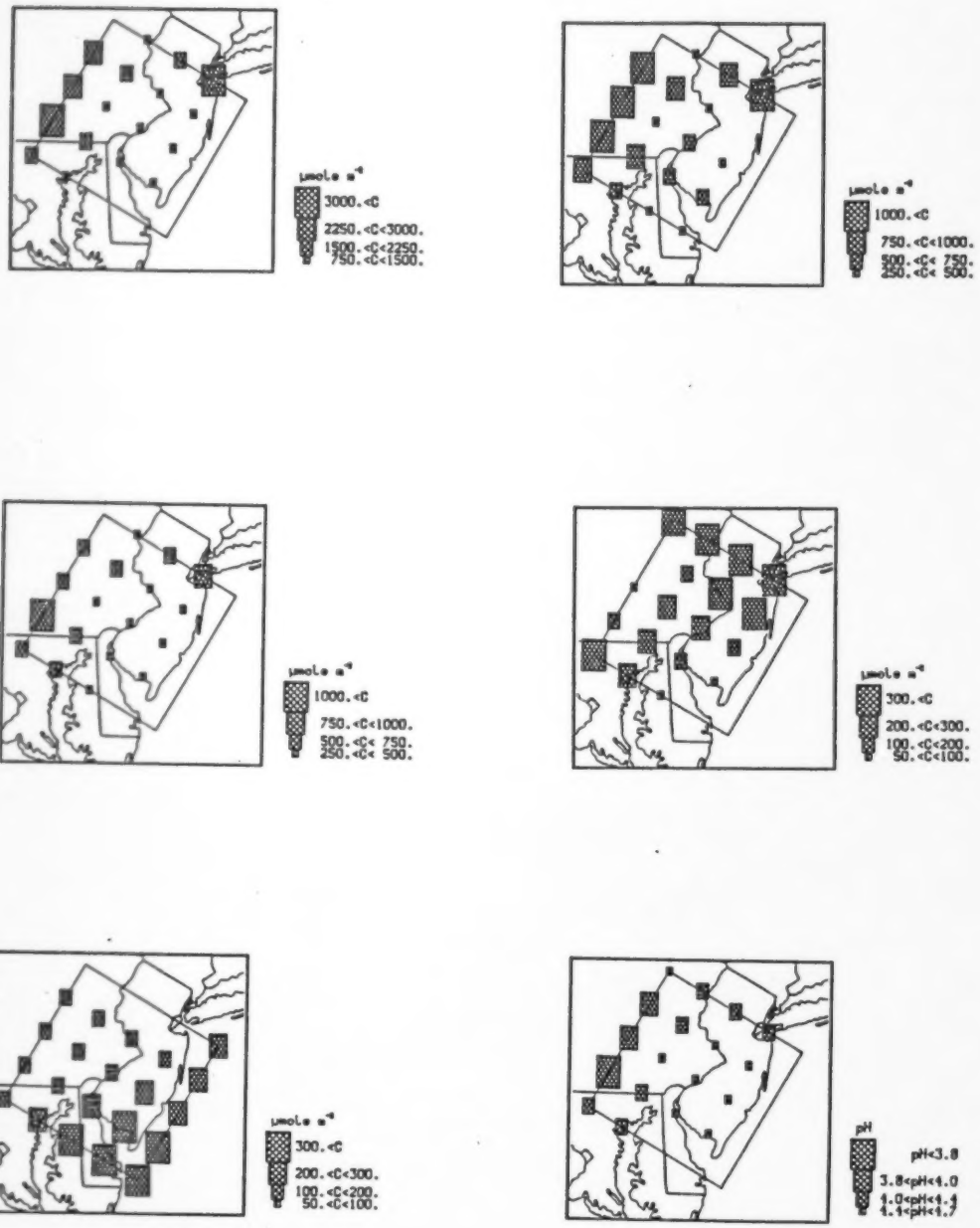

Figure 4. Predicted total deposition of (a) H^+, (b) HNO_3, (c) $SO_4^=$, (d) bisulfite, (e) H_2O_2, and (f) 18 hr averaged pH of rain during the storm.

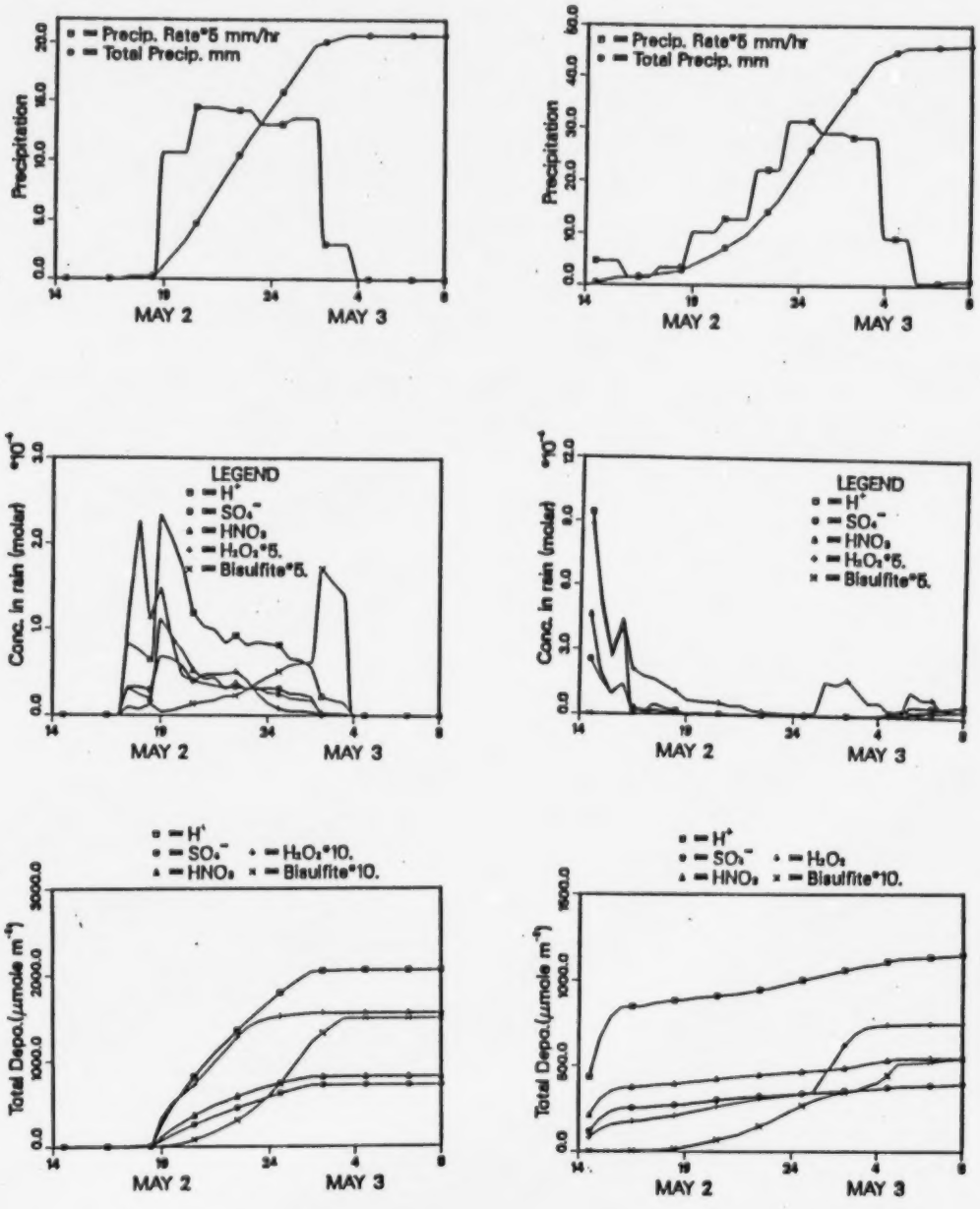

Figure 5. (a) Precipitation field at grid (2,4), (b) precipitation field at grid (4,2), (c) instantaneous deposition at grid (2,4), (d) instantaneous deposition at grid (4,2), (e) cumulative deposition at grid (2,4) and (f) cumulative deposition at grid (4,2).

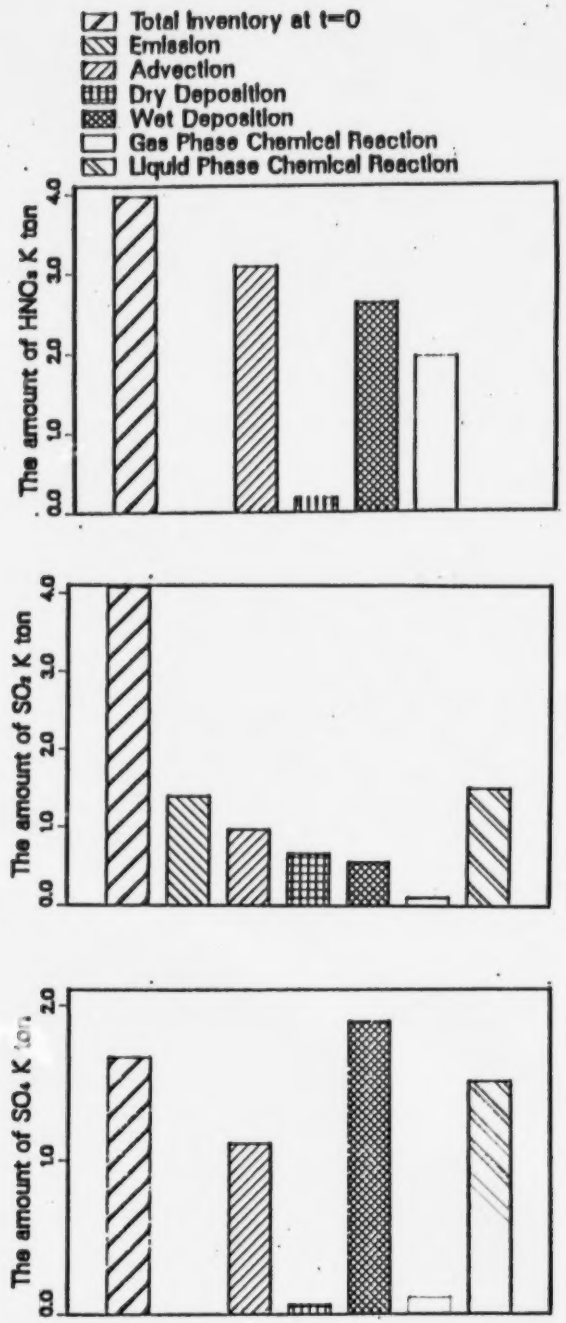

Figure 6. Inventories of (a) HNO_3, (b) SO_2, and $SO_4^{=}$.